UNIVERSITY OF CALIFORNIA
RIVERSIDE

Studies of Statistical-Mechanical Models Related to Quantum Codes

A Dissertation submitted in partial satisfaction
of the requirements for the degree of

Doctor of Philosophy

in

Physics

by

Yi Jiang

March 2021

Dissertation Committee:

Dr. Leonid P. Pryadko, Chairperson
Dr. Michael Mulligan
Dr. Shan-Wen Tsai

The Dissertation of Yi Jiang is approved:

Committee Chairperson

University of California, Riverside

Acknowledgments

First and foremost I am grateful to my advisor, Professor Leonid Pryadko, whose guidance helped me in all the time of my research and the completion of this dissertation. I want to thank him for his continuous support. His patience and immense knowledge are invaluable for my academic life.

I also want to thank the collaborators of this research. Part of this dissertation is a reprint of the material as it appears in "Duality and free energy analyticity bounds for few-body Ising models with extensive homology rank", published on May 2, 2018 on arxiv and Aug 2, 2019 on *Journal of Mathematical Physics*. Professor Pryadko directed and supervised the research. Dr. Ilya Dumer and Dr. Alexey Kovalev provided technical expertise.

I would like to thank Dr. Michael Mulligan and Dr. Shan-Wen Tsai for being on my dissertation committee.

I would like to thank my fellow research group members, Weilei Zeng and Michael Woolls, for the hardware and software they built for the research group and their selfless help when I face difficulties in my life.

ABSTRACT OF THE DISSERTATION

Studies of Statistical-Mechanical Models Related to Quantum Codes

by

Yi Jiang

Doctor of Philosophy, Graduate Program in Physics
University of California, Riverside, March 2021
Dr. Leonid P. Pryadko, Chairperson

As the beginning of the age of quantum supremacy comes closer, researches have been focusing on how to harness the full power of quantum computation. Quantum states that serve as the computational basis, known as *qubits*, are fragile. The interaction between them and the environment may result in errors, a process named *decoherence*. In the classical world, redundancy is the easiest way to protect information. But unlike classical information, it's impossible to clone an arbitrary quantum state. Fortunately, it has been shown that a small number of logical qubits can be encoded into a large number of physical ones, a technique known as *quantum error correcting codes* (QECCs). In the study of *stabilizer codes*, an important family of QECCs which shares some similarities with classical linear codes, it was discovered that the probability distribution of the decoding result can be mapped to the partition functions of spin models on graphs, a concept in statistical mechanics. Here we will explore the properties of certain families of QECCs and their corresponding statistical-mechanical models.

One of the most famous examples of stabilizer codes, the *toric code*, has the limitation that it only encodes 2 qubits regardless of how many physical qubits are used. To overcome this limitation, *hyperbolic codes* were proposed, where the physical qubits are placed on the edges of a quotient graph of a hyperbolic tessellation. Here we study the corresponding *Ising models* on such graphs with theoretical and numerical methods, and

explore their relationship to the quantum codes.

Instead of limiting ourselves to binary codes, we also consider q-ary codes where the computational basis is formed by *qudits*, a generalization of qubits to q-state quantum systems. We study the properties of qudit stabilizer codes not only in the cases where q is prime, which forms a *Galois field*, but also where q is composite, which forms a *ring of integers modulo* q. We find that their corresponding statistical-mechanical models are the *Potts models*, a q-ary generalization to Ising models. We explore the construction and parameters of such q-ary codes, and extend the known results on qubit stabilizer codes to qudit codes.

Contents

List of Figures

List of Tables

Chapter 1

Introduction

1.1 Prologue

Quantum information and quantum computation have been studied extensively based on the idea that quantum computers have the potential to be much more efficient than classical computers on certain kinds of problems, and several examples of quantum computation algorithms that outperform the best classical algorithms known so far have been discovered [1, 2]. To build a large-scale quantum computer, on the other hand, has a number of technical challenges, and one of the greatest ones is decoherence, which would result in errors in the computations. To overcome this obstacle, quantum error correction techniques are developed to protect quantum information by encoding them with a quantum error correcting code (QECC) and recover the information after decoding [3]. As long as the rate of physical qubit errors is below a certain threshold, the quantum error correction process will suppress the errors in the result, and the information can be preserved indefinitely.

A number of QECCs has been proposed, and one of the most important class of them is the *CSS* codes, named after the inventors, Robert Calderbank, Peter Shor and Andrew Steane [4, 5]. The decoding transition for such codes can be mapped to certain statistical-mechanics models, such correspondence helps the study of both research areas [6].

In some of the QECCs, qubits can be placed on the vertices or edges of a planar graph or a graph that tiles certain two-dimensional manifold. The most famous example is the toric code, which has the qubits placed on the surface of a torus [7]. The toric code has unlimited distance if given enough physical qubits, yet it can only encode 2 qubits. To explore QECCs with better code parameters, we studied quantum code constructions that locally have a lay-out of hyperbolic tessellation, which has a negative curvature. The number of logical qubits that can be encoded in such hyperbolic codes increases linearly as the number of physical qubits, so they have a finite code rate [8].

On the other hand, physics on curved space also attracts interest. For example, the AdS/CFT correspondence relates quantum gravity on curved space-time with quantum field theories [9, 10, 11, 12, 13, 14, 15]. In statistical mechanics and condensed matter physics, curvature can serve as an additional parameter to drive the criticality, or as a way to introduce geometrical frustration in toy models of amorphous solids, supercooled liquids, and metallic glasses [16, 17, 18, 19, 20, 21, 22, 23]. Models like percolation on more general expander graphs and various random graph ensembles are also common in network theory, e.g., such models occurred in relation to internet stability and spread of infectious diseases [24, 25, 26, 27, 28, 29, 30]. Understanding the relation between the decoding transition of QECCs and the phase transition of thermodynamic models on hyperbolic planes helps us to understand deeper in both areas.

Other than the QECCs on graphs, there are also QECCs that have non-local operators. One important example is the hypergraph-product code based on classical LDPC (low density parity check) codes. Such codes are also related to statistical mechanical models, but with multi-particle interactions [6, 31, 32].

While most of the QECCs are based on qubits, there are also generalizations to q-ary algebras [33]. Most often the codes are defined on Galois fields $\mathbb{F}_q$, where q is a prime or a prime power. In this work, we study qudit codes defined on modular integers $\mathbb{Z}_q$, and their correspondence with Potts model is also explored. A challenge of the generalization from binary to q-ary algebra in QECCs is that the complicated structure of modules over

the ring of modular integers requires more careful treatment than linear spaces over Galois fields, and the results could be much different. Also in statistical mechanics there are some fundamental differences, for example, the Ising model on a 2D lattice has second order phase transition, while the Potts model with $q > 4$ on the same lattice has first order transition [34]. More questions may be asked such as what are the differences when they are on a hyperbolic plane, or with multi-spin interactions. Generalizations of these studies from binary cases to q-ary cases is another topic in this thesis.

1.2 Outline

In **Chapter 2** we will introduce the background on QECCs and the correspondence between *CSS* codes and Random Bond Ising Model (RBIM).

In **Chapter 3** we introduce hyperbolic tessellations and their properties, then the construction of closed hyperbolic surfaces. Analytical and numerical results for Ising models on such graphs are given next, which are related to the hyperbolic surface codes.

In **Chapter 4** we study the generalization from binary QECC to q-ary QECC and their correspondence to Potts gauge glass model, and the construction and properties of q-ary hyperbolic surface codes, hypergraph-product codes and more general LDPC codes.

The last is **Chapter 5** which we end with a conclusion and discuss some open questions for future research.

Chapter 2

Preliminaries

2.1 Background

Modern computers utilize digital circuits to perform certain computation tasks. These circuits are large assemblies of logic gates, which implement Boolean functions on binary inputs called bits. A bit can be either in the state 0 or 1.

In quantum computation, the basic unit of information is qubit. Each qubit is a two state quantum system that has a basis $\{|0\rangle, |1\rangle\}$ which is called the computational basis. Unlike classical bits, which can only be in one of the two states, a qubit can be in a state that is a *superposition* of the computational basis, $|\psi\rangle = \alpha\,|0\rangle + \beta\,|1\rangle$, where α and β are complex numbers that satisfy the normalization condition $|\alpha|^2 + |\beta|^2 = 1$. Such a state is called a pure state. In the presence of interactions and decoherence, a qubit may turn into a mixed state, which is a statistical combination of pure states.

The state of multiple qubits is a superposition of their product basis states. A system of n qubits spans a 2^n-dimensional Hilbert space.

A quantum gate is a unitary operator that rotates the state vector. A sequence of quantum operations, including quantum gates and measurements, on a set of qubits, which are visualized as wires, is a quantum circuit.

2.2 Quantum error correction

In a quantum computation, quantum states may be affected by undesired interactions with their environment. Such quantum noise may result in errors. Unlike classical information, which one can make copies of, it is impossible to copy an arbitrary quantum state [35]. To overcome this obstacle, quantum error correction codes (QECCs) are developed to protect quantum information.

2.2.1 Stabilizer codes

Stabilizer codes are an important family of QECCs, which are similar to classical linear codes. The set of n qubit states forms a Hilbert space V_n, and the Pauli operators form a Pauli group $\mathscr{P}_n$ acting in that space. If S is a subgroup of $\mathscr{P}_n$ and V_s is a subspace of V_n such that every element of V_s is unchanged under the action of any element in S, S is called a stabilizer of V_s.

The Pauli Group on one qubit $\mathscr{P}_1$ is generated by the Pauli matrices

$$X = \sigma_1 = \begin{pmatrix} 0 & 1 \\ 1 & 0 \end{pmatrix}, \quad Y = \sigma_2 = \begin{pmatrix} 0 & -i \\ i & 0 \end{pmatrix}, \quad Z = \sigma_3 = \begin{pmatrix} 1 & 0 \\ 0 & -1 \end{pmatrix} \tag{2.1}$$

The products of the matrices and the factors -1 and $\pm i$ gives the group:

$$\mathscr{P}_1 = \{\pm I, \pm iI, \pm X, \pm iX, \pm Y, \pm iY, \pm Z, \pm iZ\} \tag{2.2}$$

The n qubit Pauli group is generated by the tensor products of the operators on each qubit.

The stabilizer group is a subgroup of the n-qubit Pauli group which acts in an n-qubit Hilbert space. The operators that are the elements of the group must commute with each other so that the measurements on the stabilizer generators don't change the state of the code. A quantum stabilizer code $\mathcal{Q}$ $[[n, k, d]]$, which encodes k logical qubits into n physical qubits that has distance d, is a 2^k-dimensional subspace of $H_2^{\otimes n}$, a common $+1$ eigenspace of all operators in the code's stabilizer, an abelian group $\mathscr{S} \subset \mathscr{P}_n$ such that $-I \notin \mathscr{S}$.

We can write the stabilizer generators as rows of a *generator matrix*,

$$\mathcal{G} = (\mathcal{G}_X, \mathcal{G}_Z)$$

where the commutativity of the stabilizers requires that

$$\mathcal{G}_X \mathcal{G}_Z^T + \mathcal{G}_Z \mathcal{G}_X^T = 0 \text{ (mod 2)}.$$

The errors of stabilizer codes is a product of Pauli operators

$$E \equiv i^m X_1^{e_1} X_2^{e_2} \dots X_n^{e_n} Z_1^{e_{n+1}} \dots Z_{2n}^{e_{2n}}$$

which can be mapped to a length $2n$ binary vector $\boldsymbol{e} = (e_1, e_2 \dots e_{2n})$ up to a phase.

An error is detectable iff it anticommutes with any of the stabilizer generators. An error that is in the stabilizer group is not detectable and doesn't need to be corrected, since it doesn't change the logical quantum state. Errors that are different by a stabilizer operator are called *degenerate*, since they act identically on the code.

An operator that commutes with the stabilizer generators and changes the logical quantum state is a codeword, represented by a length $2n$ vector $\boldsymbol{c}$.

Degenerate errors are those that are different by a linear combination of rows of $\mathcal{G}$, $\boldsymbol{e}' = \boldsymbol{e} + \boldsymbol{\alpha}\mathcal{G}$, where $\boldsymbol{\alpha}$ is an arbitrary vector.

Vectors of codewords are those that satisfy the commutativity requirement with all the rows in the generator matrix, but cannot be written as a linear combination of rows of the generator matrix. Two codewords are equivalent if they differ by a linear combination of the rows of the generator matrix.

2.2.2 *CSS* codes

An important subclass of stabilizer codes is CSS codes, which is named after the initials of the inventors: Robert Calderbank, Peter Shor and Andrew Steane [4, 5]. CSS codes can be constructed from classical linear codes.

An $[n, k, d]$ classical linear code $\mathcal{C}$ is a k-dimensional subspace of the vector space of all binary strings of length n, $\mathbb{F}_2^n$. The code distance d is the minimal weight of any

non-zero string in the code space, a code with distance d detects any error with weight up to $d-1$ and corrects any error with weight up to $\lfloor (d-1)/2 \rfloor$. The generator matrix G of the code has k rows which are the k basis vectors, and the parity check matrix H is the exact dual to G, $H \equiv G^*$, that is, the vector space of H is orthogonal to that of G, $HG^T = 0$, and also, $\operatorname{rank} H + \operatorname{rank} G = n$.

A quantum CSS code can be constructed from two generator matrices G_X and G_Z, where each of the matrices has n columns and they satisfy the orthogonal condition $G_X G_Z^T = 0$. The code dimension $k = n - \operatorname{rank} G_X - \operatorname{rank} G_Z$. The rows of G_X correspond to stabilizer generators that are tensor products of X operators, so they can detect Z type errors, which anti-commute with X. When applying the stabilizer generators to the qubits that have an error $\boldsymbol{e}$, the result is called a syndrome $\boldsymbol{s}_Z = G_X \boldsymbol{e}^T$. An error may have a zero syndrome. One possibility is that it is in the stabilizer group of the operators of the same type, for example an X error that is in the X stabilizer cannot be detected by Z stabilizer generators. Such errors would not change the code, and need not to be corrected. The other possibility is that the undetectable error is not in the stabilizer group, in this case it is a *codeword*, which changes the information to a different meaning after decoding. Two errors may have the same syndrome. If the difference between them is in the stabilizer group, they are equivalent in the code and there is no need to distinguish them, these errors are called *degenerate*. Otherwise, they are different by a codeword. The minimal weight of a codeword is the distance of the code.

2.2.3 Maximum likelihood decoding

The goal of error correction is to correct any error(s) that happened. To this end, the degeneracy class of the error that happened degeneracy must be recovered. Given a syndrome $\boldsymbol{s}$, *maximum likelihood decoding* is to find the most likely degeneracy class by summing up the probabilities of all the errors that are degenerate to an error that matches a syndrome, and compare such sums for different error degeneracy classes (such errors differ by non-trivial logical operators).

In the case of independent identically distributed (i.i.d) errors where any single X or Z error happens with probability p, the probability of an error $\boldsymbol{e} = (\boldsymbol{v}, \boldsymbol{u})$ is

$$P(\boldsymbol{e}) = \prod_{i=1}^{N_b} p^{e_i}(1-p)^{1-e_i} = p^w(1-p)^{N_b-w} \tag{2.3}$$

where $\boldsymbol{v}$ and $\boldsymbol{u}$ are both length n vectors corresponding to X errors and Z errors respectively, $N_b = 2n$, $w = \mathrm{wgt}(\boldsymbol{e}) = \mathrm{wgt}(\boldsymbol{v}) + \mathrm{wgt}(\boldsymbol{u})$ is the Hamming weight of the vector.

Since degenerate errors are equivalent, with maximum likelihood decoding one may sum up the probabilities of all the errors that are equivalent to $\boldsymbol{e}$, which is

$$P_0(\boldsymbol{e}) = \frac{1}{2^{N_g}} \sum_{\boldsymbol{\sigma}} p^w(1-p)^{N_b-w}, w \equiv \mathrm{wgt}(\boldsymbol{e} + \boldsymbol{\sigma}\mathcal{G}), \tag{2.4}$$

where $\mathcal{G}$ is the generator matrix that has dimensions $N_s \times N_b$, $N_g \equiv N_s - \mathrm{rank}\,\mathcal{G}$ is the number of linear dependent rows in $\mathcal{G}$, $\boldsymbol{\sigma}$ runs through all binary vectors of length $2n$.

As for the probability of all errors that are equivalent to $\boldsymbol{e}+\boldsymbol{c}$ where $\boldsymbol{c}$ is a codeword, we define

$$P_{\boldsymbol{c}}(\boldsymbol{e}) \equiv P_0(\boldsymbol{e} + \boldsymbol{c}), \tag{2.5}$$

so the total probability of all errors that result in a syndrome $\boldsymbol{s}$ is

$$P_{\mathrm{tot}}(\boldsymbol{s}) \equiv \sum_{\boldsymbol{c}} P_{\boldsymbol{c}}(\boldsymbol{e}). \tag{2.6}$$

where the summation should be done over all inequivalent codewords.

From all the codewords, we denote the one that maximizes $P_{\boldsymbol{c}}(\boldsymbol{e})$ by

$$P_{\max}(\boldsymbol{s}) \equiv \max_{\boldsymbol{c}} P_{\boldsymbol{c}}(\boldsymbol{e}). \tag{2.7}$$

For the decoding to return the correct codeword, $P_0(\boldsymbol{e})$ needs to be the maximum in $P_{\boldsymbol{c}}(\boldsymbol{e})$ for all $\boldsymbol{c}$, and in the limit of large n, it needs to dominate the probability distribution $P_{\mathrm{tot}}(\boldsymbol{s}_{\boldsymbol{e}})$ so that the decoding would success with probability one,

$$[P_0(\boldsymbol{e})/P_{\mathrm{tot}}(\boldsymbol{s}_{\boldsymbol{e}})] \xrightarrow{n\to\infty} 1, \tag{2.8}$$

where the brackets denote averaging over all the errors $\boldsymbol{e}$.

2.3 Mapping to Random Bond Ising Models (RBIM)

The relation between spin models and binary codes is well known [36, 37]. We define a partition function of an Ising model as the following [31]:

$$\mathcal{Z}_{\boldsymbol{e},\boldsymbol{m}}(\Theta, \{K_b\}) \equiv \frac{1}{2^{N_g}} \sum_{\{S_r=\pm 1\}} \prod_{b=1}^{N_b} R_b^{m_b} \frac{\exp(K_b(-1)^{e_b} R_b)}{2\cosh\beta}, \tag{2.9}$$

where $S_r \in \pm 1$ are the spins of the Ising model, $r = 1, \ldots, N_s$, $R_b \equiv \prod_r S_r^{\Theta_{r,b}}$ are the bond interactions, Θ is the incidence matrix of the graph that the Ising spins are defined on, $K_b \equiv \beta J_b$ where β is the inverse temperature and J_b is the bond strength. The vectors $\boldsymbol{e}, \boldsymbol{m}$ represent electric and magnetic disorder respectively.

On the other hand, we may rewrite the probability of equivalent errors as the following:

$$P_0(\boldsymbol{e}) = \frac{1}{2^{N_g}} \sum_{\boldsymbol{\sigma}} \left(\frac{p}{1-p}\right)^{\mathrm{wgt}(\boldsymbol{e}+\boldsymbol{\sigma}\mathcal{G})} (1-p)^{N_b} \tag{2.10}$$

$$= \frac{1}{2^{N_g}} \sum_{\{\sigma_r\}} \prod_{b=1}^{N_b} (1-p) \left(\frac{p}{1-p}\right)^{e_b + \sum_r \sigma_r \mathcal{G}_{r,b}} \tag{2.11}$$

By replacing $p/(1-p)$ with e^{-2K}, we can see that this quantity has the same form as the partition function. Define a simplified partition function:

$$Z_0(\boldsymbol{e}, \beta) \equiv \mathcal{Z}_{\boldsymbol{e},\boldsymbol{0}}(\mathcal{G}, \{K_b = \beta\}), \tag{2.12}$$

the probability is found to be the same of the partition function on the *Nishimori line*[36] for the random bond Ising model:

$$P_0(\boldsymbol{e}) = Z_0(\boldsymbol{e}, \beta_p) \tag{2.13}$$

where β_p satisfies $e^{-2\beta_p} = p/(1-p)$ is the definition of the Nishimori line.

For any other temperatures not on the Nishimori line $\beta \neq \beta_p$, the assumed probability of a 1-qubit X or Z error doesn't match the actual one, in which case it corresponds to

sub-optimal decoding, with the decoder given incorrect information about error probability distribution.

In the case of CSS codes, the partition function is the product of those of the two models, corresponding to the generating matrices G_X and G_Z, so we may consider G as either of them since they work likewise.

2.3.1 Toric code

Toric code is one of the most famous QECCs, where the physical qubits are located on the edges of a square lattice with periodic boundary conditions, which forms a torus, hence the name. The X and Z stabilizer operators are on the vertices and faces respectively, and the logical operators are on the non-trivial cycles. The corresponding statistical mechanics model is RBIM on 2D square lattices [6].

Chapter 3

Hyperbolic Codes and the Ising Model

Toric code is a great example of a QECC that's on a 2D plane and has a finite threshold. Yet it has the disadvantage that as the distance increases, the code rate approaches 0 asymptotically. Many finite rate QECCs have been studied, and one family of such codes are analogs of the toric code on locally planar graphs which look locally like a regular tiling of a hyperbolic plane.

To have a finite code rate, the code dimension must grow linearly with the block length. Based on toric code, an intuitive approach is to increase the number of holes on the torus, resulting in a surface with genus g that grows linearly with n so that $k = 2g \propto n$. But how do we find a symmetric graph on such a surface? For surfaces with $g > 1$, the curvature is negative, so we may find such tilings on a hyperbolic plane instead of a 2D Euclidean plane.

Similar to the toric code, to construct hyperbolic codes the qubits are placed on the edges of a graph, and one type of stabilizer checks are placed on vertices and the other on faces, except that the graph is a quotient of an infinite hyperbolic tiling, instead of a square lattice.

3.1 Hyperbolic tilings

Hyperbolic geometry is a non-Euclidean geometry, where the axiom about parallel lines is replaced so that more than one non-intersecting lines exist for any point that is not on the line [38]. A hyperbolic plane has negative Gaussian curvature everywhere. For a hyperbolic plane with constant Gaussian curvature K, denote $R \equiv \frac{1}{\sqrt{-K}}$, then for a circle of radius r the circumference is $2\pi R \sinh \frac{r}{R}$ and the area is $2\pi R^2(\cosh \frac{r}{R} - 1)$, which both grow exponentially with r asymptotically in the large r limit.

To visualize and study geometry on hyperbolic planes more easily, many models that represent hyperbolic planes on other 2D planes are used. Here we use the *Poincaré disk model* for showing the hyperbolic tilings. In this model the hyperbolic plane are mapped to a disk with radius 1, and the distance between two points on the disk is

$$d(x, y) = \cosh^{-1}\left(1 + \frac{2||x - y||^2}{(1 - ||x||^2)(1 - ||y||^2)}\right) \tag{3.1}$$

On an Euclidean plane there are only three regular tilings: the equilateral triangles, the squares and the regular hexagons, which are denoted by {3,6}, {4,4} and {6,3} in *Schläfli symbol* respectively. The symbol $\{p, q\}$ represents a tessellation that has q regular p-sided polygon faces around each vertex. A $\{p, q\}$ tessellation on 2D Euclidean plane must obey the constraint $1/p + 1/q = 1/2$, which originates from the fact that the angles around a vertex must sum to 2π on an Euclidean plane.

In the case of $1/p + 1/q > 1/2$, the tessellation is on a sphere. There are 5 possible solutions, where $\{p, q\}$ can be {3,3}, {3,4}, {4,3}, {3,5} or {5,3}. They correspond to the five Platonic solids, namely the tetrahedron, octahedron, cube, icosahedron and dodecahedron.

When $1/p + 1/q < 1/2$, the tessellation is on a hyperbolic plane, and there are infinitely many solutions for this condition, each of them forms a regular hyperbolic tessellation.

3.1.1 Tilings with open boundary

For uniform tilings on 2D Euclidean plane inside a circle of radius r, it is easy to see that the number of vertices or edges or faces along the circumference grows linearly with r, and the number of them inside the area grows as r^2. While for hyperbolic tessellations, they grow exponentially with r in the large r limit, with some base $c : n \propto c^r$.

When creating such graphs with a computer, the memory may soon be used up as the radius increases. To estimate the order and the size of a graph of $\{p, q\}$ tiling with a given distance from the origin to the boundary, it is necessary to determine the base $c(p, q)$.

Consider a $\{p, q\}$ tiling on a hyperbolic plane with constant Gaussian curvature -1, where the length of an edge is a. The base of the exponential growth of the number of vertices or edges or faces inside a circle of radius ar is given by

$$\ln(c_{\text{geo}}) = 2\cosh^{-1}\left(\frac{\cos(\frac{\pi}{p})}{\sin(\frac{\pi}{q})}\right) \tag{3.2}$$

which can be calculated from the area of the circle, Area $= 4\pi\sinh^2(r'/2) \approx \pi e^{r'}$, where r' can be converted to r, which is in the unit of the length of the edges a, $r' = ar$, so $c_{\text{geo}} = e^a$. The length of the edges is easily calculated from the trigonometry of right triangles, $\cosh(\frac{a}{2}) = \cos(\frac{\pi}{p})/\sin(\frac{\pi}{q})$.

However, to create a hyperbolic graph in a computer, it is more convenient to do it layer by layer. Thus, we also consider the growth of the size of the graph with another two definitions of radius and distance. The first one is the distance in graph theory, which is the number of edges in the shortest path between two vertices. On a square lattice, the analog is *Manhattan distance*, corresponding to *von Neumann neighborhood*, where each new layer consists of the faces that share at least one edge with the previous layer. The second definition of the distance is analogous to the *Chebyshev distance* on a square lattice, where the distance between two vertices is the minimum number of faces on any path of vertex-face pairs that are incident to each other. This construction corresponds to *Moore neighborhood*, where each new layer consists of the faces that share at least one vertex with

the previous layer.

It is easy to prove that the tiling graph inside a circle of geometric radius r from a vertex at the center is always larger than the one that has r layers with Von Neumann neighborhood for any $\{p, q\}$, and always smaller than the one that has r layers with Moore neighborhood for any $p \geq 4$. The former is true because the graph distance between any vertex and the center vertex must be less than or equal to r, so their geometric distance must be less than or equal to r. The latter is true because, if we draw a circle of radius 1 at any point on the boundary of the $(r-1)$th layer, the circle will be fully covered by the $(r-1)$th and rth layer of the faces if $p \geq 4$.

The base of the exponential growth of the graph size with radius analogous to Chebyshev distance is easier to calculate, so let us start from this one and then go back to the one with graph distance.

Suppose there is a $\{p, q\}$ tiling with $p \geq 4, q \geq 3$ of radius r in Chebyshev distance, and we want to find the number of vertices on the boundary. It is easy to see that the vertices on the boundary either have degree 3 or 2, which we denote by type a and b respectively, as shown in Fig 3.1. Denote the number of vertices of type a on the boundary of the tiling of radius n with a_n and those of type b with b_n, we find the recurrence relation:

$$\begin{cases} a_n = (q-3)a_{n-1} + (q-2)b_{n-1} \\ b_n = ((p-3)(q-3)-1)a_{n-1} + ((p-3)(q-2)-1)b_{n-1} \end{cases} \tag{3.3}$$

By solving the equation $a_n + xb_n = c(a_{n-1} + xb_{n-1})$ for c, we see that it must satisfy

$$c^2 - ((p-2)(q-2)-2)c + 1 = 0 \tag{3.4}$$

When $(p-2)(q-2) < 4$, there is no real solutions for c. When $(p-2)(q-2) = 4$, $c = 1$. When $(p-2)(q-2) > 4$, there are 2 positive solutions which have product 1, and at large radius limit the contribution from the smaller solution can be ignored, and the number of vertices grows as c^n. These are the cases corresponding to spherical tiling, Euclidean plane tiling and hyperbolic plane tiling respectively.

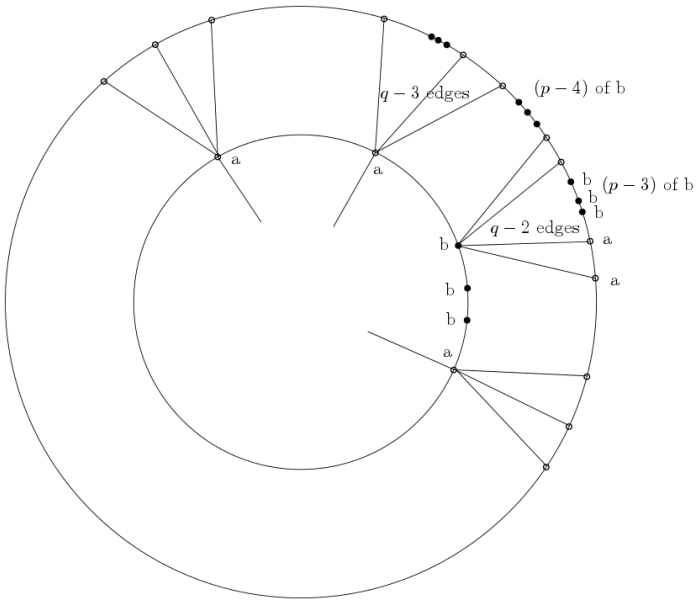

Figure 3.1: Constructing the next layer with Moore neighborhood for $p \geq 4$.

The recurrence equations above don't work for $p = 3$, so we must calculate it separately. The situation for $p = 3$ is similar, where the recurrence relation becomes:

$$\begin{cases} a_n = (q-5)a_{n-1} + (q-6)b_{n-1} \\ b_n = a_{n-1} + b_{n-1} \end{cases} \tag{3.5}$$

And c satisfies

$$c^2 - (q-4)c + 1 = 0 \tag{3.6}$$

which is the same as the previous case with $p = 3$.

The calculation for the case where radius is the graph distance is more complicated, since each time we add a layer of edges instead of faces, which means the new layer depends on many layers backwards. So instead of 2 recurrence equations, there will be $p/2$ of them if p is even or $p-1$ of them if p is odd.

To find the recurrence equations, we may partition the polygon layer by layer into triangles and quadrilaterals. When p is even, we name these pieces of a face A_1, A_2, ..., A_k where $k = p/2$, A_1 and A_k are triangles and the rest are quadrilaterals. When p is odd, we

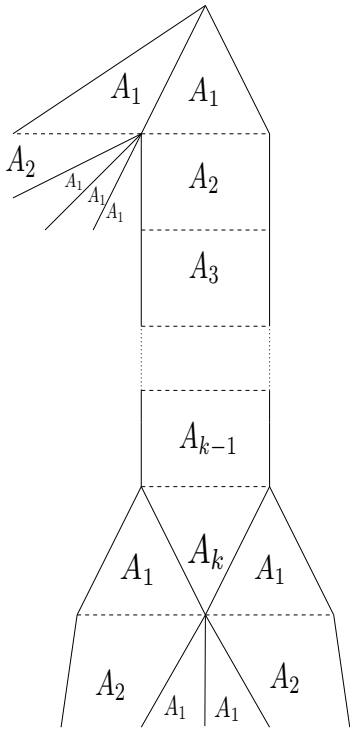

(a) p is even

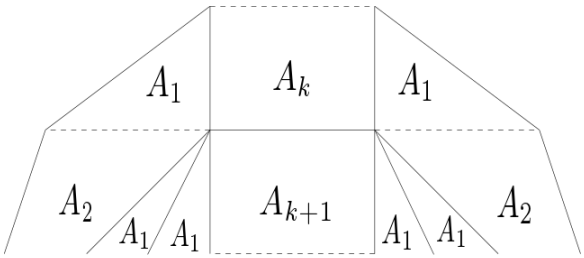

(b) p is odd

Figure 3.2: Constructing the graph with von Neumann neighborhood for $q = 5$ as an example.

must also include the polygon of the opposite direction, so we have A_1, A_2, ..., A_k, A_{k+1}, ..., A_{2k}, where $k = (p-1)/2$, A_1 and A_{2k} are triangles and the rest are quadrilaterals.

In the case that p is even, if we label each layer with a string, e.g. the first layer is $\overbrace{A_1 A_1 \dots A_1}^{q \text{ of } A_1}$, the next layer can be found by the substitution rules:

$$\begin{cases} A_1 \to A_2 \overbrace{A_1 \dots A_1}^{q-2} \\ A_2 \to A_3 \overbrace{A_1 \dots A_1}^{q-2} \\ \quad \vdots \\ A_{k-1} \to A_{k-2} \overbrace{A_1 \dots A_1}^{q-2} \\ A_k \to - A_1 \end{cases} \tag{3.7}$$

as shown in Fig 3.2a.Then we define the number of each pieces on layer n to be $a_{1,n}, a_{2,n}, \ldots, a_{k,n}$, the recurrence equations are

$$\begin{cases} a_{1,n+1} = (q-2)a_{1,n} + (q-2)a_{2,n} + \cdots + (q-2)a_{k-1,n} - a_k \\ a_{2,n+1} = a_{1,n} \\ a_{3,n+1} = a_{2,n} \\ \quad\vdots \\ a_{k-1,n+1} = a_{k-2,n} \\ a_{k,n+1} = a_{k-1,n} \end{cases} \tag{3.8}$$

solving these equations for the base c gives

$$c^k - (q-2)c^{k-1} - (q-2)c^{k-2} - \cdots - (q-2)c + 1 = 0 \tag{3.9}$$

We may re-arrange the equation to be $(c-(q-1))(c^{k-1}+c^{k-2}+\cdots+c+1)+q=0$ and notice that as $k \to +\infty$ the solution approaches $q-1$, which is expected since the graph becomes a regular tree of degree q asymptotically.

If p is odd, the construction goes similarly from A_1 to A_{2k} except for A_k where it becomes

$$A_k \to -A_1 A_{k+1} \overbrace{A_1 \ldots A_1}^{q-3} \tag{3.10}$$

since it is the end of the first face and is the neighbor of the next face as shown in Fig 3.2b, which means that the coefficient of $a_{k,n}$ in the recurrence equation for $a_{1,n+1}$ is $q-4$ instead of $q-2$. The equation for c becomes

$$c^{2k} - (q-2)c^{2k-1} - (q-2)c^{2k-2} - \cdots - (q-4)c^k - \cdots - (q-2)c + 1 = 0 \tag{3.11}$$

We see that the equations for c above are different from them of the Moore neighborhood construction, except for $p = 3$.

On an Euclidean plane, the tiling grows polynomially, so c must equal 1. Replacing c with 1 in either of the equations for p even or odd gives the same constraint $(p-2)(q-2) = 4$, which is also the same condition we found out for Moore neighborhood construction on Euclidean plane.

3.1.2 Compact tilings by group theory

A regular tiling can be constructed with *Wythoff construction*, which partition the polygons into *Schwarz triangles*. E.g. if we connect the vertices of a regular polygon of p edges to its center, we partition it into p isosceles triangles, and further we may partition it into $2p$ congruent right triangles. So start from a right triangle, we can construct the polygon by reflection and rotation. The rest of the polygons in the tiling can be constructed by rotation of the polygon with respect to the vertices. The infinite tiling can be constructed by identifying a right triangle with identity element e and all the other triangles are generated by rotation and reflection group operations in the *triangle group*.

To form a compact surface from an infinite tiling, we may pick a few pairs of elements and identify the two elements in each pair. To make sure the transformation is orientation-preserving, we may express the tiling with *von Dyck group* which is a subgroup of the triangle group. Hence the infinite $\{p, q\}$ tiling can be seen as the elements of the group $D(p, q, 2) = \langle a, b | a^p, b^q, (ab)^2 \rangle$, where a and b are group generators that act as a clockwise rotation with respect to the center of the polygon or to the vertex respectively, and the terms on the right hand side are relators that equal identity. By adding additional relators, we may find a finite *quotient group* which corresponds to a tiling on a closed surface. With this presentation, the faces, edges and vertices of the tiling correspond to the right cosets with respect to the subgroups $\langle a \rangle$, $\langle ab \rangle$ and $\langle b \rangle$, respectively. More details can be found in [39].

Similar to toric codes, the hyperbolic codes on such graphs have physical qubits placed on edges and logical operators on non-trivial cycles, so the code rate $R = \frac{k}{n}$ is

$$R = \frac{k}{n} = \frac{2g}{|E|} = \frac{2-\chi}{|E|} = \frac{2-|V|+|E|-|F|}{|E|} = 1 - \frac{2}{q} - \frac{2}{p} + \frac{2}{n} \tag{3.12}$$

where g is the genus, χ is the Euler characteristic. Since $1/p + 1/q < 1/2$ for hyperbolic codes, the code rate approaches a positive constant asymptotically with large n.

To find additional relators that gives a finite group, we repeated creating a pseudo random string of generators as the additional relator until a finite group is obtained. The

vertex-edge and face-edge incidence matrices are obtained from the coset tables. Namely, non-zero matrix elements are in positions where the corresponding pair of cosets share an element.

Another way to find an additional relator is by traversing every element in the graph and check if identifying it with identity results in a finite group. A traversal algorithm can be found readily with the "layer by layer" recurrent construction we described in the previous section. Either a breadth-first search or a deep-first search would work. The former is straight-forward, since we can construct the graph layer by layer, but each time we have to store the information of all the elements in one layer in memory. The latter is more space-efficient. Noticing that by removing certain types of edges (e.g., the edges connecting B and C type pieces and the left or right side edges that connect D and A type pieces in Fig. 3.3), it is easy to create a spanning tree of the tiling graph. The resulting tree is a *tree of finite cone type*, which retains the feature of recurrent construction [40]. Traversing every edge in the tree and traverse the elements that are incident to it, every element can be reached exactly once with this method.

Taking $\{5, 5\}$ tiling as an example, denoting the 4 pieces of face as A, B, C, D, the first layer is $AAAAA$, and each edge is between AA pieces. To find the next layers of edges in the spanning tree, take any edge and construct the next layer which is $BAAAB$, as Fig 3.3 shows on the top-left.

The other possibilities include $AB/BA, AC/CA, AD/DA$, which are also shown in Fig 3.3. So if we know the pieces of faces that is incident to the edge, we can construct the edges on the next layer. A depth-first search can be performed by recording the neighboring pieces of the edges from the root to the current location, and the ordinal number of each edge according to the vertex above it.

To traverse all the group elements on the graph up to a radius, we can do so by traversing all the edges. Each edge has 1 element on each side of it, as shown in Fig 3.4. We may choose one of them as the moving element (gray-filled triangles), and the other element

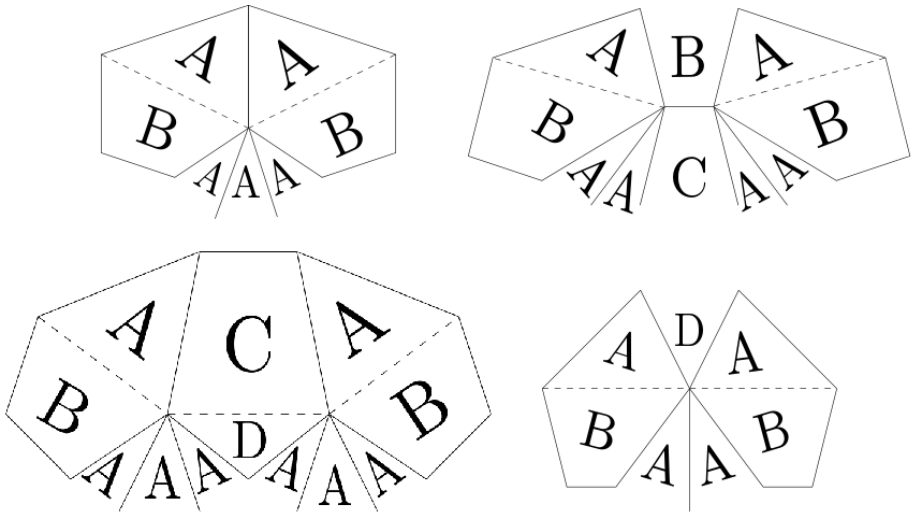

Figure 3.3: Constructing the next layer of the edges of a {5,5} tiling.

(blue-filled triangles) can be found by reflection operation. The change of the location of the element can be expressed by multiplication of the rotation operations a and b.

3.2 Ising models on hyperbolic tilings

In section 2.3 we discussed the mapping from maximum likelihood decoding of QECCs to random bond Ising models. Here we study the Ising models on the hyperbolic tiling graphs. We consider pairs of few-body Ising models where each spin enters a bounded number of interaction terms (bonds), such that each model can be obtained from the dual of the other after freezing k spins on large-degree sites. Such a pair of Ising models can be interpreted as a two-chain complex with k being the rank of the first homology group. Our focus is on the case where k is extensive, that is, scales linearly with the number of bonds n. Flipping any of these additional spins introduces a homologically non-trivial defect (generalized domain wall). In the presence of bond disorder, we prove the existence of a low-temperature weak-disorder region where additional summation over the defects have no effect on the free energy density $f(T)$ in the thermodynamical limit, and of a high-temperature region where in the ferromagnetic case an extensive homological defect does not affect $f(T)$. We also discuss

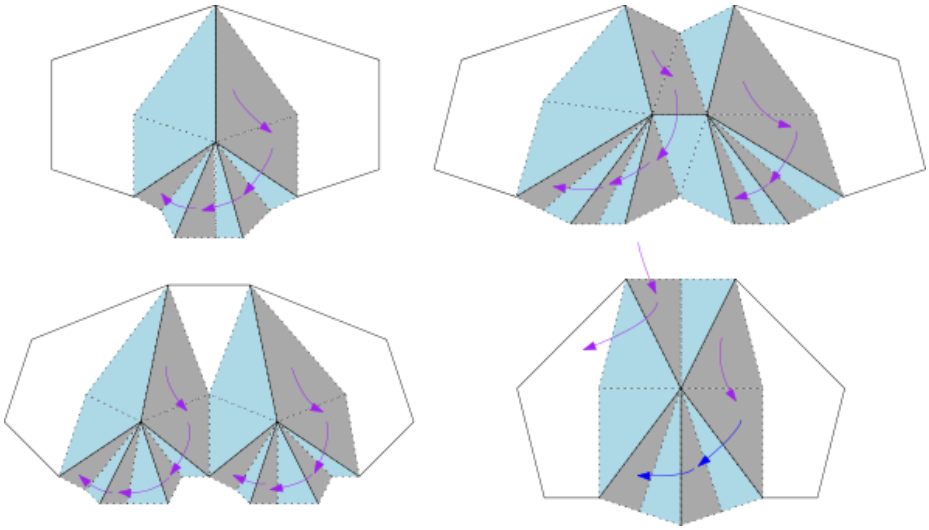

Figure 3.4: Traversing every element on the {5,5} tiling graph.

the convergence of the high- and low-temperature series for the free energy density, prove the analyticity of limiting $f(T)$ at high and low temperatures, and construct inequalities for the critical point(s) where analyticity is lost. As an application, we prove multiplicity of the conventionally defined critical points for Ising models on all $\{f, d\}$ tilings of the infinite hyperbolic plane, where $df/(d+f) > 2$. Namely, for these infinite graphs, we show that critical temperatures with free and wired boundary conditions differ, $T_c^{(\mathrm{f})} < T_c^{(\mathrm{w})}$. Most of the results in this subsection are summarized in Ref.[8].

3.2.1 Introduction

Singular behavior associated with a phase transition may emerge only in the thermodynamical limit, as the system size goes to infinity. One example are spin models on any finite-dimensional lattice, where both the interaction strength and its range are finite. Then the thermodynamical limit is well defined thanks to the fact that boundary contribution scales sublinearly with the system size[41]. Respectively, e.g., in the case of an Ising model, the same transition can be alternatively defined as the temperature where spontaneous magnetization appears, spin susceptibility diverges, spin correlations start to decay exponentially,

domain wall tension is lost, or as a singular point of the free energy[42, 43, 44, 41].

Situation is different if we have a model on a *non-amenable* graph characterized by a non-zero Cheeger constant, the lower bound on the perimeter to size ratio for all its finite subgraphs[45, 46]. Examples include infinite transitive expander graphs like a degree-regular tree, and regular $\{f, d\}$ tilings of the hyperbolic plane, with $(f-2)(d-2) > 2$. Physically, non-amenability of a graph implies that the boundary gives a finite contribution to any bulk average, so that both the location of a transition and its properties may depend on both the quantity being probed and the boundary conditions used to define the infinite-graph limit.

A number of general results are known that relate properties of a statistical-mechanical model to amenability/non-amenability of the underlying graph. In particular, for a random walk on a bounded-degree graph, the return probability decays exponentially with time iff the graph is non-amenable[47]. In the case of Bernoulli percolation, an infinite cluster is necessarily unique on amenable graphs, but it is conjectured that on any transitive non-amenable graph there is necessarily an interval where multiple infinite clusters coexist[48, 49, 50]. Among other cases, this conjecture has been verified for planar transitive graphs with bounded-degree duals[51]. In the case of the Ising model, there is never a phase transition with a finite coupling and a non-zero magnetic field on an amenable transitive graph, while such a transition necessarily exists on any bounded-degree non-amenable graph[52]. Further, phase transition points in Bernoulli percolation, Ising, and q-state Potts models (these have the Fortuin-Kasteleyn random cluster representation with parameter 1, 2, and q, respectively[53, 54]) are known to depend on the boundary conditions when the Cheeger constant is sufficiently large[55], and on planar non-amenable graphs with regular duals when q is large enough[56].

From physics perspective, non-amenable graphs are non-local, in the sense that they cannot be embedded in a Euclidean space without infinitely stretching some edges. Most natural geometry for such graphs is hyperbolic, with constant negative curvature. Interest in quantum field theory models on curved space-time is motivated by quantum

gravity and, in particular, the AdS/CFT correspondence[9, 10, 11, 12, 13, 14, 15]. There is an independent interest in models on curved spaces in statistical mechanics and condensed matter communities, e.g., since curvature can serve as an additional parameter to drive the criticality, or as a way to introduce geometrical frustration in toy models of amorphous solids, supercooled liquids, and metallic glasses[16, 17, 18, 19, 20, 21, 22, 23]. Models like percolation on more general expander graphs and various random graph ensembles are also common in network theory, e.g., such models occurred in relation to internet stability and spread of infectious diseases[24, 25, 26, 27, 28, 29, 30]. Finally, the strongest motivation to study non-local Ising models comes from their relation[6, 31, 32] to certain families of finite-rate quantum error-correcting codes (QECCs).

The Ref.[32] studied pairs of *weakly-dual* few-body Ising models where each spin enters a bounded number of interaction terms (bonds). Each model can be obtained from the exact dual of the other after freezing k spins which enter a large number of bonds. For the related QECC, k is the number of encoded qubits, and its ratio to the number of bonds, $R \equiv k/n$, is the code rate. One can also map such a pair of Ising models to a 2-chain complex Σ, in which case k is the rank of the first homology group $H_1(\Sigma)$. In particular, Ref. [32] introduced the *homological difference* $\Delta F \geq 0$, the difference of the free energies of two models with and without the additional summation over the homological defects, and gave the sufficient conditions for the existence of a low-temperature low-disorder region on the phase diagram where in the large-system limit $\Delta F = 0$.

In this Chapter we study duality and phase transitions in general Ising models, focusing on the case where the homology rank k scales linearly with the number of bonds n. Our main tool is the *specific homological difference* scaled by the number of bonds, $\Delta f = \Delta F/n$. Upon duality Δf is mapped to $R \ln 2 - \Delta f^*$, where Δf^* is the homological difference for the other model in the pair, at the dual temperature. Existence of a low-temperature *homological* region where asymptotically $\Delta f = 0$ implies that at high temperatures $\Delta f^* = R \ln 2$; with $R > 0$ this implies the existence of at least two distinct points where Δf is non-analytic as a function of temperature. Combining with the analysis of convergence of the

high-temperature series expansion for the free energy density, we obtain several bounds for critical temperatures associated with the non-analyticity of the limiting free energy densities of the two models. Main result is the inequality for the change of thus defined critical point due to summation over the homological defects.

Second, we discuss applications of these general results to two-body Ising models on transitive graphs, with the infinite graph G obtained as the weak limit of the sequence of finite transitive graphs. Finite rate R implies that the corresponding infinite graph has to be non-amenable. In particular, we prove multiplicity of the conventionally defined critical points for Ising models on all $\{f, d\}$ tilings of the hyperbolic plane with $df/(d+f) > 2$. That is, we show that transition temperatures with wired and free boundary conditions differ, $T_c^{(\mathrm{w})} > T_c^{(\mathrm{f})}$, which extends the results of Refs. [57, 55, 56].

The rest of this section is organized as follows. We introduce the notations and review some known facts from theory of general Ising models and theory of QECCs in Sec. 3.2.2. Our results are given in Sec. 3.2.3, where we first discuss properties of the homological difference Δf, analyze the convergence and analyticity of free energy density for a sequence of weakly-dual Ising model pairs, and finally apply the obtained results to Ising models on $\{f, d\}$ tilings of the hyperbolic plane, additionally illustrating the conclusions with numerical simulations. We summarize the results and list some related open questions in Sec. 3.2.4. Most of the proofs are given in the Appendices.

3.2.2 Notations and background

We consider general Ising models in Wegner's form[58], which describes joint probability distribution of $r \equiv |\mathcal{V}|$ Ising spin variables, $S_v \in \{-1, 1\}$, associated with elements of the vertex set, $\mathcal{V}$,

$$\mathrm{Prob}_{\mathbf{e}}[\{S\}; \Theta; K, h] = \frac{1}{Z} \prod_{b \in \mathcal{B}} e^{K(-1)^{e_b} R_b} \prod_{v \in \mathcal{V}} e^{h S_v}, \tag{3.13}$$

where each bond $R_b \equiv \prod_{v \in \mathcal{V}} S_v^{\Theta_{vb}}$, $b \in \mathcal{B}$, $|\mathcal{B}| = n$, is a product of the spin variables corresponding to non-zero positions in the corresponding column of the $r \times n$ binary coupling

matrix Θ, the binary "error" vector $\mathbf{e}$ with components e_b, $b \in \mathcal{B}$, describes quenched disorder, and the dimensionless coupling coefficients are $K \equiv \beta J$ and $h \equiv \beta h'$, where J is the Ising exchange constant, h' is the magnetic field, and $\beta \equiv 1/T$ the inverse temperature in energy units. The normalization constant $Z \equiv Z_{\mathbf{e}}(\Theta; K, h)$ in Eq. (3.13) is the *partition function*,

$$Z \equiv Z_{\mathbf{e}}(\Theta; K, h) \equiv \sum_{\{S_v = \pm 1\}} \prod_{b \in \mathcal{B}} e^{K(-1)^{e_b} R_b} \prod_{v \in \mathcal{V}} e^{h S_v}. \tag{3.14}$$

The partition function is commonly written in terms of the corresponding logarithm, the *free energy*, $F = -\ln Z$, or the free energy density (per bond), $f = F/n$.

The binary coupling matrix Θ in Eq. (3.13) can be interpreted geometrically in terms of a bipartite *Tanner* graph[59], or, equivalently, as the vertex-edge incidence matrix for a hypergraph $\mathcal{H} = (\mathcal{V}, \mathcal{B})$ with vertex set $\mathcal{V}$ and hyperedge (bond) set $\mathcal{B}$, with each hyperedge $b \in \mathcal{B}$ a non-empty subset of the vertex set, $b \subseteq \mathcal{V}$. In comparison, in a (simple undirected) graph $\mathcal{G} = (\mathcal{V}, \mathcal{E})$, each edge $b \in \mathcal{E}$ is an unordered pair of vertices, $b = \{i, j\} \subseteq \mathcal{V}$. The *degree* d_v of a vertex $v \in \mathcal{V}$ in a (hyper)graph is the number of edges that contain v, it is equal to the number of non-zero entries in the v th row of the vertex-edge incidence matrix Θ. Similarly, the size of an edge in a hypergraph is called its degree, $d_b = |b|$, $b \in \mathcal{B}$. In a graph, all edges are pairs of vertices, and all columns of the incidence matrix Θ have exactly two non-zero entries.

The probability distribution (3.13) can be characterized via the corresponding marginals, the spin correlations

$$\langle S_{\mathcal{A}} \rangle \equiv \sum_{\{S_v = \pm 1\}} S_{\mathcal{A}} \, \mathrm{Prob}_{\mathbf{e}}(\{S\}; \Theta; K, h), \tag{3.15}$$

where $\mathcal{A} \subseteq \mathcal{V}$ is a set of vertices, $S_{\mathcal{A}} = \prod_{v \in \mathcal{A}} S_v$; by convention, $S_\emptyset = 1$. At $h = 0$, on a finite system and with $\mathbf{e} = \mathbf{0}$, non-zero expectation is obtained for the sets (and only the sets) that can be constructed as products of bonds[58],

$$S_{\mathcal{A}} = \prod_{b : m_b \neq 0} R_b = \prod_v \prod_b S_v^{\Theta_{vb} m_b}, \tag{3.16}$$

where bonds in the product correspond to non-zero positions $m_b \neq 0$ in the binary vector $\mathbf{m} \in \mathbb{F}_2^n$ of *magnetic charges*. A number of *correlation inequalities* for spin averages have been constructed, see, e.g., Refs. [60, 61]. Particularly important for this work are Griffiths-Kelly-Sherman (GKS) inequalities[62, 63],

$$\langle S_{\mathcal{A}} \rangle \geq 0, \tag{3.17}$$

$$\langle S_{\mathcal{A}} S_{\mathcal{B}} \rangle \geq \langle S_{\mathcal{A}} \rangle \langle S_{\mathcal{B}} \rangle, \tag{3.18}$$

valid in the ferromagnetic case, $\mathbf{e} = \mathbf{0}$, for any $\mathcal{A}, \mathcal{B} \subseteq \mathcal{V}$.

The second GKS inequality (3.18) can also be written[62, 63] in terms of the derivative of $\langle S_{\mathcal{A}} \rangle$ with respect to $K_{\mathcal{B}}$, the coupling constant corresponding to the product of spins $S_{\mathcal{B}}$,

$$\frac{d\langle S_{\mathcal{A}} \rangle}{dK_{\mathcal{B}}} \geq 0. \tag{3.19}$$

This implies the monotonicity of any average with respect to all coupling constants and, as a consequence, the existence of two extremal Gibbs states describing (generally different) thermodynamical limit(s) for the Ising model on an infinite hypergraph $\mathcal{H} = (\mathcal{V}, \mathcal{B})$, with free and wired boundary conditions, respectively. Namely, one considers an increasing sequence $\mathcal{V}_t$, $t \in \mathbb{N}$, of sets of vertices, $\mathcal{V}_t \subsetneq \mathcal{V}_{t+1} \subset \mathcal{V}$ which converges weakly to $\mathcal{V} = \cup_{t \in \mathbb{N}} \mathcal{V}_t$, and the sequence of sub-hypergraphs $\mathcal{H}_t = (\mathcal{V}_t, \mathcal{B}_t)$ induced by the sets $\mathcal{V}_t$. For each $\mathcal{H}_t$, consider also the hypergraph $\mathcal{H}'_t = (\mathcal{V}'_t, \mathcal{B}'_t)$, obtained from $\mathcal{H}$ by contracting all vertices outside $\mathcal{V}_t$ into one. Denote the vertex-edge incidence matrices of $\mathcal{H}_t$ and $\mathcal{H}'_t$ as Θ_t^{f} and Θ_t^{w}, respectively. Here "f" and "w" stand for "free" and "wired" boundary conditions in the Ising models (3.13) defined with the help of these matrices. Clearly, $\mathcal{H}_t$ can be obtained from $\mathcal{H}_{t+1}$ by reducing some couplings to zero, while $\mathcal{H}'_t$ can be obtained from $\mathcal{H}'_{t+1}$ by increasing some couplings to infinity. This implies that for any set of vertices $\mathcal{A} \subset \mathcal{V}$, and t large enough so that $\mathcal{A} \subset \mathcal{V}_t$, the averages $\langle S_{\mathcal{A}} \rangle_t^{\mathrm{f}} \leq \langle S_{\mathcal{A}} \rangle_t^{\mathrm{w}}$ are, respectively, non-decreasing and non-increasing with t. They are also bounded, which proves the existence of the corresponding pointwise limits, $\langle S_{\mathcal{A}} \rangle^{\mathrm{f}} \leq \langle S_{\mathcal{A}} \rangle^{\mathrm{w}}$ at any K and h.

The two limits are known to coincide [41] for degree-limited graphs embeddable in D-dimensional space, e.g., the hypercubic lattice $\mathbb{Z}^D$. Indeed, the increasing sequence of subgraphs $\mathcal{G}_t = (\mathcal{V}_t, \mathcal{E}_t)$ can be chosen so that the boundary grows sublinearly with the total number of spins $|\mathcal{V}_t|$. Such a property is violated in the case of a non-amenable graph $\mathcal{G}$, which has a non-zero edge expansion (Cheeger) constant, $\iota_E(\mathcal{G}) > 0$, defined as

$$\iota_E(\mathcal{G}) \equiv \sup_{\mathcal{W}\subset\mathcal{V}:|\mathcal{W}|<\infty} \frac{|\partial_E \mathcal{W}|}{|\mathcal{W}|}, \tag{3.20}$$

where $\partial_E(\mathcal{W})$ is the set of edges connecting $\mathcal{W}$ with its complement, $\mathcal{V}\setminus\mathcal{W}$. The dependence of the critical temperatures (as seen by the magnetization) on the boundary conditions, $T_c^{\rm w} > T_c^{\rm f}$, where the superscripts stand for "wired" and "free" boundary conditions, respectively, is called the "multiplicity" of critical points[57, 55, 56]. Examples are the infinite d-regular trees $\mathcal{T}_d$ (in this case $T_c^{\rm f} = 0$, $T_c^{\rm w} = (d-1)^{-1}$, see, e.g., Ref. [45]), and the regular $\{f, d\}$ tilings $\mathbf{H}(f, d)$ of the infinite hyperbolic plane, $df/(f+d) > 2$, where in each vertex d regular f-gons meet. In the latter case multiplicity of the critical points have been demonstrated for self-dual graphs, $d = f$, and for graphs with large enough curvature [57, 55, 56]. In Sec. 3.2.3.3 we prove the multiplicity of critical points for all hyperbolic tilings $\mathbf{H}(f, d)$ with $df/(d+f) > 2$.

Another important result for the Ising model (3.13) is the duality transformation[64, 58]. In particular, in the absence of bond disorder, $\mathbf{e} = 0$, and at $h = 0$, one has

$$Z_{\mathbf{0}}(\Theta; K) = Z_{\mathbf{0}}(\Theta^*; K^*)\, 2^{r-n_g^*} (\sinh K \cosh K)^{n/2}, \tag{3.21}$$

where K^* is the Kramers-Wannier dual of K, namely $\tanh K^* = e^{-2K}$, the degeneracy $n_g^* = r^* - \operatorname{rank}\Theta^*$ ($2^{n_g^*}$ is the number of distinct ground-state spin configurations in the dual representation), and Θ^* is a binary $r^* \times n$ matrix exactly dual to Θ (binary rank is used),

$$\Theta^*\Theta^T = 0, \quad \operatorname{rank}\Theta + \operatorname{rank}\Theta^* = n. \tag{3.22}$$

Notice that in Eq. (3.21), and elsewhere in this work, we simplify the notations by suppressing the argument corresponding to a zero magnetic field, $h = 0$.

Exact duality also works in the presence of sign bond disorder, except the corresponding bonds ("electric charges") are mapped by duality to extra factors in front of the exponent, "magnetic charges". The resulting expression is not positive-definite and thus cannot be interpreted as a probability measure; instead it is proportional to the average of a product of the corresponding bonds. The duality in this case reads[58]

$$\frac{Z_{\mathbf{e}}(\Theta;K)}{Z_{\mathbf{0}}(\Theta;K)} = \left\langle \prod_{b\in\mathcal{B}} R_b^{e_b} \right\rangle_{\Theta^*;K^*}, \tag{3.23}$$

where the average on the right is computed in the dual model with all bonds ferromagnetic, cf. Eq. (3.16).

There is a natural notion of equivalence between defects $\mathbf{e}$ that produce identical averages in Eq. (3.23). For the electric charges in the l.h.s., equivalent are any two defects which differ by a linear combination of rows of Θ, $\mathbf{e} \simeq \mathbf{e}' = \mathbf{e} + \boldsymbol{\alpha}\Theta$, where $\boldsymbol{\alpha}$ is a length-r binary vector. Such defects are related by Nishimori's spin-glass *gauge symmetry*[36] generated by local spin flips $\alpha_v \in \mathbb{F}_2$, $v \in \mathcal{V}$, and simultaneous update of the components of $\mathbf{e}$ on the adjacent bonds,

$$S_v \to (-1)^{\alpha_v} S_v, \quad e_b \to e'_b \equiv e_b + \sum\nolimits_v \alpha_v \Theta_{vb}. \tag{3.24}$$

For such a defect $\mathbf{e}$, it is convenient to introduce an invariant distance $d_{\mathbf{e}}$, the minimum number of flipped bonds among all defects in the same equivalence class,

$$d_{\mathbf{e}} \equiv d_{\mathbf{e}}(\Theta) = \min_{\boldsymbol{\alpha}} \mathrm{wgt}(\mathbf{e} + \boldsymbol{\alpha}\Theta), \tag{3.25}$$

where $\mathrm{wgt}(\mathbf{e})$ is the Hamming weight. An identical equivalence relation for the magnetic charges which define the product of spins in the r.h.s. of Eq. (3.23) can be interpreted as a result of introducing a product of (dual) bonds that form a cycle, i.e., does not change the spins that actually enter the average.

For a finite system and a finite $K > 0$, both sides of Eq. (3.23) are strictly positive. The logarithm of the l.h.s. is proportional to the free energy increment due to the addition of the defect,

$$\delta_{\mathbf{e}} \equiv \delta_{\mathbf{e}}(\Theta;K) \equiv \ln Z_{\mathbf{0}}(\Theta;K) - \ln Z_{\mathbf{e}}(\Theta;K); \tag{3.26}$$

in turn, it is proportional to dimensionless defect tension

$$\tau_{\mathbf{e}} \equiv \tau_{\mathbf{e}}(\Theta; K) \equiv \delta_{\mathbf{e}}(\Theta; K)/d_{\mathbf{e}}. \tag{3.27}$$

Respectively, the scaling of the spin average in the r.h.s. of Eq. (3.23) with the minimum number of bonds in the product is called the *area-law* exponent,

$$\alpha_{\mathbf{e}} \equiv \alpha_{\mathbf{e}}(\Theta^*; K^*) = -d_{\mathbf{e}}^{-1} \ln \left\langle \prod_{b \in \mathcal{B}} R_b^{e_b} \right\rangle_{\Theta^*; K^*}. \tag{3.28}$$

Second GKS inequality (3.18) implies subadditivity,

$$d_{\mathbf{e}_1+\mathbf{e}_2} \alpha_{\mathbf{e}_1+\mathbf{e}_2} \leq d_{\mathbf{e}_1} \alpha_{\mathbf{e}_1} + d_{\mathbf{e}_2} \alpha_{\mathbf{e}_2}. \tag{3.29}$$

Thus electric-magnetic duality (3.23) also implies an exact relation between the defect tension and area-law exponent in a pair of dual models,

$$\tau_{\mathbf{e}}(\Theta; K) = \alpha_{\mathbf{e}}(\Theta^*; K^*). \tag{3.30}$$

Combined with Eq. (3.29), this implies subadditivity for defect free energy cost

$$\delta_{\mathbf{e}_1+\mathbf{e}_2} \leq \delta_{\mathbf{e}_1} + \delta_{\mathbf{e}_2}. \tag{3.31}$$

In the special case of a model with two-body couplings defined on a graph $\mathcal{G} = (\mathcal{V}, \mathcal{E})$, a correlation decay exponent can be defined in terms of pair correlations,

$$\alpha \equiv \alpha(\mathcal{G}; K) = \inf_{i,j \in \mathcal{V}} \left[-\frac{\ln \langle S_i S_j \rangle}{d_{ij}} \right], \tag{3.32}$$

where d_{ij} is the graph distance between i and j. Subadditivity (3.29) implies that the value of α corresponds to that for pairs with large d_{ij}, although the decay rate is not necessarily uniform for all pairs. In addition, on an infinite graph, we will also use

$$\bar{\alpha} \equiv \bar{\alpha}(\mathcal{G}; K) = \limsup_{d_{ij} \to \infty} \left[-\frac{\ln \langle S_i S_j \rangle}{d_{ij}} \right]. \tag{3.33}$$

The limit here exists since the expression in the square brackets is bounded by $|\ln \tanh K|$. In particular, finite magnetization on a transitive graph, $\langle S_i \rangle = m > 0$, implies by the

second GKS inequality (3.18), $\langle S_i S_j \rangle \geq m^2$, thus $\bar{\alpha} = 0$, which is a stronger statement than just $\alpha = 0$.

We are interested in the Ising models (3.13) with few-body couplings. More specifically, we consider *weight-limited* Ising models with vertex and bond degrees bounded by some fixed ℓ and m, respectively, so that $d_v \leq m$, $v \in \mathcal{V}$, and $d_b \leq \ell$, $b \in \mathcal{B}$. With fixed ℓ and m, we call such a model (ℓ, m)-sparse. This refers to the sparsity of the corresponding coupling matrix Θ: ℓ and m, respectively, are the maximum weights of a column and of a row of Θ.

Further, we would like to consider models whose duals are in the same class of weight-limited Ising models, with some maximum vertex, ℓ^*, and bond, m^*, degrees. However, such a condition would be very restrictive if one insists on the exact duality (3.22). For example, in the case of the square-lattice Ising model with periodic boundary conditions on an $L \times L$ square ($\ell = 2$ and $m = 4$), the dual model can be chosen to have the same vertex and bond degrees, $\ell^* = 2$ and $m^* = 4$, except for $k = 2$ additional summations over periodic/antiperiodic boundary conditions in each direction. These summations can be introduced as additional spins entering $d_v \geq L$ bonds, where the lower bound is the length of the shortest domain wall on the $L \times L$ square-lattice tiling of a torus. The two additional summations give no contribution to the asymptotic free energy density at $L \to \infty$, both in the low- and high-temperature phases, and are often ignored.

Such a *weak* duality with additional defects for models on locally planar graphs can be generalized by considering a pair of weight-limited binary matrices with n columns each, G and H, such that their rows be mutually orthogonal, $G H^T = 0$. Since we do not require exact duality (3.22), there are exactly

$$k \equiv n - \operatorname{rank} G - \operatorname{rank} H \tag{3.34}$$

distinct *defect* vectors $\mathbf{c}_i \in \mathbb{F}_2^n$, $i \in \{1, \ldots, k\}$, which are orthogonal to rows of H and whose non-trivial linear combinations are linearly-independent from rows of G.

Just as for the spin glasses on locally planar graphs, the matrix H can be used

to define *frustration*, $\mathbf{s} \equiv \mathbf{e}\, H^T$, a gauge-invariant characteristic of bond disorder. As common in spin-glass theory[36], we will consider independent identically-distributed (i.i.d.) components of the quenched disorder vector $\mathbf{e}$, such that $e_b = 1$ with probability p. The corresponding averages are denoted with square brackets, $[\,\cdot\,]_p$.

In theory of quantum error correcting codes[65, 66, 3, 67], a pair of binary matrices with orthogonal rows, $G\, H^T = 0$, can be used to define a Calderbank-Shor-Steane[4, 68] (CSS) stabilizer code $\mathcal{Q}(G, H)$ which encodes k qubits in n, see Eq. (3.34). Such a quantum code has a convenient representation in terms of *classical* binary codes. Given a matrix G with n columns, one defines the classical code $\mathcal{C}_G \subseteq \mathbb{F}_2^n$, a linear space of dimension $\operatorname{rank} G$ generated by the rows of G. One also defines the corresponding *dual* code $\mathcal{C}_G^\perp$ of all vectors in $\mathbb{F}_2^n$ orthogonal to rows of G; such a code is generated by the corresponding dual matrix (3.22), $\mathcal{C}_G^\perp \equiv \mathcal{C}_{G^*}$. By orthogonality, we necessarily have $\mathcal{C}_H \subseteq \mathcal{C}_G^\perp$ and $\mathcal{C}_G \subseteq \mathcal{C}_H^\perp$, where equality is achieved when the two matrices are exact dual of each other, in which case $k = 0$. The defect vectors $\mathbf{c}$ are non-zero CSS *codewords* of G type, $\mathbf{c} \in \mathcal{C}_H^\perp \setminus \mathcal{C}_G$; there are exactly $2^k - 1$ inequivalent (mutually *non-degenerate*[66]) vectors of this type. Similarly, there are also $2^k - 1$ inequivalent H-type vectors $\mathbf{b}$ in $\mathcal{C}_G^\perp \setminus \mathcal{C}_H$, where equivalence is defined in terms of rows of H, $\mathbf{b}' \simeq \mathbf{b}$ iff $\mathbf{b}' = \mathbf{b} + \alpha^T H$. For any quantum code, important parameters are its rate, $R \equiv k/n$, and the distance, $d \equiv \min(d_G, d_H)$,

$$d_G \equiv \min_{\mathbf{c} \in \mathcal{C}_H^\perp \setminus \mathcal{C}_G} \operatorname{wgt}(\mathbf{c}), \quad d_H \equiv \min_{\mathbf{b} \in \mathcal{C}_G^\perp \setminus \mathcal{C}_H} \operatorname{wgt}(\mathbf{b}). \tag{3.35}$$

As yet another interpretation of the algebraic structure in the pair of weakly-dual Ising models with vertex-bond incidence matrices G and H of dimensions $r \times n$ and $r' \times n$, respectively, consider a two-chain complex $\Sigma \equiv \Sigma(G, H)$,

$$\Sigma : \; C_2 \equiv \mathbb{F}_2^{r'} \xrightarrow{\partial_2} C_1 \equiv \mathbb{F}_2^{n} \xrightarrow{\partial_1} C_0 \equiv \mathbb{F}_2^{r}, \tag{3.36}$$

where the modules C_j, $j \in \{0, 1, 2\}$ are the linear spaces of binary vectors with dimensions r, n, and r', respectively, and the boundary operators ∂_1 and ∂_2 are two linear maps defined by the matrices G and H^T. The required composition property, $\partial_1 \circ \partial_2 = 0$, is guaranteed

by the orthogonality between the rows of G and H. The number of independent defect vectors (3.34) is exactly the rank of the first homology group $H_1(\Sigma)$.

3.2.3 Results

3.2.3.1 Properties of specific homological difference

We first quantify the effect of homological defects on the properties of general Ising models. To this end, given a pair of binary matrices G and H with n columns each and mutually orthogonal rows, $GH^T = 0$, consider the specific homological difference [32] (per bond),

$$\begin{aligned} \Delta f_{\mathbf{e}} &\equiv \Delta f_{\mathbf{e}}(G, H; K) \\ &= \frac{1}{n} \left\{ \ln Z_{\mathbf{e}}(H^*; K) - \ln Z_{\mathbf{e}}(G; K) \right\}, \end{aligned} \tag{3.37}$$

where, to fix the normalization, the dual matrix H^* [see Eq. (3.22)] is constructed from G by adding exactly k row vectors[1], linearly-independent inequivalent codewords $\mathbf{c} \in \mathcal{C}_H^{\perp} \setminus \mathcal{C}_G$. This quantity satisfies the inequalities[32]

$$\begin{aligned} 0 \leq \Delta f_{\mathbf{0}}(G, H; K) \leq \Delta f_{\mathbf{e}}(G, H; K), \\ \Delta f_{\mathbf{0}}(G, H; K) \leq R \ln 2, \end{aligned} \tag{3.38}$$

where $R \equiv k/n$, and k is the homology rank given by Eq. (3.34). The lower and the upper bounds are saturated, respectively, in the limits of zero and infinite temperatures. In addition, in the absence of disorder, the specific homological difference is a non-increasing function of K (and non-decreasing function of $T = J/K$),

$$\frac{d}{dK} \Delta f_{\mathbf{0}}(G, H; K) \leq 0. \tag{3.39}$$

Our starting point is the following Theorem (related to Theorem 2 in Ref. [32]), proved in Appendix A.1:

[1] Notice that any other construction of the dual matrix would at most change the partition function multiplicatively by a power of two.

Theorem 3.1 *Consider a sequence of pairs of weakly dual Ising models defined by pairs of finite binary matrices with mutually orthogonal rows, $G_t H_t^T = 0$, $t \in \mathbb{N}$, where row weights of each H_t do not exceed a fixed m. In addition, assume that the sequence of the CSS distances d_{G_t} is increasing. Then the sequence $\Delta f_t \equiv [\Delta f_{\mathbf{e}}(G_t, H_t; K)]_p$, $t \in \mathbb{N}$, converges to zero in the region*

$$(m-1)[e^{-2K}(1-p) + e^{2K}p] < 1. \tag{3.40}$$

REMARKS: 3.1-1. The bound in Theorem 3.1 guarantees the existence of a *homological* region where Δf_t converges to zero. Generally, such a region may be wider than what is granted by the sufficient condition (3.40). We will denote $K_h(G, H; p)$ the smallest $K > 0$ such that the series Δf_t converges to zero at any $K' > K$. The corresponding temperature, $T_h(G, H; p) \equiv J/K_h(G, H; p)$, is the upper boundary for the homological region at this p. Eq. (3.40) implies, in particular, that $K_h(G, H; 0) \geq \ln(m-1)/2$.

3.1-2. In the homological region, the sequence of the average free energy densities $[f_{\mathbf{e}}(G_t, K)]_p$ converges iff the sequence $[f_{\mathbf{e}}(H_t^*, K)]_p$ converges, and the corresponding limits coincide.

3.1-3. In analogy with Eq. (3.27), we introduce the defect tension in the presence of disorder,

$$\tau_{\mathbf{c},\mathbf{e}} \equiv \tau_{\mathbf{c},\mathbf{e}}(G; K) \equiv \frac{1}{d_{\mathbf{c}}} \left\{ F_{\mathbf{e}+\mathbf{c}}(G; K) - F_{\mathbf{e}}(G; K) \right\}, \tag{3.41}$$

where $d_{\mathbf{c}} \geq d_G$ is the minimum weight of the codeword equivalent to $\mathbf{c} \in \mathcal{C}_H^{\perp} \setminus \mathcal{C}_G$. While the tension (3.41) is not necessarily positive, it satisfies the inequalities

$$|\tau_{\mathbf{c},\mathbf{e}}| \leq \tau_{\mathbf{c},\mathbf{0}} \leq 2K. \tag{3.42}$$

We also define the weighted average defect tension,

$$\bar{\tau}_p \equiv \frac{\sum_{\mathbf{c} \neq \mathbf{0}} d_{\mathbf{c}} [\tau_{\mathbf{c},\mathbf{e}}]_p}{\sum_{\mathbf{c} \neq \mathbf{0}} d_{\mathbf{c}}}, \tag{3.43}$$

where the average is over disorder and the $2^k - 1$ non-trivial defect classes. This quantity satisfies the following bound in terms of the average homological difference,

$$\zeta\, \bar{\tau}_p \geq R \ln 2 - [\Delta f_{\mathbf{e}}]_p, \tag{3.44}$$

where the dimensionless constant $\zeta \leq 1/2$, see Eq. (A.3) in the Appendix. In the homological phase this gives $\bar{\tau}_p \geq 2R \ln 2$. (A related bound was previously obtained for the boundary of *decodable* phase in Ref. [31].)

In the absence of disorder, $\mathbf{e} = \mathbf{0}$, the specific homological difference is self-dual[32], up to an exchange of the matrices G and H, and an additive constant,

$$\Delta f_{\mathbf{0}}(G, H; K) = R \ln 2 - \Delta f_{\mathbf{0}}(H, G; K^*). \tag{3.45}$$

Comparing with the general inequalities (3.38), one sees that a point close to the lower bound is mapped to a point close to the corresponding upper bound. This implies a version of Theorem 3.1 applicable for high temperatures:

Theorem 3.2 *Consider a sequence of pairs of weakly dual Ising models defined by pairs of finite binary matrices with mutually orthogonal rows, $G_t H_t^T = 0$, $t \in \mathbb{N}$, where row weights of each G_t do not exceed a fixed m, CSS distances d_{H_t} are increasing with t, and the sequence of CSS rates $R_t \equiv k_t/n_t$ converges, $\lim_t R_t = R$. Then, for any $K \geq 0$ such that $(m-1)\tanh K < 1$, the sequence $\Delta f_t \equiv [\Delta f_{\mathbf{e}}(G_t, H_t; K)]_p$, $t \in \mathbb{N}$, converges to $R \ln 2$.*

Remarks: 3.2-1. Since duality is used in the proof, we had to switch the conditions on the matrices G_t and H_t. Similarly, the bound for $\tanh K$ is the Kramers-Wannier dual of that in Eq. (3.40) at $p = 0$.

3.2-2. We will call the temperature region where the sequence Δf_t in Theorem 3.2 converges to $R \ln 2$ the *dual homological* region. Given that the homological region in the absence of disorder extends throughout the interval $K \geq K_h(G, H)$, the corresponding interval for the dual homological region is $K \leq K_h^*(H, G)$, where K^* denotes the Kramers-Wannier dual, see Eq. (3.21). Respectively, $T_h^*(H, G) \equiv J/K_h^*(H, G)$ is the low temperature boundary of the dual homological region at $p = 0$.

3.2-3. In the dual homological region, the sequence of the free energy densities $f_{\mathbf{0}}(H_t^*, K)$ converges iff the sequence $f_{\mathbf{0}}(G_t, K)$ converges, and the corresponding limits $f_{H^*}(K)$ and $f_G(K)$ satisfy

$$f_G(K) = f_{H^*}(K) + R \ln 2. \tag{3.46}$$

Notice that when both sets of matrices H_t and G_t, $t \in \mathbb{N}$, have bounded row weights, the same sequence $\Delta f_{\mathbf{0}}(G_t, H_t; K)$ converges to zero in the homological region, $K \geq K_h(G, H)$, and to $R \ln 2$ in the dual homological region, $K \leq K_h^*(H, G)$. Since the magnitude of the derivative of the free energy density with respect to K (proportional to the energy per bond) is bounded, for any $R > 0$ this implies the existence of a minimum gap between the boundaries of the homological and the dual homological regions. We have the inequality

$$K_h(G, H) - K_h^*(H, G) \geq R \ln 2. \tag{3.47}$$

3.2.3.2 Free energy analyticity and convergence

The end points, $T_h(G, H)$ and $T_h^*(H, G)$ of the two flat regions in the temperature dependence of the homological difference $\Delta f_{\mathbf{0}}$ are clearly the points of singularity. What is the relation between these points and the singular points of the limiting free energy density in individual models, which are usually associated with phase transitions?

To establish such a relation, let us analyze the convergence of free energy density and the analyticity of the corresponding limit as a function of parameters. To this end, consider the high-temperature series (HTS) expansion of the free energy density (3.14),

$$f_{\mathbf{e}}(\Theta; K, h) \equiv \sum_{s=1}^{\infty} \kappa_{\mathbf{e}}^{(s)}(\Theta; J, h') \frac{\beta^s}{s!}, \tag{3.48}$$

where both parameters are scaled with the inverse temperature, $K \equiv \beta J$ and $h \equiv \beta h'$. The coefficient in front of β^s is proportional to an order-s cumulant of energy; it is a homogeneous polynomial of the variables h' and J of degree s. A general bound on high-order cumulants from Ref. [69] gives the following

Statement 3.3 *Consider any model in the form (3.13), with an (ℓ, m)-sparse $r \times n$ coupling matrix Θ. The coefficients of the HTS expansion of the free energy density satisfy*

$$|\kappa_{\mathbf{e}}^{(s)}(\Theta; J, h')| \leq 2^{s-1} s^{s-2} C (\Delta + 1)^{s-1} A^s, \tag{3.49}$$

where $A \equiv \max(|J|, |h'|)$ *and (**a**) with* J *and* h' *both non-zero,* $\Delta = \ell m$ *and* $C = r/n + 1$*, while (**b**) with* $h' = 0$*,* $\Delta = (\ell - 1)m$ *and* $C = 1$*.*

Such a bound implies the absolute convergence of the HTS in a finite circle in the complex plane of β and, thus, the analyticity of $f_{\mathbf{e}}(\Theta; K, h)$ and all of its derivatives as a function of both variables in a finite region with $|K|$ and $|h|$ small enough, in any finite (ℓ, m)-sparse Ising model, at any given configuration of flipped bonds $\mathbf{e}$. The same is true for the average free energy $[f_{\mathbf{e}}(\Theta; J, h')]_p$.

In this region, at $p = 0$, convergence and analyticity of the limiting free energy density for models defined by a sequence of binary matrices Θ_t, $t \in \mathbb{N}$, is equivalent to existence of the (pointwise) limit $\lim_t \kappa_{\mathbf{0}}^{(s)}(G_t; J, h')$ for the individual coefficients (remember, each of them is a homogeneous two-variate polynomial of degree s). With the help of the cluster theorem for the HTS coefficients, the existence of the limit can be guaranteed by the Benjamini-Schramm convergence[70] of the corresponding Tanner graphs, see Refs. [71, 72] for the corresponding discussion for general models with up to two-body couplings. For our present purposes, the following subsequence construction at $h = 0$ is sufficient:

Corollary 3.4 *Any infinite sequence of* (ℓ, m)*-sparse Ising models, specified in terms of the matrices* Θ_j*,* $j \in \mathbb{N}$*, has an infinite subsequence* $\Theta_{j(t)}$*,* $t \in \mathbb{N}$*, where* $j : \mathbb{N} \to \mathbb{N}$ *is strictly increasing, such that (**a**) for each* s*, the sequence of the coefficients* $\kappa_{\mathbf{0}}^{(s)}(\Theta_t; J, 0)$ *converges with* t*, and (**b**) the sequence of free energy densities* $f(\Theta_{j(t)}; K)$ *has a limit,* $\varphi_\Theta(K)$*, which is an analytic function of* K *in the interior of the circle* $|K| \leq \{2e\,[(\ell - 1)m + 1]\}^{-1}$*. Here* e *is the base of natural logarithm.*

Remarks: 3.4-1. Similar analyticity bounds apply to a very general class of (ℓ, m)-sparse models with up to ℓ-body interactions, where each variable is included in up to m interaction terms, and magnitudes of different interaction terms are uniformly bounded: the dependency graph used in the proof can be used in application to all such models. Examples include a variety of discrete models, e.g., Potts and clock models with few-body couplings, as well as compact continuous models with various symmetry groups, Abelian

and non-Abelian, where interaction terms are constructed as traces of products of unitary matrices. This is a generalization of the "right" convergence established for models with two-body couplings ($\ell = 2$) in Refs. [71, 72].

3.4-2. The subsequence construction is not necessary in the special case where the Tanner graphs defined by the bipartite matrices Θ_t are transitive, with weak infinite-graph limit Θ and a center $0 \in \mathcal{V}(\Theta)$, such that a ball of radius ρ_t in Θ_t is isomorphic to the ball of the same radius centered around 0 in Θ; here the sequence of the radii is increasing, $\rho_{t+1} > \rho_t$, $t \in \mathbb{N}$. In this case the cluster theorem[73] guarantees that the coefficients $\kappa_s(\Theta_t)$ do not depend on t for $\rho_t > s$.

To make precise statements applicable outside of the convergence radius of the high-temperature series, we need to ensure that a sequence of free energy densities converges. The question of convergence for a general sequence of Ising models being far outside the scope of this work, we will assume the use of yet another subsequence construction to guarantee the existence of the thermodynamical limit for the free energy density. This is based on the following Lemma proved in Appendix A.6.

Lemma 3.5 *Consider a sequence of $r_t \times n_t$ binary matrices Θ_t, where $0 < r_t \le n_t$, and $t \in \mathbb{N}$. For any $M > 0$, define a closed interval $I_M \equiv [0, M]$. (a) There exists a subsequence $\Theta_{t(i)}$, $i \in \mathbb{N}$, where the function $t : \mathbb{N} \to \mathbb{N}$ is strictly increasing, $t(i+1) > t(i)$ for all $i \in \mathbb{N}$, such that the sequence of Ising free energy densities converges for any $K \in I_M$, $f_i(K) \equiv f_{\mathbf{0}}(\Theta_{t(i)}; K) \to f(K)$. (b) The limit $f(K)$ is a continuous non-increasing concave function with left and right derivatives uniformly bounded,*

$$-1 \le f'_+(K) \le f'_-(K) \le 0, \tag{3.50}$$

for all $K \in I_M$.

Let us now assume that we have a sequence of pairs of weakly-dual weight-limited Ising models which (a) satisfy the conditions of Theorems 3.1 and 3.2 with the asymptotic rate R, (b) such that the coefficients of the corresponding HTSs converge, so that the sequences of free energy densities $f(G_t; K)$ and $f(H_t; K)$ both converge to analytic functions,

$\varphi_G(K)$ and $\varphi_H(K)$ respectively, at $|K|$ sufficiently small (Corollary 3.4), and, in addition, (c) the sequences of free energy densities both converge on an interval of real axis I_M, with $M > \ln(m-1)/2$.

The interval in (c) is such that Theorems 3.1 and 3.2 can be used to extend the convergence to the entire real axis; we denote the corresponding limits $f_G(K)$ and $f_H(K)$. The continuity of the functions $f_G(K)$ and $f_H(K)$ (and the corresponding duals), along with the inequality (3.39) which also survives the limit, guarantee that in the range of temperatures between the homological and the dual homological regions, $T_h(G,H) < T < T_h^*(H,G)$, the specific homological difference $\Delta f(K) \equiv f_G(K) - f_{H^*}(K)$ satisfies the strict inequality

$$0 < \Delta f(K) < R \ln 2. \tag{3.51}$$

Notice that the existence of the limit on the real axis does not guarantee analyticity which is only guaranteed by condition (b) in a finite vicinity of $K = 0$. Hereafter, we will assume that $f_G(K)$ is analytic on the interval $0 \le K < K_c(G)$. That is, for any $\epsilon > 0$, there exists a simply-connected open complex region $\Omega_\epsilon \in \mathbb{C}$ which includes the union of the circle of convergence of HTS for $\varphi_G(K)$ from Corollary 3.4 and the interval I_M, $M = K_c(G) - \epsilon$, such that the sum of HTS series $\varphi_G(K)$ can be analytically continued to Ω_ϵ, and the result coincides with the limit $f_G(K)$ on the real axis, $K \in I_M$. Further, we will assume that $K_c(G)$ is the largest value at which this is possible. Such a threshold may arise either (i) because $K_c(G)$ is a singular point of $\varphi_G(K)$, e.g., the intersection of the natural boundary of $\varphi_G(K)$ with the real axis, or (ii) the limit on the real axis, $f_G(K)$, starts to deviate from the result of the analytic continuation. In either case, this guarantees that the limit on the real axis, $f_G(K)$, has a singular point of some sort at $K_c(G)$.

According to this definition, $T_c(G) = J/K_c(G)$ is the highest-temperature point of non-analyticity of the limiting free energy density $f_G(K)$; $f_G(J/T)$ is analytic for $T > T_c(G)$. By duality and Theorem 3.1, $f_G(K)$ is also analytic at low temperatures. We denote $T_c'(G) \le T_c(G)$ the lowest-temperature singular point of $f_G(J/T)$.

We make similar assumptions about the properties of the limiting free energy density $f_H(K)$, and use similar definitions of the critical temperatures $T_c'(H) \leq T_c(H)$ for $f_H(J/T)$. We will also use the dual functions, $f_{G^*}(K)$ and $f_{H^*}(K)$, which coincide with $f_G(K^*)$ and $f_H(K^*)$ up to an addition of analytic functions of K, see Eq. (3.21). The corresponding lowest- and highest-temperature singular points are exchanged by duality, e.g., $T_c'(H^*) = T_c^*(H)$, $T_c'(H) = T_c^*(H^*)$. Convergence of $\Delta f(G_t, H_t; K)$ to zero implies that $f_G(K) = f_{H^*}(K)$ for $K > K_h(G, H)$, thus $f_G(K)$ is an analytic function in a complex vicinity of any $K > \max\left(K_c^*(H), K_h(G, H)\right)$. Equivalently,

$$T_c'(G) \geq \min\left(T_c^*(H) = T_c'(H^*), T_h(G, H)\right). \tag{3.52}$$

Once we are assured of convergence of the homological difference, the first observation is that the limit, $\Delta f(K)$, is necessarily a strictly convex function at $T_h(G, H)$, and a strictly concave function at $T_h^*(H, G)$, the singular points which are also the boundaries of the region separating the dual homological region at small K and the homological region at large K. On the other hand, both $f_G(K)$ and $f_{H^*}(K)$ are concave functions. Therefore, the convexity at $T_h(G, H)$ must originate from $f_{H^*}(G, H)$.

Unfortunately, this does not guarantee that $T_h(G, H)$ be a singular point of $f_{H^*}(K)$. A higher-order phase transition, with a continuous specific heat but discontinuity or divergence in its first or higher derivative, cannot be eliminated on the basis of the general thermodynamical considerations alone. Therefore, we formulate Theorem 3.6 below (proved in Appendix A.7) with a list of independently-sufficient conditions.

Theorem 3.6 *Let us assume that any one of the following Conditions is true:*

1. *The transition at $T_c'(G)$ is discontinuous or has a divergent specific heat;*
2. *The derivative of $\Delta f(K) = f_G(K) - f_{H^*}(K)$ is discontinuous at $K_h \equiv K_h(G, H)$, or the derivative of $\Delta f(K)$ is continuous at K_h, but its second derivative diverges at K_h;*
3. *Summation over homological defects does not increase the critical temperature, $T_c(G^*) \leq T_c(H)$.*

Then the Kramers-Wannier dual of the critical temperatures $T_c(H)$ satisfies

$$T_c^*(H) \leq T_h(G,H). \tag{3.53}$$

REMARKS: 3.6-1. We are making the same assumptions about the properties of $f_H(K)$, which gives $T_c^*(G) \leq T_h(H,G)$. Combining with Eq. (3.47), we have

$$K_c(H^*) - K_c(G) \geq R \ln 2. \tag{3.54}$$

This implies a strict inequality, $T_c(G) > T_c(H^*)$, when the homological rank scales extensively, $R > 0$, which is superficially similar to the multiplicity of critical points on nonamenable infinite graphs[57, 55, 56], see Sec. 3.2.2. The difference is that our critical temperatures correspond to points of non-analyticity of the limiting free energy density in zero magnetic field; we do not have a direct connection to magnetic transitions.

3.6-2. It is known that stabilizer codes with generators local in $\mathbb{Z}^D$ and divergent distances have asymptotically zero rates[74, 75]. This is perfectly consistent with the known fact that weight-limited models local in $\mathbb{Z}^D$ have well-defined thermodynamical limits, independent of the boundary conditions[41]. For example, inequality (3.54) with $R = 0$ is saturated in the case of planar self-dual Ising models, where the transition is in the self-duality point, which is the only non-analyticity point of the free energy density.

3.6-3. Most important application of Theorem 3.6 and Eq. (3.54) are few-body Ising models that correspond to finite-rate quantum LDPC codes with distances scaling as a power of the code length n, $d \geq An^\alpha$ with $A, \alpha > 0$. Examples are quantum hypergraph-product (QHP) and related codes[76, 77], and higher-dimensional hyperbolic codes[78]. Because of higher-order couplings, generic mean-field theory gives a discontinuous transition, which is the case of Condition 1 in Theorem 3.6. The discontinuous nature of the transition has been verified numerically for one class of QHP codes[32].

3.6-4. Ising models on expander graphs are known to have mean-field criticality[79, 55]. A combination of an analytic $f_{H^*}(K)$ and a finite specific heat jump in $f_G(K)$ at $K_h(G,H)$

is not eliminated by the Conditions 1 or 2. We discuss the important case of Ising models on hyperbolic graphs in the next subsection.

3.6-5. GKS inequalities imply that any spin average satisfies $\langle S_{\mathcal{A}} \rangle_{G;K} \geq \langle S_{\mathcal{A}} \rangle_{H^*;K}$. Physically, this ought to be sufficient to guarantee Condition 3, but we are not aware of a general proof.

3.2.3.3 Application to models on hyperbolic graphs

3.2.3.3.1 Bounds for infinite-graph transition temperatures

While the inequalities (3.47) are (3.54) are certainly important results, they address unconventionally defined critical points. Both the homological critical point, $T_h(G, H)$, and the end points of the interval of possible non-analyticity, $T_c'(G) \leq T_c(G)$, are defined for sequences of Ising models without boundaries. They are not immediately related to the critical temperatures $T_c^{\mathrm{f}} \leq T_c^{\mathrm{w}}$ defined on related infinite systems in terms of extremal Gibbs states with free/wired boundary conditions.

To bound these critical temperatures, consider a sequence of pairs of weakly dual Ising models which satisfy the conditions of Theorems 3.1 and 3.2 with the asymptotic rate $R > 0$, with an additional assumption that matrices G_t and H_t are incidence matrices of graphs, that is, they have uniform column weights $\ell = \ell^* = 2$. In addition we assume that the graph sequences converge weakly to a pair of infinite transitive graphs, which we denote $\mathcal{G} = (\mathcal{V}, \mathcal{E})$ and $\mathcal{H} = (\mathcal{F}, \mathcal{E})$, where $\mathcal{F}$ is the set of faces in $\mathcal{G}$. Weak convergence is defined as follows: for some chosen vertex $0 \in \mathcal{V}$, there is an increasing sequence $\rho_t \in \mathbb{N}$ such that a ball $\mathcal{B}(0, \rho_t) \subset \mathcal{G}$ of radius ρ_t centered at 0, is isomorphic to a ball in $\mathcal{G}_t$.

These conditions necessarily imply that matrices G_t and H_t describe mutually-dual locally-planar graphs, and also that the graphs $\mathcal{G}$ and $\mathcal{H}$ are mutually dual.

Examples of such a sequence are given by sequences of finite hyperbolic graphs constructed[80, 19] as finite quotients of the regular $\{f, d\}$ tilings of the infinite hyperbolic plane, $\mathbf{H}(f, d)$, with $df/(d + f) > 2$. A graph in such a sequence gives a tiling of certain

surface, with d regular f-gons meeting in each vertex. Hyperbolic graphs have been extensively discussed in relation to quantum error correcting codes[81, 82, 83, 84, 85, 86, 39]. Given such a finite locally-planar transitive graph with n edges, the quantum CSS code is a surface code[87, 6]; it is constructed from the vertex-edge and plaquette-edge incidence matrices, G and H respectively. Here H is also a vertex-edge incidence matrix of a dual graph, which corresponds to the dual tiling $\{d, f\}$ of the same surface. Such a code has the minimal distance scaling logarithmically with n, and it encodes $k = 2g = 2 + nR$ qubits into n, where g is the genus of the surface and $R = 1 - 2/d - 2/f$ is the asymptotic rate.

An extremal Gibbs ensemble on any infinite locally planar transitive graph can be characterized by the average magnetization m, the asymptotic correlation decay exponents α [Eq. (3.32)] and $\bar{\alpha} \geq \alpha$ [Eq. (3.33)], and similarly defined asymptotic domain wall tensions

$$\tau \equiv \tau(\mathcal{G}; K) = \inf_{\{i,j\} \subset \mathcal{F}} \tau_{\mathbf{e}(i,j)}, \quad \bar{\tau} \equiv \bar{\tau}(\mathcal{G}; K) = \limsup_{d_{ij} \to \infty} \tau_{\mathbf{e}(i,j)}, \tag{3.55}$$

where $\mathbf{e}(i, j)$ is a defect that connects a pair of frustrated plaquettes i and j. Generally, $\bar{\alpha} = \alpha = 0$ whenever spontaneous magnetization m is non-zero. A non-zero magnetization on a locally planar transitive graph also implies $\tau > 0$. [This is a generalization of the result from Ref. [44], see Appendix A.8.] Respectively, electro-magnetic duality (3.30) implies

Statement 3.7 *Let $\mathcal{G}$ and $\mathcal{H}$ be a pair of infinite mutually dual locally-planar transitive graphs. Denote $T_c^{\mathrm{f}}(\mathcal{G})$ and $T_c^{\mathrm{w}}(\mathcal{H})$ the critical temperatures of the extremal Gibbs ensembles for Ising models on $\mathcal{G}$ and $\mathcal{H}$ with free and wired boundary conditions, respectively. Then these temperature are Kramers-Wannier duals of each other,*

$$T_c^{\mathrm{f}}(\mathcal{G}) = [T_c^{\mathrm{w}}(\mathcal{H})]^*. \tag{3.56}$$

For each model, in the ordered phase, $T < T_c$, $\bar{\alpha} = 0$ and $\tau > 0$, while in the disordered phase, $T > T_c$, $\alpha > 0$ and $\bar{\tau} = 0$.

We can now prove the following:

Theorem 3.8 *For any regular $\{f,d\}$ tiling of an infinite hyperbolic plane, $fd/(f+d)>2$, the critical temperatures of the Ising model with free and wired boundary conditions, $T_c^{\rm f}=1/K_c^{\rm f}$ and $T_c^{\rm w}=1/K_c^{\rm w}$, satisfy*

$$K_c^{\rm f}-K_c^{\rm w}\geq R\ln 2,\quad R=1-2/f-2/d. \tag{3.57}$$

Proof. For any regular $\{f,d\}$ tiling $\mathcal{G}\equiv\mathbf{H}(f,d)$ of the hyperbolic plane, consider a sequence of finite mutually dual locally planar transitive graphs $\mathcal{G}_t$ and $\mathcal{H}_t$, where the sequence $\mathcal{G}_t$ weakly converges to $\mathcal{G}$. The corresponding sequence of incidence matrices satisfies the conditions of Theorems 3.1 and 3.2 with the asymptotic rate $R>0$. Transitivity implies that the free energy density converges in a finite circle around $K=0$, see Remark 3.4-2. While we are not sure of convergence for larger K, Lemma 3.5 guarantees the existence of a subsequence of graphs, and corresponding pairs of incidence matrices G_t, H_t, $t\in\mathbb{N}$, such that the sequences of free energy densities $f(G_t;K)$ and $f(H_t;K)$ converge. For such a sequence, the specific homological difference $\Delta f(G_t,H_t;K)$ also converges, which guarantees $\Delta f<R\ln 2$ outside of the dual homological phase, $K>K_h^*(H,G)$. Such an inequality implies the existence of an $\epsilon>0$ such that $\Delta f(G_t,H_t;K)<R\ln 2-\epsilon/2$ at all sufficiently large t. In turn, Eq. (3.44) implies that the average defect tension is bounded away from zero, $\bar\tau_0(G_t)\geq\epsilon$.

While defects that contribute to the average $\bar\tau_0(G_t)$ have large weights, we notice that the free energy increment (3.26) associated with an arbitrary defect is subadditive, see Eq. (3.31). Thus, a large-weight defect can be separated into smaller pieces; subadditivity (3.31) ensures that $\max(\tau_{\mathbf{e}_1},\tau_{\mathbf{e}_2})\geq\tau_{\mathbf{e}_1+\mathbf{e}_2}$ as long as $d_{\mathbf{e}_1+\mathbf{e}_2}=d_{\mathbf{e}_1}+d_{\mathbf{e}_2}$. Thus, if we start with a homological defect with the tension $\tau_{\mathbf{c}}\geq\epsilon>0$, at each division we can select a piece with the tension not smaller than ϵ. Moreover, since homological defects are cycles on the dual graph, we can first separate $\mathbf{c}$ into simple cycles of weight not smaller than the corresponding CSS distance which increases with t, and then cut such a cycle into pieces to obtain a defect compatible with the definition (3.55).

Further, GKS inequalities imply that tension $\tau_{\mathbf{e}}$ is monotonously non-decreasing

when individual bonds' coupling is increased. Thus, for the same defect $\mathbf{e} = \mathbf{e}(i,j)$ connecting frustrated plaquettes i and j on $\mathcal{G}_t$ and on the corresponding planar subgraph with wired boundary conditions, $\tau_{\mathbf{e}(i,j)}(G_t^{\rm w}; K) \geq \tau_{\mathbf{e}(i,j)}(G_t; K) \geq \epsilon$. Subadditivity construction in the previous paragraph guarantees the existence of such pairs for any t, and that pairs separated by arbitrarily large dual-graph distances d_{ij} can be chosen with t sufficiently large. Definition (3.55) then gives $\bar{\tau} \geq \epsilon > 0$ for the Ising model with wired boundary conditions on the infinite graph $\mathcal{G}$, at temperatures below the dual homological point, $K > K_h^*(H, G)$. Necessarily, $K_c^{\rm w}(\mathcal{G}) \leq K_h^*(H, G)$.

Duality (3.56) also ensures that $K_c^{\rm f}(\mathcal{H}) \geq K_h(G, H)$; inequality (3.47) gives Eq. (3.57). ■

REMARKS: 3.8-1. An interesting fact about systems with finite rates $R > 0$ is that electro-magnetic duality (3.30) does not guarantee that area-law exponent $\alpha_{\mathbf{m}}(G; K)$ be zero at low temperatures. While "area" is the defect distance $d_{\mathbf{m}}$, the smallest number of bonds in an equivalent defect, the "perimeter" is the number of spins involved in the product, the syndrome weight $\mathrm{wgt}\,\mathbf{s}$, where $\mathbf{s} = \mathbf{m}G^T$. Standard area/perimeter law argument assumes that perimeter can be parametrically smaller than the area; this is not necessarily true for systems with non-amenable Tanner graphs.

3.8-2. Even in the case of a pair of locally planar graphs, a linear domain wall $\mathbf{e}$ connecting a pair of frustrated plaquettes may have a large perimeter in the dual model, because of the additional spins corresponding to the homological defects. Any such defect that crosses the domain wall (changes the sign of the corresponding spin average) increases the perimeter in the dual model. Such additional defects are absent with free boundary conditions as considered in Theorem 3.8.

3.2.3.3.2 Numerical results

In addition to analytical bounds presented above, we also analyzed numerically Ising models on several finite transitive hyperbolic graphs constructed[80, 19] as finite quotients of the regular $\{5, 5\}$ tilings of the infinite hyperbolic plane. We used canonical ensemble simula-

tions with both local Metropolis updates[88] and Wolff cluster algorithm[89], to compute the average magnetization $m = \langle M \rangle / N$, susceptibility $\chi = (\langle M^2 \rangle - \langle M \rangle^2)/NT$, average energy per bond $\varepsilon \equiv \langle E \rangle / n$, specific heat $C = (\langle E^2 \rangle - \langle E \rangle^2)/nT^2$, and the fourth Binder cumulant[90] $U_4 = 1 - \langle S^4 \rangle / (3\langle S^2 \rangle^2)$. Here $M = |\sum_i S_i|$ is the (magnitude of the) total magnetization, $E = -\sum_{\langle ij \rangle} S_i S_j$ is the total energy, N and n respectively denote the number of spins and bonds, and $\langle \cdot \rangle$ denotes the ensemble average. For Metropolis simulations, each run consisted of 128 cooling-heating cycles, with 1024 full graph sweeps at each temperature, with additional averaging over 64 independent runs of the program. The number of sweeps at each temperature was sufficient to make any hysteresis unnoticeable. For Wolff algorithm simulations, each run consisted of 16 cooling-heating cycles, with 4096 cluster updates at each temperature, and additional averaging over 64 independent runs of the program. The resulting averages are shown in Figs. 3.5 to 3.8, where lines (dots) show the data obtained with cluster (local Metropolis) updates, respectively. The results obtained using the two methods are very close.

The parameters of the graphs used in the simulations are listed in Tab. 3.1. The first three graphs we obtained from N. P. Breuckmann[39]. We generated the remaining graphs with a custom `gap`[91] program, which constructs coset tables of freely presented groups obtained from the infinite von Dyck group $D(5,5,2) = \langle a, b | a^5, b^5, (ab)^2 \rangle$ [here a and b are group generators, while the remaining arguments are *relators* which corresponds to imposed conditions, $a^5 = b^5 = (ab)^2 = 1$] by adding one or more relator obtained as a pseudo random string of generators, until a finite group is obtained. Given such a finite group $\mathcal{D}$, the vertices, edges, and faces are enumerated by the right cosets with respect to the subgroups $\langle a \rangle$, $\langle ab \rangle$, and $\langle b \rangle$, respectively. The vertex-edge and face-edge incidence matrices G and H are obtained from the coset tables. Namely, non-zero matrix elements are in positions where the corresponding pair of cosets share an element. Finally, the distance d of the CSS code $\mathcal{Q}(G, H)$ was computed using the random window algorithm, which has

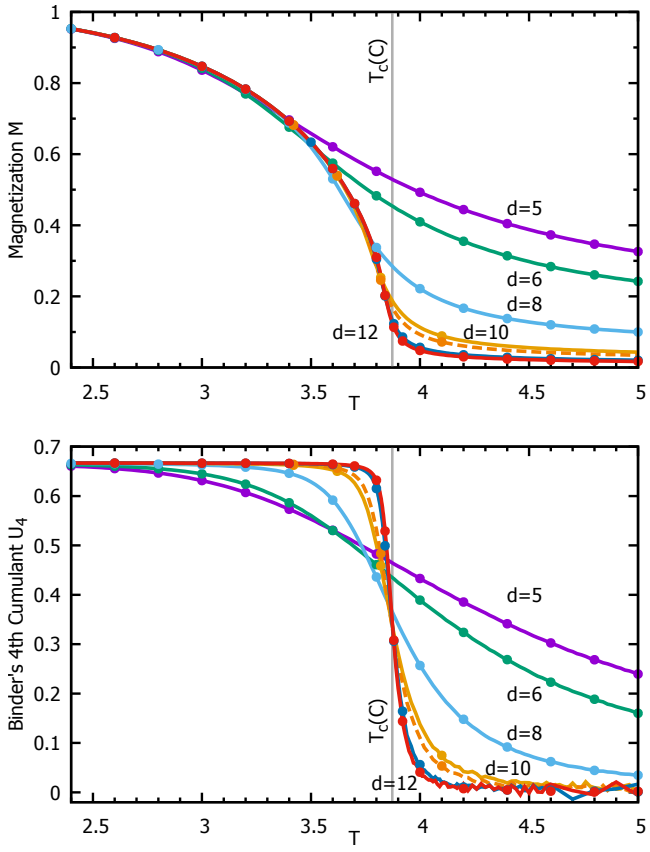

Figure 3.5: (Color online) Average magnetization (top) and Binder's fourth cumulant (bottom) as a function of temperature, for transitive graphs listed in Tab. 3.1 with minimal distances as indicated. Dashed lines show the data for the larger $d = 10$ graph. Lines show the data obtained using cluster updates; points show the data from simulations using local Metropolis updates. Vertical line shows the critical temperature $T_c(C)$ extrapolated from the positions of the specific heat maxima, see Fig. 3.9. While both sets of data do cross near $T_c(C)$, there is significant drift with increased graph size. In addition, the curves are near parallel which makes reliable extraction of the critical temperature difficult.

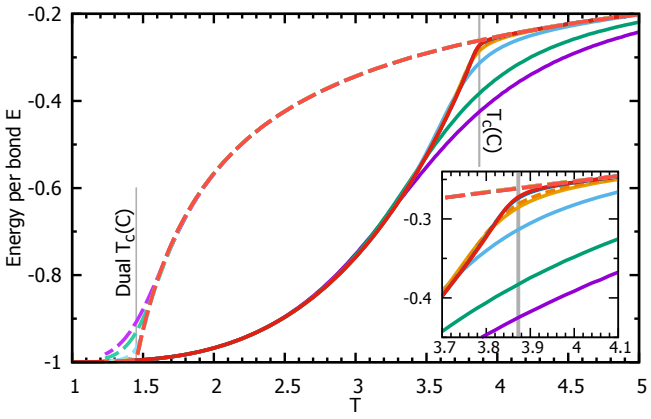

Figure 3.6: (Color online). Solid lines: energy per bond from Wolff cluster calculations as a function of temperature, as in Fig. 3.5. These data are converted with the help of the exact duality (3.21) to give energies in the dual model (long dashes). With increasing graph sizes, the difference between the original and dual energies decreases above the empirically found $T_c(C)$ (Fig. 3.9) and below the corresponding Kramers-Wannier dual, $T_c^*(C)$. Inset: close up of the plots near $T_c(C)$.

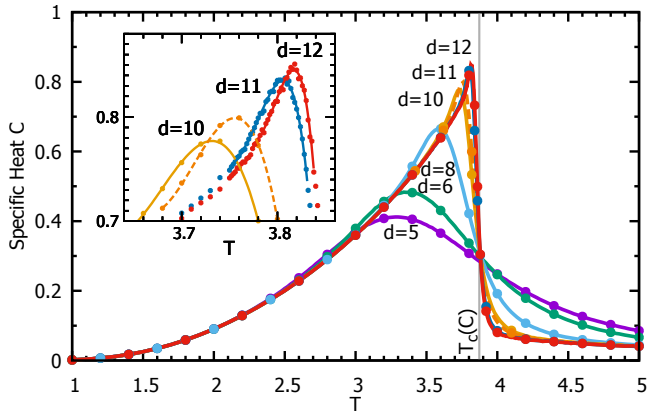

Figure 3.7: (Color online). As in Fig. 3.5 but for the specific heat. Inset: fitting for maxima. Data points in the inset are from the Wolff cluster calculations, while the lines are obtained using non-linear fits with general quartic polynomials of the form $y = y_m + a_2(x - x_m)^2 + \ldots + a_4(x - x_m)^4$, which give the coordinates of the maximum (x_m, y_m) nearly independent from the rest of the coefficients.

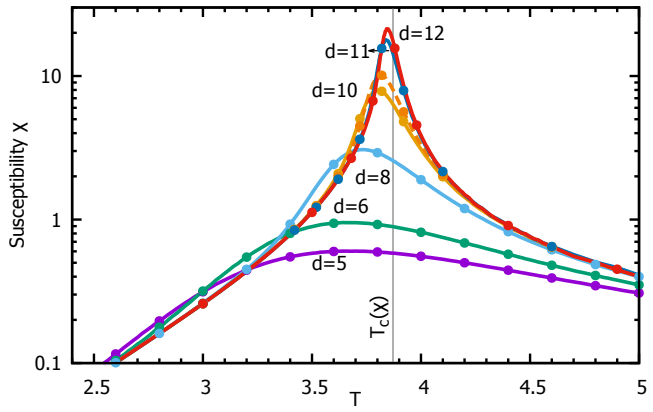

Figure 3.8: (Color online). As in Fig. 3.5 but for the susceptibility $\chi(T)$, plotted in semi logarithmic scale. The vertical line shows the critical temperature extrapolated from the susceptibility maxima, see Fig. 3.9.

the advantage of being extremely fast when distance is small[92, 93]. With the exception of the graph with $n = 7440$, the graphs used have the smallest size for the given distance.

vertices r	edges n	homology rank k	CSS distance d
32	80	18	5
60	150	32	6
360	900	182	8
1920	4800	962	10
2976	7440	1490	10
8640	21600	4322	11
12180	30450	6092	12

Table 3.1: Parameters of the graphs used in the simulations.

The obtained plots of magnetization and Binder's fourth cumulant are shown in Fig. 3.5; the corresponding curves on largest graphs are nearly indistinguishable, consistent with convergence at large n. We note that the crossing point in the Binder's fourth cumulant show a significant drift with the system size, see lower plot on Fig. 3.5. This is not surprising, given that the original scaling analysis[90] only applies to locally flat systems, whereas the hyperbolic graphs have a uniform negative curvature. On both plots, the curves for larger system sizes are near parallel to each other, which makes the identification of the phase transition point from the corresponding crossing points difficult.

Fig. 3.6 shows energy per bond as a function of temperature. To illustrate the properties of the specific homological difference, see Theorems 3.1 and 3.2, we also plot the energy per bond of the exact dual models obtained from the same data using $\varepsilon^*(K^*) = -\sinh(2K)\,\varepsilon(K) - \cosh(2K)$, derived from Eq. (3.21). The plot shows that as the size of the graph increases, the difference between the energies $\varepsilon^*(T)$ and $\varepsilon(T)$ decreases with increasing graph size both above $T_c(C)$ and below the corresponding Kramers-Wannier dual, $T_c^*(C)$, while a finite difference remains for the intermediate temperatures. This is consistent with the identification $T_h^* = T_c(C)$. The area between the 2 curves converges to $\ln 2/5$ asymptotically, which supports the result in Theorem 2.

The plots for specific heat $C(T)$ (Fig. 3.7) and magnetic susceptibility $\chi(T)$ (Fig. 3.8) show well developed maxima which become sharper and higher with increasing system sises. Notice that a unique point of divergence of the specific heat necessarily coincides with the dual homological temperature T_h^*.

We obtained the positions of the specific heat and magnetic susceptibility maxima by fitting the data in the vicinity of the corresponding maxima with quartic polynomials as explained in the caption of Fig. 3.7. The resulting positions of the maxima are plotted in Fig. 3.9 as a function of $x = 1/n^{1/2}$. The error bars of the positions of the maxima have errors in the third digit; the observed minor scattering of the data is a feature of the corresponding graphs.

While the size dependence is not monotonic in the case of susceptibility maxima, the data points for larger graphs show approximately linear dependence on x. Linear extrapolation to infinite size ($x = 0$) gives $T_c \approx 3.872 \pm 0.003$ for both sets of data. This value is consistent with the lower bound (3.54) for the infinite graph with wired boundary conditions, which gives in the present case $T_c \geq 2.668$. In comparison, the transition for a square-lattice Ising model is in the self-dual point, $T_{\text{s.d.}} = 2/\ln(1+\sqrt{2}) \approx 2.269$.

We note that even though we expect Ising model on hyperbolic graphs to have mean field criticality, conventional finite size scaling theory does not apply here. In partic-

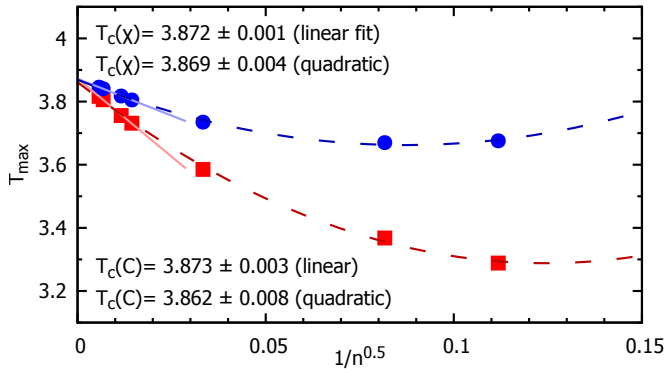

Figure 3.9: (Color online). Extrapolation of the specific heat and susceptibility maxima to infinite system size. Red squares (blue circles) show the positions of the specific heat (susceptibility) maxima extracted from the data on Figs. 3.7 and 3.8, respectively for graphs of different size, plotted as a function of $1/n^{1/2}$, where n is the number of edges in the corresponding graphs, see Tab. 3.1. Solid (dashed) lines are obtained as linear (quadratic) fits to the data, where only the four leftmost points were used for the linear fits. This results in the extrapolated critical temperature values as indicated.

ular, this is seen from the absence of the well defined crossing point in the data for Binder's fourth cumulant, see the lower plot on Fig. 3.5. Therefore, we had to experiment on how to extrapolate the positions of the maxima to estimate the critical temperature. The scaling with $x = 1/n^{1/2}$ was chosen since it gives near identical estimates for the critical temperatures from the maxima of $C(T)$ and $\chi(T)$, cut off at different maximum sizes (we tried $d_{\max} = 8$ and above).

This kind of scaling of the critical region size with the system size n can be obtained from the mean-field critical exponent for the correlation length $\nu_{\mathrm{MF}} = 1/2$ and the value of the critical dimension $D_{\mathrm{c}} = 4$. Namely, in dimension $D > D_{\mathrm{c}}$, above the critical dimension, the system size L no longer serves as the cut-off parameter; it is replaced with the system volume n. With the crossover at the critical dimension, we write $n^{1/D_{\mathrm{c}}} \sim L \sim \Delta T^{-\nu}$, which gives for the width of the critical region $\Delta T \sim n^{1/(D_{\mathrm{c}}\nu_{\mathrm{MF}})}$, with the exponent $1/(D_{\mathrm{c}}\nu_{\mathrm{MF}}) = 1/2$. In the case of percolation where the critical dimension is six, the same argument gives the exponent of $1/3$, which recovers the correct scaling for percolation on large random graphs and transitive hyperbolic graphs[94, 95, 96, 97].

We also note that the data shows good convergence with increased system size, without the need for the subsequence construction described in Sec. 3.2.3.2.

3.2.4 Discussion

3.2.4.1 Summary of the results

We considered pairs of weakly dual Ising models with few-body couplings, defined via sequences of degree-limited bipartite coupling graphs, with the focus on the case where the rank k of the first homology group of the corresponding two-chain complex scales extensively with the system size. This construction is needed to avoid introducing the boundaries, which are known to affect the position of the critical point in non-amenable graphs, and also to connect to applications, e.g., in quantum information theory, where results for large but finite systems are of interest. Here, extensive scaling of k corresponds to quantum error correcting codes with finite rates $R > 0$. Important examples include two-body Ising models on families of finite transitive hyperbolic graphs which weakly converge to regular $\{f, d\}$-tilings of the hyperbolic plane with $df/(d+f) > 2$; the corresponding limiting rates $R = 1 - 2/d - 2/f$ are non-zero.

Our main technical result is Theorem 3.1, which guarantees the existence of a low-temperature, low-disorder region where homological defects are frozen out—in the thermodynamical limit they have no effect on the free energy density. Duality guarantees the existence of a high-temperature phase where extensive homological defects have near zero free energy cost, see Theorem 3.2. At all temperatures below this phase, the average defect tension is non-zero, see Eq. (3.44).

With the help of duality and a known bound on high-order cumulants, we established the absolute convergence of both the high- and low-temperature series expansions of the free energy density in finite regions which include vicinities of the real temperature axis around the zero and infinite temperatures, respectively. We used a subsequence construction to ensure the convergence of free energy density at all temperatures, and defined the

critical temperatures as the real-axis points of non-analyticity of the limiting free energy density. For these critical temperatures, we derived several inequalities, in particular, an analog of multiplicity of the critical points, which guarantees that with $R > 0$, critical point of the free energy density is affected by the summation over the topological defects.

As an application of obtained bounds, we proved the multiplicity of phase transitions on all regular tilings $\mathbf{H}(f, d)$ of the infinite hyperbolic plane, $df/(d + f) > 2$.

We also simulated the phase transition on a sequence of self-dual $\{5, 5\}$ transitive hyperbolic graphs without boundaries, with up to $n_{\max} = 30450$ bonds numerically. Our data shows good convergence with increasing system sizes, with a single specific heat maximum which sharpens with the increasing system size. If the corresponding position $T_c(C) \approx 3.872 \pm 0.003$ is the only singularity of the free energy, then necessarily it coincides with the dual homological point, $T_h^* = T_c(C)$.

3.2.4.2 Open questions

1. The rightmost point of the homological region established in Theorem 3.1 on the p-T plane has the same value $p_{\max}$ as can be also obtained using the energy-based arguments[98], which apply at $T = 0$. Either of these results also implies[36, 31] that the portion of the Nishimori line at $p < p_{\max}$ is in the homological region. It should be possible to establish the existence of a homological region in the intermediate temperature points, but we could not find the corresponding arguments.

2. The proof of Statement 3.3 is based on overly generic bounds[69] for cumulants of a sum of random variables with a given dependency graph. In the case of the Ising model, it should be possible to construct a stronger lower bound for absolute convergence of the HTS. We expect that the same bound as in Theorem 3.2 should apply. Such a bound would be consistent with that from high-temperature series expansions for spin correlations[99], and it would also be consistent with the analysis of the higher-order derivatives of free energy[100], as well as the naive expectation that $T_c(G) = T_h^*(H, G)$.

3. In addition to the case in Remark 3.4-2, the infinite subsequence construction of Corollary

3.4 is also not needed when the sequence of Tanner graphs has a well defined distributional limit (Benjamini-Schramm or "left" convergence[70, 71, 72]). Important examples are given by the Tanner graphs of hypergraph-product and related codes[76, 77] based on specific families of sparse random matrices. For such sequences, it would be nice to establish the conditions for convergence of the free energy density or spin averages for all $K > 0$, to supercede the subsequence construction of Lemma 3.5.

3.3 Combinatorial solution for Ising models on hyperbolic plane

First introduced by Kac and Ward [101], the combinatorial method for solving Ising models on a planar graph is well known [102]. We generalized this method to RBIM on hyperbolic lattices with open boundary condition to find the partition functions and correlation functions.

Given a finite planar graph G with set of vertices $V(G)$ and edges $E(G)$, the partition function of a spin glass Ising model without external field on this graph is defined as

$$Z \equiv \sum_{\{S_v=\pm 1\}} \prod_{e\in E} e^{\beta J_e S_{e_1} S_{e_2}} \tag{3.58}$$

where β is the inverse temperature, e_1 and e_2 denote the two vertices of the edge e, J_e is -1 for flipped bonds and 1 for other bonds. The spin correlation of two spins A and B is defined as

$$\langle S_A S_B \rangle \equiv \frac{Z_{AB}}{Z} \tag{3.59}$$

where Z_{AB} is defined to be

$$Z_{AB} \equiv \sum_{\{S_v=\pm 1\}} S_A S_B \prod_{e\in E} e^{\beta J_e S_{e_1} S_{e_2}} \tag{3.60}$$

To calculate the partition function and the correlation function on the hyperbolic graphs, we start with finding the coordinates of the vertices on the Poincare disk model and

the direction of each oriented edge $e(u,v)$. Denote $o(e)=u$ and $t(e)=v$ to be the origin and the terminal vertex of e respectively. A $2|E|$ by $2|E|$ matrix T, where columns or rows correspond to oriented edges, is defined as

$$T(e,e')=\begin{cases}\tanh(\beta), & \text{case 1}\\ i\tanh(\beta), & \text{case 2}\\ -i\tanh(\beta), & \text{case 3}\\ 0, & \text{otherwise}\end{cases} \tag{3.61}$$

where in cases 1,2,3, they all require that $t(e)=o(e')$ and $e\neq\bar{e'}$, where $\bar{e'}$ is the reverse of e'. The differences are: Case 1: e and e' are on different sides of the horizontal line that passes through their common vertex, Case 2: e and e' are on the same side and it makes a counter-clockwise rotation, Case 3: e and e' are on the same side and it makes a clockwise rotation. They are illustrated in Fig. 3.10. In the case one of the edges or both of them are horizontal, we may assume that the horizontal line is rotated counter-clockwise by an infinitesimal angle, so that it belongs to one of the 3 cases.

Notice that this is different from the convention that the elements $T(e,e')=e^{\frac{i}{2}w(e,e')}\tanh(\beta)$, where $w(e,e')$ is the counterclockwise rotation angle between the two vectors [102]. But it retains the feature that any closed loop without self-intersection gives a product of -1, which is the reason this method works. In numeric calculations, as the number of edges in the loops becomes large, the errors in calculating the angles may accumulate, which may affect the accuracy of the result. Our convention has the advantage that there is no need to calculate the angles, which may help increasing the accuracy of the numerical calculation.

Define matrix

$$T_e\equiv I_eTI_e \tag{3.62}$$

where I_e is a diagonal matrix that has element i for the edges of both orientations that correspond to the flipped bonds ($J_e=-1$) and element 1 elsewhere on the diagonal.

Finally, the matrix K_e is defined as

$$K_e\equiv UJ(I-T_e) \tag{3.63}$$

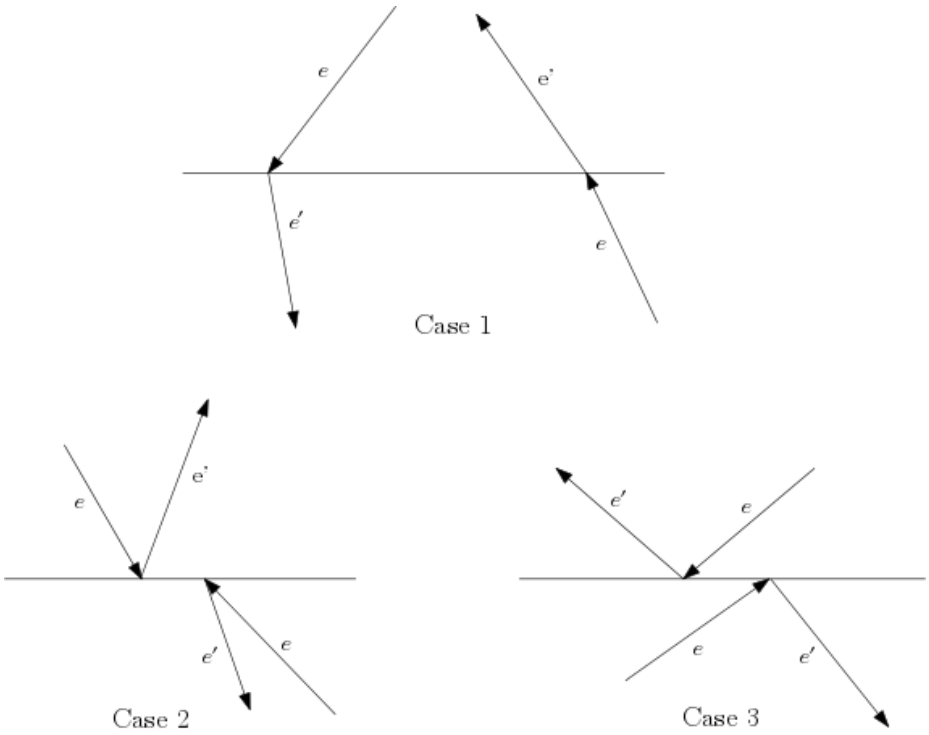

Figure 3.10: Different cases for the elements in the matrix T.

where I is the identity matrix, $J(e,e') = \delta(\bar{e},e')$, U is diagonal and $U(e,e) = -1$ if e has an angle $\in (0,\pi]$ with respect to horizontal $+x$ direction and 1 otherwise. It turns out that K_e is an anti-symmetric matrix, and the *Pfaffian* of K_e is related to the partition function as the following:

$$Z = (2^{|V|}\cosh^{|E|}(\beta))(\pm\mathrm{Pf}(K_e)) \tag{3.64}$$

where the sign before $\mathrm{Pf}(K_e)$ is chosen to guarantee that Z is positive.

To find the correlation function of two spins S_A and S_B, first we need to find a path connecting them, all paths are equivalent in the result. The correlation function is given by

$$\langle S_A S_B\rangle = (-1)^x \frac{\mathrm{Pf}(K_{em})}{\mathrm{Pf}(K_e)} \tag{3.65}$$

where $K_{em} \equiv UJ(I - T_{em})$, $T_{em} \equiv I_e I_m T I_m I_e$, I_m is a diagonal matrix depending on the path:

$$I_m(e,e) = \begin{cases} \tanh^{-1}\beta & \text{if } e \text{ or } \bar{e} \text{ is on the path} \\ 0 & \text{otherwise} \end{cases} \tag{3.66}$$

and x is the number of flipped bonds on that path.

It has been shown that the complexity of computing the Pfaffian of an $n\times n$ matrix scales with $n^3/3$ [103]. While the Monte Carlo simulations of RBIMs suffer from the rugged energy landscapes, where the configuration can be trapped in many local minima for a long time, the combinatorial solution is an alternative method which gives the free energy and correlation function directly.

In the case of hyperbolic lattices on a closed surface, this method requires summation over all the *spin structures* [102], which are the non-trivial cycles in this case. Since the spin structures grows exponentially with the size of the lattice, it is impractical to perform the calculation on large hyperbolic graphs, thus other approaches are needed.

Chapter 4

Qudit Quantum Error Correcting Codes and the Potts Model

4.1 Introduction

4.1.1 Classical q-ary code

A q-ary classical error correcting code $(n, \mathcal{K}, d)_q$ is a collection of $\mathcal{K}$ strings of length n, using an alphabet with q symbols. Each string (called a codeword) represents a different message. Any two different codewords must have at least d symbols different, where d is the distance of the code. Such a code can detect up to $d-1$ errors in any message, and correct up to $\lfloor (d-1)/2 \rfloor$ errors.

4.1.2 Linear codes over $\mathbb{F}_q$

In a linear code, a linear combination of any codewords is also a codeword. Such property requires that the alphabet forms an algebraic structure closed under addition and multiplication. When q is a power of a prime, the elements can form a *Galois field* $\mathbb{F}_q$, where there is an identity element "1" and each element a has a unique multiplicative inverse a^{-1} such that $a * a^{-1} = 1$. The vector space of a length-n linear code is a subset of $\mathbb{F}_q^n$. A *generator*

matrix G is a matrix whose rows are the basis of the code. The number of codewords that G can encode is q^k, where $k = \text{rank}(G)$. The distance of the code, d, is the minimum *Hamming weight* of the codewords. Such a code is called a $[n, k, d]_q$ linear code. A *parity check* matrix H is the exact dual of the generator matrix G,

$$GH^T = 0,\ \text{rank}(G) + \text{rank}(H) = n.$$

In the presence of errors, the received vector $\boldsymbol{x}$ may be different from its original value. By multiplying the check matrix, the result is called a *syndrome*, $\boldsymbol{s} = H\boldsymbol{x}^T$. A codeword or a non-detectable error will result in a zero syndrome, while other errors result in a non-zero syndrome.

4.1.3 Linear codes over $\mathbb{Z}_q$

For a composite q, here we consider codes over commutative ring $\mathbb{Z}_q$, where addition and multiplication are defined mod q. Such a code (denoted by $\mathcal{C}$) is a subset of $\mathbb{Z}_q^n$. The dimension of $\mathcal{C}$ is the number of rows in the minimal generating set forming the generator matrix G (the number of rows after removing the rows in G that can be written as linear combinations of the other rows, where the rows left are not necessarily linear independent). Then, any linear combination of rows of G is a codeword in $\mathcal{C}$. The distance of the code is the minimum weight of a non-zero codeword.

A check matrix H of a linear code C is a generator matrix of the dual code $C^\perp = \{x \in \mathbb{Z}_q^n \mid \langle x, c\rangle = 0\ \forall\ c \in C\}$, where $\langle , \rangle$ is the inner product of the two vectors in $\mathbb{Z}_q$.

4.1.4 Smith normal form

The *Smith normal form* of a matrix is a unique diagonal matrix which can be obtained by multiplying invertible matrices on the left and right of the original matrix [104]. In most cases the entries of the matrices are defined in a principal ideal domain (PID), but the concept can be generalized to any principal ideal ring (PIR) [105, Theorem 15.9]. For example, a code $\mathcal{C}$ over $\mathbb{Z}_q$ is a free module over a PIR, so the generator matrix G has a

Smith normal form $G = VDU$, where $\det V = \pm 1$ and $\det U = \pm 1$ and D has the form:

$$D = \left[\begin{array}{cccc|cc} d_1 & 0 & \dots & 0 & \dots & 0 \\ 0 & d_2 & \dots & 0 & \dots & 0 \\ \vdots & \vdots & \ddots & \vdots & \ddots & \vdots \\ 0 & 0 & \dots & d_k & \dots & 0 \\ 0 & 0 & \dots & 0 & \dots & 0 \\ \vdots & \vdots & \ddots & \vdots & \ddots & \vdots \\ 0 & 0 & \dots & 0 & \dots & 0 \end{array}\right]$$

where d_i are integers called the *invariants* and $0 < d_1 \leq d_2 \leq \cdots \leq d_k < q$, each d_i is a factor of d_{i+1}, and d_k divides q. The number of codewords $K = \frac{q}{d_1} \cdot \frac{q}{d_2} \cdot \cdots \cdot \frac{q}{d_k}$.

4.1.5 Dual matrix over $\mathbb{Z}_q$

The *dual matrix* $\tilde{G}$ of a matrix G is a matrix such that any vector $\boldsymbol{v}$ that satisfies $G\boldsymbol{v}^T = 0$ is a linear combination of the rows of $\tilde{G}$. If we write the generator matrix G in Smith normal form $G = VDU$, we find the dual of D to be

$$\tilde{D} = \left[\begin{array}{ccccccc|ccc} 0 & \dots & 0 & \frac{q}{d_{l+1}} & 0 & \dots & 0 & 0 & \dots & 0 \\ 0 & \dots & 0 & 0 & \frac{q}{d_{l+2}} & \dots & 0 & 0 & \dots & 0 \\ \vdots & & & & & \ddots & & & & \vdots \\ 0 & \dots & 0 & 0 & \dots & \dots & \frac{q}{d_k} & 0 & \dots & 0 \\ 0 & \dots & 0 & 0 & \dots & \dots & 0 & 1 & \dots & 0 \\ \vdots & & & & & & & & \ddots & \vdots \\ 0 & \dots & 0 & 0 & \dots & \dots & 0 & 0 & \dots & 1 \\ 0 & \dots & \dots & \dots & \dots & \dots & \dots & \dots & \dots & 0 \\ \vdots & & & & & & & & & \vdots \\ 0 & \dots & \dots & \dots & \dots & \dots & \dots & \dots & \dots & 0 \end{array}\right]$$

assuming $d_1, \dots, d_l = 1$ and $d_{l+1}, \dots, d_k \neq 1$.

Since $D\tilde{D}^T = 0$ and U is invertible, we find that the dual matrix of G has the form $\tilde{G} = M\tilde{D}(U^{-1})^T$, where M is an arbitrary matrix that is invertible over $\mathbb{Z}_q$.

4.1.6 q-ary LDPC codes

In classical binary error correcting codes, low-density parity-check (LDPC) codes are known for their reliability and high performance [106]. They are defined as to have a sparse check

matrix. A number of ensembles of random LDPC codes have been proposed [107], where the row weight and/or column weight are upper bounded. An (l, m)-regular LDPC code has a check matrix with column weight l and row weight m.

Similarly, a LDPC code can be defined over $\mathbb{Z}_q$. The code dimension depends on its Smith normal form. We performed numeric experiments of finding the Smith normal form of random (l, m)-regular matrices of dimension r by n, where $r/n < 1$. Numerical results show that with high likelihood their Smith normal form invariants are all 1 for a large n.

4.1.7 Distance distributions of q-ary LDPC codes

The following result on the code distance function $N(l)$ of an (n, j, k) ensemble of $(0, 1)$ check matrices over $\mathbb{Z}_q$ is given by Gallager:

Theorem 4.1 (Theorem 5.1 of Ref.[106]) *Define the ensemble of (n, j, k) codes as the ensemble resulting from random permutations of the columns of each of the bottom $j - 1$ submatrices of a (n, j, k) parity-check matrix with equal probability assigned to each permutation.*

For each code in an (n, j, k) ensemble with alphabet size q, the number $N_1(l)$ of sequences of weight l that satisfies any one of the j blocks of n/k checks is bounded by

$$N_1\left[\frac{n}{k}\mu_q'(s)\right] \leq \exp\frac{n}{k}[\mu_q(s) - s\mu_q'(s) + (k-1)\ln q]$$

where s is an arbitrary parameter and $\mu_q(s)$ is defined by

$$\mu_q(s) = \ln q^{-k}\left\{[1 + (q-1)e^s]^k + (q-1)(1-e^s)^k\right\}$$

$$\mu_q'(s) = \frac{d\mu_q(s)}{ds}$$

where an (n, j, k) parity-check matrix is a matrix of n columns that has j ones in each column, k ones in each row, and zeros elsewhere.

Following this result, it can be shown that the minimum distance typical of most codes in the ensemble increases linearly with n. See [106, p.51,17-18] for details.

For LDPC codes over $\mathbb{F}_q$, consider an ensemble of matrices in the following, which is the q-ary generalization of ensemble C in Ref [107],

Definition 4.2 *Ensemble: Matrix H is chosen with uniform probability from the ensemble of $m \times n$ $\mathbb{F}_q$-matrices with column Hamming weights equal l.*

Let $\Delta_n^{l,\alpha}$ stand for the ensemble of such matrices, where $\alpha \equiv m/n$, and let $\Delta_{n,\theta}^{l,\alpha}$ represent the ensemble of matrices that is orthogonal to a codeword of weight w, where $\theta \equiv w/n$. Let

$$p_{n,\theta}^{l,\alpha} \equiv \frac{|\Delta_{n,\theta}^{l,\alpha}|}{|\Delta_n^{l,\alpha}|}$$

Theorem 4.3 *The distance distribution of the ensemble of matrices (Definition 4.2) is given by*

$$\lim_{n\to\infty} \frac{1}{n} \ln p_{n,\theta}^{l,\alpha} = -\alpha \ln q + \max_{\eta \in [0, 1-\frac{1}{q}]} \left\{ \alpha H_q(\eta) \ln q + \theta l \ln \left(1 - \frac{q}{q-1}\eta \right) \right\}$$

and the maximum is at the only solution for η of

$$\left(1 - \frac{1}{q} - \eta\right) \left(\ln \frac{1-\eta}{\eta} + \ln(q-1) \right) = \frac{\theta l}{\alpha}$$

where $H_q(x)$ is the q-ary entropy function,

$$H_q(x) \equiv x \log_q(q-1) - x \log_q x - (1-x) \log_q (1-x).$$

The proof is given in Appendix B.1.

4.2 q-ary quantum codes and the Potts gauge glass model

4.2.1 Qudit and error correction

A qudit is an isolated quantum system that has q different states available, described as vectors in a q-dimensional Hilbert space $\mathbb{H}_q$. Denote the orthonormal basis states as $|0\rangle, |1\rangle, |2\rangle, \ldots$

$, |q-1\rangle$. The generalization of X and Z Pauli operators for such a system can be defined as:

$$Z|j\rangle = e^{i\frac{2\pi j}{q}}|j\rangle, X|j\rangle = |j+1 \pmod q\rangle, j = 0, 1, \ldots, q-1 \tag{4.1}$$

which are given the names "clock" and "shift" operators.

To simplify the notation, we will omit the "mod q" in the following, since all arithmetic on the quantum states or on the spin values of the corresponding statistical mechanical models are over $\mathbb{Z}_q$.

Qudits can be used as the basic unit of quantum computations just like qubits, except that they have q quantum states instead of 2.

Due to random noise and interactions with the environment, the quantum state of a single qudit may change randomly, and the information will be lost. Qudit error correction is to encode a small number of logical qudits into a large number of physical qudits, and to use quantum circuits to attempt to return the quantum state of the system, which went through a noisy channel, back to the original logical state, thus correcting the error. If the system is in a different logical quantum state afterwards, a logical error happens and the error correction fails.

4.2.2 Stabilizer codes and *CSS* codes on qudits

The space of n qudit quantum states is the product of their Hilbert spaces, $\mathbb{H}_q^{\otimes n}$. The n-qudit Pauli operators are tensor products of single-qudit clock Z_i and shift X_i operators in different powers, $i \in \{1, 2, \ldots, n\}$; they form an n-qudit Pauli group $\mathscr{P}_n$. Let V_s be a subspace of $\mathbb{H}_q^{\otimes n}$. If $\mathscr{P}$ is a subgroup of $\mathscr{P}_n$ such that every element of V_s is unchanged under the action of any element in $\mathscr{P}$, $\mathscr{P}$ is called a stabilizer of V_s.

In the stabilizer group, the operators must commute with each other so that the measurements don't change the state of codewords, which are the common eigenstates of all of the operators.

An error of stabilizer codes is a Pauli operator

$$E \equiv \omega^m X_1^{e_1} X_2^{e_2} \dots X_n^{e_n} Z_1^{e_{n+1}} \dots Z_{2n}^{e_{2n}}$$

where $\omega \equiv i\frac{2\pi}{q}$. It can be mapped to a length $2n$ vector $\boldsymbol{e} = (e_1, e_2 \dots e_{2n})$ up to a phase.

An error is detectable iff it anticommutes with any of the stabilizer generators. An error that is in the stabilizer group is not detectable and doesn't need to be corrected, since it doesn't change the logical quantum state. Errors that are different by a stabilizer operator are called *degenerate*, since they act identically on the code.

An operator that commutes with the stabilizer generators and changes the logical quantum state is a codeword, represented by a length $2n$ vector $\boldsymbol{c}$.

An n-qudit quantum stabilizer code $\mathcal{Q}\ ((n, \mathcal{K}, d))_q$ is a $\mathcal{K}$-dimensional subspace of $\mathbb{H}_q^{\otimes n}$, a common $+1$ eigenspace of all operators in the code's stabilizer, an Abelian group $\mathscr{S} \subset \mathscr{P}_n$ such that $\omega^j \notin \mathscr{S}$ for $j \in \{1, \dots, q-1\}$. When q is prime, it is an $[[n, k, d]]_q$ code where k is the number of logical qudits it encodes, $\mathcal{K} = q^k$. For general q,

$$\mathcal{K} = \frac{q^n}{|\mathscr{S}|} \tag{4.2}$$

where $|\mathscr{S}|$ is the size of the stabilizer group $\mathscr{S}$ [108].

The distance of the code, d, is the minimum of the weights of the undetectable errors outside of the stabilizer group. Any non-trivial error of weight up to $d-1$ can be detected, and those that have weights up to $\lfloor (d-1)/2 \rfloor$ can be corrected.

The generator matrix $\mathcal{G}$ consists of rows that correspond to stabilizer generators. For any operator on an n-qudit system $O(\boldsymbol{a}, \boldsymbol{b}) \equiv X_1^{a_1} X_2^{a_2} \dots X_n^{a_n} Z_1^{b_1} Z_2^{b_2} \dots Z_n^{b_n}$, we see that $O(\boldsymbol{a}, \boldsymbol{b}) O(\boldsymbol{c}, \boldsymbol{d}) = \omega^{\boldsymbol{b}\cdot\boldsymbol{c} - \boldsymbol{a}\cdot\boldsymbol{d}} O(\boldsymbol{c}, \boldsymbol{d}) O(\boldsymbol{a}, \boldsymbol{b})$. So two operators $O(\boldsymbol{a}, \boldsymbol{b})$ and $O(\boldsymbol{c}, \boldsymbol{d})$ commute iff $\boldsymbol{b}\cdot\boldsymbol{c} - \boldsymbol{a}\cdot\boldsymbol{d} = 0$. We may separate the parts of Pauli X and Z operators in $\mathcal{G}$ and write

$$\mathcal{G} = (\mathcal{G}_X, \mathcal{G}_Z)$$

where the commutativity condition requires that $\mathcal{G}_X \mathcal{G}_Z^T - \mathcal{G}_Z \mathcal{G}_X^T = 0$.

Degenerate errors are those that are different by a linear combination of rows of $\mathcal{G}$, $\boldsymbol{e}' = \boldsymbol{e} + \boldsymbol{\alpha}\mathcal{G}$, where $\boldsymbol{\alpha}$ is an arbitrary vector.

Vectors of codewords are those that satisfy the commutativity requirement with all the rows in the generator matrix, but cannot be written as a linear combination of rows of the generator matrix. Two codewords are equivalent if they differ by a linear combination of the rows of the generator matrix.

A subclass of the stabilizer codes, the qudit CSS codes, have the property that the stabilizer operators only contain powers of Pauli X operators or powers of Pauli Z operators, in which case we can treat X and Z errors separately. Thus in CSS codes, we use a length n vector to represent an error $\boldsymbol{e}$ or a codeword $\boldsymbol{c}$, and the generator matrix $\mathcal{G}$ has the form

$$\mathcal{G} = \mathrm{diag}(G_X, G_Z)$$

Since the stabilizer generators consist of only X or Z operators, the commutativity requirement can be simplified, namely, $O_X(\boldsymbol{a})$ and $O_Z(\boldsymbol{b})$ commute iff $\boldsymbol{a} \cdot \boldsymbol{b} = 0$. So the generator matrices satisfy $G_X G_Z^T = 0$.

In the following sections, we only consider CSS codes, so X errors and Z errors can be treated separately, and we use G to represent G_X or G_Z since they work in the same fashion. We specifically concentrate on the cases where matrices G_X and G_Z have all Smith normal form invariants equal to one. The advantage is that in this case the code contains an integer number k of logical qudits. Indeed, with all SNF invariants equal to one, the matrices G_X and G_Z have well defined ranks equal to the numbers of non-zero invariants. Denoting the ranks as r_X and r_Z, respectively, Eq.(4.2) gives $\mathcal{K} = q^{n-r_X-r_Z}$, thus $k = n - r_X - r_Z$.

4.2.3 Families of quantum LDPC codes over $\mathbb{Z}_q$

Quantum LDPC codes for qubits have also been studied extensively, since the low weight of the stabilizer generators are important for low complexity and high performance of quantum error correction [109]. Here we study q-ary generalizations of such codes. Some examples include:

- Quantum codes on a quotient of $G(4)$ graph, which is a square lattice on a plane with periodic boundary condition, known as the toric code [87]. The dimension of the code is $k = 2, n = L^2, d = L$, where L is the side length of the square lattice.

- Quantum codes on a quotient of $G(5)$ graph, which is a graph of pentagon tiling that has 5 pentagons around each vertex with proper boundary conditions. In general, we denote $G(m)$ as a regular graph of m-side polygon tiling that has m polygons around each vertex. For $m \geq 5$, the graph $G(m)$ is on a hyperbolic plane. Codes with dimension $k = (1 - 4/m)n + 2$ exist on such quotient graphs [81].

- Quantum hypergraph-product (QHP) codes [76], which is a *CSS* code generated by generator matrices $G_x = (I \otimes H_2, H_1 \otimes I)$ and $G_z = (H_1^T \otimes I, -I \otimes H_2^T)$, where H_1 and H_2 are sparse check matrices over $\mathbb{Z}_q$.

- Higher-dimensional quantum hypergraph-product codes [110], a generalization of the QHP codes and all families of toric codes on m-dimensional hypercubic lattices.

4.2.3.1 Qudit toric and surface code

Similar to the construction of binary toric code, we can construct a q-ary toric code. The qudits are placed on the edges, and the stabilizer operators are located on each vertex and plaquette,

$$A_v(a) = \prod_{i \in \{v+\}} X_i^a \prod_{i \in \{v-\}} X_i^{-a} \tag{4.3}$$

$$B_p(b) = \prod_{i \in \{p+\}} Z_i^b \prod_{i \in \{p-\}} Z_i^{-b} \tag{4.4}$$

for some non-zero a and b in $\mathbb{Z}_q$, where v runs through all vertices and p runs through all plaquettes, $\{v+\}$ includes the qudits to the right or up of vertex v, $\{v-\}$ includes those to the left or down of v; $\{p+\}$ includes the qudits to the right or below plaquette p, and $\{p-\}$ includes those to the left or above p.

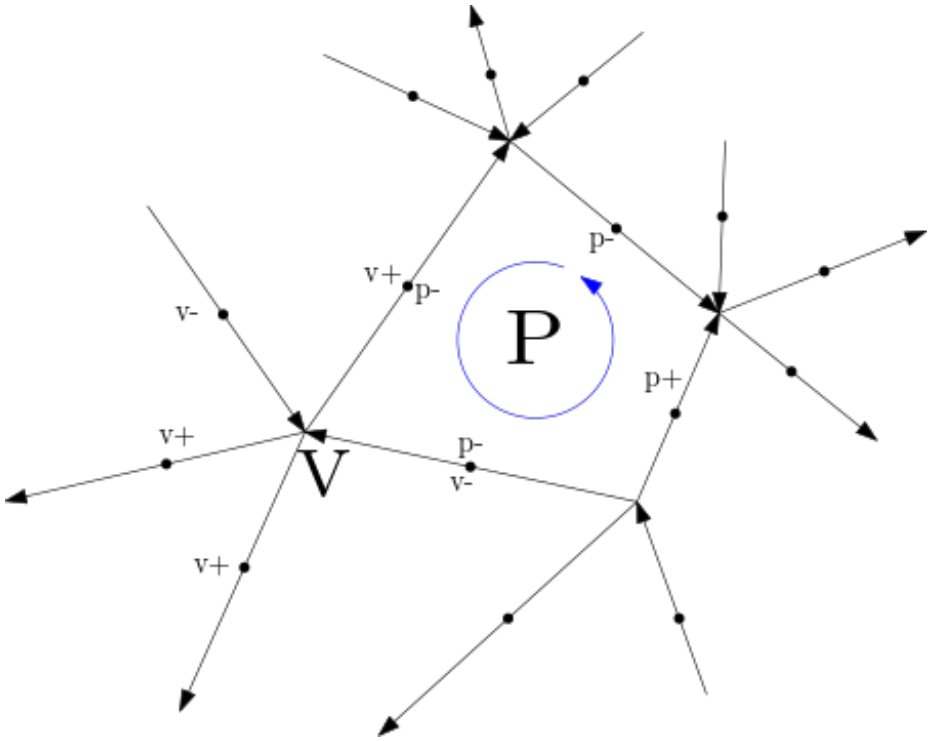

Figure 4.1: Example of surface code construction on any orientable surface.

This construction of stabilizer operators can be generalized to any graph on an orientable surface by assigning an arbitrary orientation on each edge, where $\{v+\}$ includes the subset of the neighboring qudits such that the direction of it in relative to v is parallel with the orientation of the edge, and $\{v-\}$ includes those that are anti-parallel; $\{p+\}$ includes the qudits that are on the edges whose orientation is parallel to the counter-clockwise direction in relative to p, and $\{p-\}$ includes those that are anti-parallel, as shown in Fig. 4.1. That is because any plaquette and any vertex have zero or two overlapping edges. If there are two, the direction relative to the plaquette and the direction relative to the vertex must be the same on one edge and different on the other. So on one edge, they are both parallel or anti-parallel to the orientation of the graph, while on the other edge, one is parallel and the other is anti-parallel. So that $\boldsymbol{a} \cdot \boldsymbol{b} = ab + (-ab) = 0$, A_v and B_p commute.

In the case q is prime, the dimension of a quantum code on such a graph is $k = 2g$, where g is the genus of the surface. The X and Z distances of the code are the minimum length of a non-trivial cycle on the graph and on the dual graph, respectively [111].

The same applies if we take the stabilizer group with all vertex and plaquette generators with $a = b = 1$. In this case it is easy to check that all non-zero Smith normal form invariants of the stabilizer generator matrices G_X and G_Z are equal to one, so that both the dimension k and the distances (d_X, d_Z) of the code over $\mathbb{Z}_q$ coincides with those of the conventionally defined qubit code.

4.2.3.2 Qudit hypergraph-product codes

In the binary case, a finite rate hypergraph-product code can be constructed with generator matrices $G_x = (I \otimes H_2, H_1 \otimes I)$ and $G_z = (H_1^T \otimes I, I \otimes H_2^T)$, where H_1 is an r_1 by n_1 binary matrix and H_2 is an r_2 by n_2 matrix. Denote the distances of the binary codes with parity check matrices H_1 and H_2 as d_1 and d_2, and of the binary codes with the same parity check matrices transposed as $\tilde{d_1}$ and $\tilde{d_2}$, respectively. The distance of this CSS code is bounded as following [76]:

- The upper bound of the distance of the code is $d \leq d_1$ when $k_2 \neq 0$ and $d \leq d_2$ when $k_1 \neq 0$; similarly, $d \leq \tilde{d_1}$ when $\tilde{k}_2 \neq 0$ and $d \leq \tilde{d_2}$ when $\tilde{k}_1 \neq 0$.
- The lower bound is $d \geq \min(d_1, d_2)$ and $d \geq \min(\tilde{d_1}, \tilde{d_2})$.
  When $H_2 = H_1^T$, this code has parameters $n = n_1^2 + (n_1 - k_1)^2$, $k = k_1^2$, $d = d_1$.

In the q-ary case, we can use a similar construction $G_x = (I \otimes H_2, H_1 \otimes I)$ and $G_z = (H_1^T \otimes I, -I \otimes H_2^T)$. We can prove the lower bound:

Theorem 4.4 *Given that the distances of the codes $C_{H_1}^{\perp}$ and $C_{H_2}^{\perp}$ are d_1 and d_2 respectively and the corresponding codes with transposed matrices are $\tilde{d_1}$ and $\tilde{d_2}$ respectively, the lower bound of the distance d of the code $\mathcal{C}$ is $d \geq \min(d_1, d_2)$ and $d \geq \min(\tilde{d_1}, \tilde{d_2})$.*

Moreover, as mentioned in Sec.4.1.6, sparse rectangular matrices with random 0,1 entries with high likelihood have all non-zero Smith normal form invariants equal to one. It is easy to check that the same will be true for the generators of the qudit hypergraph-product codes. In this case, also the upper bound on the distance can be proved. Details can be found in Appendix B.7. From above we can construct a code with parameters $n = n_1^2 + (n_1 - k_1)^2$, $k = k_1^2$, $d = d_1$. Since there exist classical LDPC codes with $k \propto n$ and $d \propto n$ (Theorem 4.1 and 4.3), we can construct a quantum code with dimension $k \propto n$ and distance $d \propto \sqrt{n}$.

4.2.3.3 Qudit higher-dimensional QHP codes

The QHP codes can be generalized to higher dimensions, which form a m dimensional *chain complex*, as shown in Ref. [110]. The distance of such a code has the following lower bound,

Theorem 4.5 (Theorem 1 from Ref. [110]) *Consider m-complex $\mathcal{A}$:*

$$\mathcal{A} : \{0\} \xleftarrow{\partial_0} \mathcal{A}_0 \xleftarrow{A_1} \mathcal{A}_1 \ldots \xleftarrow{A_m} \mathcal{A}_m \xleftarrow{\partial_{m+1}} \{0\},$$

and assume that homological groups $H_j(\mathcal{A})$ have distances d_j, $0 \le j \le m$. Given an $r \times c$ binary matrix P of rank u, construct matrices C_j with:

$$C_{j+1} = \left(\begin{array}{c|c} A_{j+1} \otimes E_r & (-1)^j E_{n_j} \otimes P \\ \hline & A_j \otimes E_c \end{array}\right)$$

Denote δ the minimum distance of a binary code with the parity check matrix P; by our convention, $\delta = \infty$ if $u = c$. The minimum distance $d'_j \equiv d_j(C)$ of the homology group $H(C_j, C_{j+1})$, $0 \le j \le m+1$, satisfies the following lower bounds:

1. *if $r > u$, $d'_j \ge \min(d_j, d_{j-1}\delta)$, otherwise,*
2. *if $r = u$, $d'_j \ge d_{j-1}\delta$.*

We formulate this theorem in application to chain complexes over $\mathbb{Z}_q$ without a proof. The proof for the binary case was given in Ref. [110], and in the case of $\mathbb{F}_q$, with q a power

of a prime in Ref. [112]. Again, most interesting case from the practical point of view corresponds to torsion-free complexes such that all matrices have Smith normal forms with non-zero invariants equal to one.

4.2.4 Distances verification complexity

The following result is an improvement of the results in Ref. [93].

Theorem 4.6 *A codeword of weight δn in any q-ary (l,m)-limited quantum or classical LDPC code can be found with complexity 2^{Fn}, where*

$$F = \delta \log_2(\gamma_m(m-1)),$$

$\gamma_m \in (1, \gamma_\infty)$ grows monotonically with m and is upper bounded as the following:
If all entries of the parity check matrix are coprime with q, γ_m is upper bounded by

$$\gamma_m \leq \min\left[\frac{q-2}{(m-1)((q-1)^{\frac{1}{m-1}}-1)}, \frac{1}{q^{\frac{1}{q-1}}-1}\right] \tag{4.5}$$

More generally, with some entries in the parity check matrix that are not coprime with q, γ_m is upper bounded by

$$\gamma_m \leq \frac{q-2}{(m-1)((3-\frac{4}{q})^{\frac{1}{m-1}}-1)}.$$

The upper bound of γ_m is improved from the value in the original paper for codes on $\mathbb{F}_q$, and an upper bound for $\mathbb{Z}_q$ is also given. Details can be found in Appendix B.5.

4.2.5 Minimum energy decoding on LDPC codes

Minimum energy decoding is to find the codeword correcting the most likely error for a given syndrome, ignoring any degenerate errors. This corresponds to maximum likelihood decoding at zero temperature ($\beta = +\infty$), where only the codewords that have minimum Hamming distance to the error are important. Without the summation of probabilities of all possible errors for each codeword, the minimum energy decoding is less complicated

than maximum likelihood decoding, but usually it has a lower error threshold since it is sub-optimal decoding.

For a regular quantum CSS LDPC code with row weight m, we discovered the lower bound of the decodable threshold of error probabilities on physical qudits as a function of q and m, based on *irreducible cluster* method [98]:

Theorem 4.7 *Any sequence of q-ary CSS codes whose distances scale with n at least logarithmically ($d \geq D \ln n$, $D > 0$) with generator weights not exceeding m_X, m_Z can be decoded with vanishing error probabilities if channel probabilities (p_X, p_Z) for independent X/Z errors satisfy*

$$\begin{aligned} (m_X - 1)\Upsilon_{CSS}(p_Z) &\leq e^{-1/D} \\ (m_Z - 1)\Upsilon_{CSS}(p_X) &\leq e^{-1/D} \end{aligned} \tag{4.6}$$

where $\Upsilon_{CSS}(p) \equiv \left(\sqrt{1-p} + \sqrt{p(q-1)}\right)^2 - 1$.

The proof is given in Appendix B.4.

Notice that $\Upsilon_{CSS}(p) \propto \sqrt{p}$, $\lim p \to 0$, so the inequality must have positive solutions, showing that there is a positive minimum energy decoding threshold for p.

As an example, for the $\{5,5\}$ hyperbolic quotient graphs listed in Table 3.1, a linear fit of d vs $\ln n$ shows that $d = 0.854 \ln n$. Eq. (4.6) gives the minimum energy decoding threshold

$$p_{\mathrm{ME}\{5,5\}} \geq \frac{2.078}{q} - \frac{2.155}{q^2} - \frac{\sqrt{4.644 - 8.954q + 4.310q^2}}{q^2}.$$

4.2.6 Maximum likelihood decoding

Maximum likelihood (ML) decoding requires us to find the most probable codeword from the $\mathcal{K}$ codewords by comparing the probabilities of inequivalent errors. Given an error $\boldsymbol{e}$ corresponding to the syndrome $\boldsymbol{s}$, we need to choose the largest of the probabilities $P_{\boldsymbol{e}+\boldsymbol{c}}(\boldsymbol{s})$ for each inequivalent codeword, where $P_{\boldsymbol{e}}(\boldsymbol{s})$ is given by the sum of probabilities of all errors equivalent to $\boldsymbol{e}$ that will result in the syndrome $\boldsymbol{s}$ for each codeword, $P_{\boldsymbol{e}+\boldsymbol{c}}(\boldsymbol{s})$. Since X and Z error corrections are independent in CSS codes, let us take X errors as an example.

We only consider i.i.d errors where any operator X^j acts on any qudit with the same probability $\frac{p}{q-1}$ for any $j \in \{1, \ldots, q-1\}$. The probability of an X error described by a length n q-ary vector $\boldsymbol{e}$ is

$$P(\boldsymbol{e}) = \prod_{i=1}^{N_b} (\frac{p}{q-1})^{\delta(e_i,0)} (1-p)^{1-\delta(e_i,0)} = (\frac{p}{q-1})^{\mathrm{wgt}(\boldsymbol{e})} (1-p)^{N_b - \mathrm{wgt}(\boldsymbol{e})} \tag{4.7}$$

where $N_b = n$ is the number of physical qudits and $\mathrm{wgt}(\boldsymbol{e})$ is the Hamming weight of the error.

Degenerate errors are the errors that are equivalent in the code, the difference between them is a linear combination of the rows of the generator matrix. Consider all the degenerate errors that have the same effect as $\boldsymbol{e}$, the probability of that is given by

$$P_0(\boldsymbol{e}) \equiv \sum_{\boldsymbol{e}' \simeq \boldsymbol{e}} P(\boldsymbol{e}') = \frac{1}{q^{N_s - r} \prod_{i=1}^{r} d_i} \sum_{\boldsymbol{\sigma} \in \{0,\ldots,q-1\}^{N_s}} (\frac{p}{q-1})^{\mathrm{wgt}(\boldsymbol{e} - \boldsymbol{\sigma} G)} (1-p)^{N_b - \mathrm{wgt}(\boldsymbol{e} - \boldsymbol{\sigma} G)} \tag{4.8}$$

where N_s is the number of stabilizer generators, d_i are the invariants of G in Smith normal form, r is the number of the invariants, G is the generator matrix which has dimensions $N_s \times N_b$.

Expanding the weight $\mathrm{wgt}(\boldsymbol{e} - \boldsymbol{\sigma} G) = \sum_b (1 - \delta(e_b - \sum_s \sigma_s G_{sb}, 0))$, where $\delta(x, y)$ denotes the discrete Kronecker delta function which is equal to one whenever $x = y$ and zero otherwise. We have

$$P_0(\boldsymbol{e}) = \frac{1}{q^{N_s - r} \prod_{i=1}^{r} d_i} (1-p)^{N_b} \sum_{\boldsymbol{\sigma}} \prod_b \left(\frac{p}{(1-p)(q-1)} \right)^{1 - \delta(e_b - \sum_s \sigma_s G_{sb}, 0)} \tag{4.9}$$

If we substitute $\frac{(1-p)(q-1)}{p}$ with e^{K_p}, we can simplify the expression as

$$P_0(\boldsymbol{e}) = \frac{1}{q^{N_s - r} \prod_{i=1}^{r} d_i} \sum_{\boldsymbol{\sigma}} \prod_b \frac{e^{K_p \delta(e_b - \sum_s \sigma_s G_{sb}, 0)}}{e^{K_p} + q - 1} \tag{4.10}$$

The sum can be interpreted as the partition function of the Potts model with disorder, at the inverse Potts temperature K_p. In fact, here K_p is related to the error probability p; this is an analog of the Nishimori line for the q-state Potts model, which we define in the following section.

4.2.7 Potts gauge glass model

To study the qudit code, we may relate it with another physics model. Because of Eq.(4.9), A natural choice is the Potts model [34]. Potts model is a generalization of the Ising model. It is defined on a set of spins, where each spin can take any number from $\{0, 1, 2, \ldots, q-1\}$. The standard Potts model has the Hamiltonian

$$H = -\sum_{\langle i,j \rangle} J\delta(s_i, s_j) - \sum_i h\delta(s_i, 0) \tag{4.11}$$

where J is the interaction energy on each bond, h is the external field, the first summation runs over all the nearest neighbor site pairs and the second summation runs over all the sites, and $\delta()$ is the Kronecker delta function.

It is well known that the qubit error correcting codes can be mapped to the $\pm J$ *Ising spin glass model* [6], where the external field is absent, $h = 0$, and the interaction energy takes the value $-J$ or J with probability p and $1-p$ respectively. Because of the symmetry in the system, a gauge transformation can be applied on spins and interactions to solve for important physical quantities of the system. For example, the internal energy can be solved exactly on the Nishimori line [36], which is defined as $e^{2J/k_B T_p} = \frac{p}{1-p}$.

In the case of qudit code with i.i.d. X or Z errors, the corresponding model is the *Potts gauge glass model* [113], where the external field is absent and the interaction energy takes the values $-J\delta(s_i, s_j + e_{ij})$, where $e_{ij} = 0$ with probability $1-p$ and $e_{ij} = 1, .., q-1$ each with probability $p/(q-1)$.

The standard Potts model can be generalized to include multi-spin couplings with interaction energy $-J\delta(\sum_i \sigma_i \Theta_{ib}, 0)$ (all arithmetic are in mod q), where Θ_{ib} is the incidence matrix whose rows correspond to spins, and columns to bonds. When each column of Θ has exactly two non-zero entries equal 1 and -1, it can be interpreted as a vertex-edge incidence matrix of a directed graph, in which case Eq. (4.10) is recovered. More generally, each bond may include multi-spin interactions, in which case the model is defined on a hypergraph. Introducing flipped bonds results in a Potts gauge glass model, which has the

partition function

$$Z_{\text{Potts}} = \sum_{\{\sigma_i\}} \exp\left(\sum_b \beta J \delta(\sum_i \sigma_i \Theta_{ib} - e_b, 0)\right) \tag{4.12}$$

where

$$e_b \begin{cases} = 0, & \text{with probability } (1-p) \\ = j \in \{1, \ldots, q-1\}, & \text{each with probability } p/(q-1) \end{cases}.$$

The Nishimori line of Potts gauge glass model is given by [114]

$$\beta_p \equiv \frac{1}{J} \ln\left[\frac{(1-p)(q-1)}{p}\right]$$

Using gauge transformation, the internal energy on the Nishimori line can be solved exactly $E = \frac{N_B J}{q} - \frac{N_B J e^{\beta_p J}}{e^{\beta_p J}+q-1}$, and the specific heat is upper bounded: $C \leq \frac{k_B N_B (\beta_p J)^2 e^{\beta_p J}(q-1)}{(e^{\beta_p J}+q-1)^2}$.

The probability of degenerate errors $P_0(\boldsymbol{e})$ can be mapped onto the partition function of Potts gauge glass model up to a multiplicative factor,

$$Z_0(\boldsymbol{e}, \beta) = \frac{1}{q^{N_s - r} \prod_{i=1}^{r} d_i} \sum_{\boldsymbol{\sigma}} \prod_b \frac{e^{\beta J \delta(\sum_s \sigma_s G_{sb} - e_b, 0)}}{e^{\beta J} + q - 1} \tag{4.13}$$

so the probability of errors $P_0(\boldsymbol{e})$ coincides with the partition function on the Nishimori line

$$P_0(\boldsymbol{e}) = Z_0(\boldsymbol{e}, \beta_p) \tag{4.14}$$

where $\beta_p = K_p/J$.

We define $Z_{\boldsymbol{c}}(\boldsymbol{e}, \beta) \equiv Z_0(\boldsymbol{e}+\boldsymbol{c}, \beta)$, where $\boldsymbol{c}$ is a codeword. The maximum of $Z_{\boldsymbol{c}}(\boldsymbol{e}, \beta)$ over all codewords $\boldsymbol{c}$ for a given syndrome is $Z_{\max}(\boldsymbol{s}, \beta) \equiv Z_{\boldsymbol{c}_{\max}}(\boldsymbol{e}, \beta)$; it depends only on the syndrome but not on the chosen representative error $\boldsymbol{e}$. We also denote $Z_{\text{tot}}(\boldsymbol{e}, \beta) \equiv \sum_{\boldsymbol{c}} Z_{\boldsymbol{c}}(\boldsymbol{e}, \beta)$ the sum of the partition functions over all inequivalent codewords; this quantity also depends only on the syndrome $\boldsymbol{s}$ and can be interpreted as the probability of all the errors that give the same syndrome as $\boldsymbol{e}$.

4.2.8 Finite-T decoding threshold and homological difference convergence

The overall probability of successful ML decoding can be written as $[Z_{\max}/Z_{\text{tot}}]_{\boldsymbol{e}}$, where $[\cdot]_{\boldsymbol{e}}$ denotes the averaging over binary error vectors with probability (4.7). For a decodable

region on the $p - T$ diagram, the successful decoding probability must converge to 1 as $d \to \infty$.

Theorem 4.8 *Consider a sequence of quantum CSS codes $Q(G_t, H_t)$, $t \in \mathbb{N}$, of increasing lengths n_t, where row weights of each G_t and H_t do not exceed a fixed m, and the code distances $d_t \geq D \ln n_t$, with some $D > 0$. Then the sequence $\Delta F_t \equiv [\Delta F_{\boldsymbol{e}}(G_t, H_t; K)]_p$, $t \in \mathbb{N}$, converges to zero in the region*

$$(m-1)\left((1-p)(q-1)e^{-K} + pe^{K} + (q-2)p\right) < e^{-1/D} \tag{4.15}$$

This is the q-ary generalization of Theorem 2 of [32].

Notice that this lower bound on error rate threshold p is the same as the one with minimum energy decoding (Eq 4.6).

The corresponding Potts model has converging free energy density homological difference in a larger region [8]:

Theorem 4.9 *Consider a sequence of pairs of weakly dual Potts models defined by pairs of finite q-ary matrices with mutually orthogonal rows, $G_t H_t^T = 0$, $t \in \mathbb{N}$, where row weights of each H_t do not exceed a fixed m. In addition, assume that the sequence of the CSS distances d_{G_t} is increasing. Then the sequence $\Delta f_t \equiv [\Delta f_{\mathbf{e}}(G_t, H_t; K)]_p$, $t \in \mathbb{N}$, converges to zero in the region*

$$(m-1)\left((1-p)(q-1)e^{-K} + pe^{K} + (q-2)p\right) < 1. \tag{4.16}$$

The proofs are given in Appendix B.6.

4.2.9 Duality of Potts gauge glass model

In 2-D Ising model, a high temperature system is related to a low temperature system on the dual graph via Kramers–Wannier duality [64], from which we can find the critical temperature T_c on an infinite square lattice which is self-dual. The critical temperature of Ising model on a square lattice is given by $\sinh\left(\frac{2J}{kT_c}\right) = 1$. Similar duality relationship can

be found in standard Potts model. Here we generalize the duality transform to Potts gauge glass model, following the formalization in [31].

We introduce the *magnetic disorder* $\boldsymbol{m}$, which enters the partition function of Potts gauge glass model as

$$Z_{\boldsymbol{e},\boldsymbol{m}}(\Theta, K) \equiv \frac{1}{q^{N_s - r}(\prod_{i=1}^{r} d_i)(e^K + q - 1)^{N_b}} \sum_{s_i} \prod_{b} \omega^{\sum_i s_i \Theta_{ib} m_b} e^{K\delta(\sum_i s_i \Theta_{ib} - e_b, 0)} \tag{4.17}$$

where $K = J/k_B T$, $\boldsymbol{e}$ is the electric charge error and $\boldsymbol{m}$ is the magnetic charge error. Applying discrete Fourier transform, we find the duality relationship to be

$$\left(\frac{\prod_{i=1}^{r} d_i}{q^r}\right)^{\frac{1}{2}} \left(\frac{\sqrt{e^K - 1}}{e^K}\right)^{N_b} Z_{\boldsymbol{e},\boldsymbol{m}}(\Theta, K) = \left(\frac{\prod_{i=1}^{r^*} d_i^*}{q^{r^*}}\right)^{\frac{1}{2}} \left(\frac{\sqrt{e^{K^*} - 1}}{e^{K^*}}\right)^{N_b} \omega^{\boldsymbol{e}\cdot\boldsymbol{m}} Z_{\boldsymbol{e}^*,\boldsymbol{m}^*}(\Theta^*, K^*) \tag{4.18}$$

where $\boldsymbol{m}^* \equiv \boldsymbol{e}$, $\boldsymbol{e}^* \equiv -\boldsymbol{m}$, $K^* \equiv \ln(1 + \frac{q}{e^K - 1})$, and Θ^* is the exact dual of Θ (details in Appendix B.2).

In the case of $K^* = K$, we find the self-dual inverse temperature to be $K_{s.d} = \ln(\sqrt{q} + 1)$, which asymptotically approaches $\frac{\ln q}{2}$ in the limit of large q.

4.2.10 Spin correlations and Griffiths inequalities

Here we introduce the spin correlations similar to Eq.(3.15) and Eq.(3.16)

$$\langle S_{\mathcal{A}} \rangle_{\boldsymbol{e}} \equiv \sum_{\{s_i\}} S_{\mathcal{A}} \, \mathrm{Prob}_{\mathbf{e}}(\{S\}; \Theta; K) \tag{4.19}$$

$$S_{\mathcal{A}} = \prod_{v} \omega^{\sum_b s_v \Theta_{vb} m_b} \tag{4.20}$$

where the probability of a certain configuration $\mathrm{Prob}_{\boldsymbol{e}}(\{S\}; \Theta; K)$ is defined according to the partition function (4.13)

$$\mathrm{Prob}_{\boldsymbol{e}}(\{S\}; \Theta; K) = \frac{\prod_b e^{K\delta(\sum_i s_i \Theta_{ib} - e_b, 0)}}{\sum_{\{s_i\}} \prod_b e^{K\delta(\sum_i s_i \Theta_{ib} - e_b, 0)}} \tag{4.21}$$

Similar to Eq.(3.23), the duality relationship (4.18) in this case reads

$$\frac{Z_{\boldsymbol{e},\boldsymbol{0}}(\Theta, K)}{Z_{\boldsymbol{0},\boldsymbol{0}}(\Theta, K)} = \left\langle \prod_b R_b^{e_b} \right\rangle_{0,\Theta^*;K^*} \tag{4.22}$$

where we define

$$R_b \equiv \omega^{\sum_v s_v \Theta_{vb}}$$

From the partition function (4.17), by changing the order of the summation $s_i \to -s_i$, it is easy to see that

$$Z_{\boldsymbol{e},\boldsymbol{m}} = Z_{-\boldsymbol{e},-\boldsymbol{m}} \tag{4.23}$$

and when there is no flipped bond: $\boldsymbol{e} = 0$, we have

$$Z_{\boldsymbol{0},\boldsymbol{m}} = Z_{\boldsymbol{0},-\boldsymbol{m}}$$

Noticing that the rhs is the complex conjugate of the lhs, which implies that in the clean model where there is no flipped bonds, the correlation must be real: $\langle S_{\mathcal{A}} \rangle_0 \in \mathbb{R}$, and we may replace the complex function with only the real part, i.e. replacing $S_{\mathcal{A}} = \omega^{\sum_v \sum_b s_v \Theta_{vb} m_b}$ with $S'_{\mathcal{A}} = \cos(\frac{2\pi}{q} \sum_v \sum_b s_v \Theta_{vb} m_b)$.

The correlation of spins in the clean model satisfies the Griffiths–Kelly–Sherman (GKS) inequalities [62, 63, 115, 116]:

$$\langle S_{\mathcal{A}} \rangle_0 \geq 0, \tag{4.24}$$

$$\langle S_{\mathcal{A}} S_{\mathcal{B}} \rangle_0 \geq \langle S_{\mathcal{A}} \rangle_0 \langle S_{\mathcal{B}} \rangle_0, \tag{4.25}$$

The derivative of $\langle S_{\mathcal{A}} \rangle$ with respect to $K_{\mathcal{B}}$ gives

$$\frac{d\langle S_{\mathcal{A}} \rangle}{dK_{\mathcal{B}}} = \langle S_{\mathcal{A}} \delta_{\mathcal{B}} \rangle - \langle S_{\mathcal{A}} \rangle \langle \delta_{\mathcal{B}} \rangle \tag{4.26}$$

where we denote $\delta_{\mathcal{B}} \equiv \delta(\sum_v s_v \Theta_{vb} - e_b, 0)$. Here we may expand the Kronecker delta as a summation of cosine functions, $\delta(x, 0) = \frac{1}{q} \sum_{j=0}^{q-1} \cos(\frac{2\pi}{q} j x)$. In the case $\boldsymbol{e} = 0$, with this substitution, we can write $\delta_{\mathcal{B}}$ as a summation of $S'_{\mathcal{B}} = \cos(\frac{2\pi}{q} \sum_v s_v \Theta_{vb} m_b)$.

Then from the GKS inequality (4.25), we find that this quantity is non-negative in the clean model

$$\frac{d\langle S_{\mathcal{A}} \rangle_0}{dK_{\mathcal{B}}} \geq 0 \tag{4.27}$$

Next we may introduce the invariant distance for a defect $\boldsymbol{e}$,

$$d_{\boldsymbol{e}} \equiv d_{\boldsymbol{e}}(\Theta) = \min_{\boldsymbol{\alpha}} \mathrm{wgt}(\boldsymbol{e} + \boldsymbol{\alpha}\Theta) \tag{4.28}$$

The free energy increment due to the addition of the defect can be found by taking the logarithm of the lhs of (4.22),

$$\delta_{\boldsymbol{e}} \equiv \delta_{\boldsymbol{e}}(\Theta; K) \equiv \ln Z_0(\Theta; K) - \ln Z_{\boldsymbol{e}}(\Theta; K) \tag{4.29}$$

and the defect tension is defined to be

$$\tau_{\boldsymbol{e}} \equiv \tau_{\boldsymbol{e}}(\Theta; K) \equiv \delta_{\boldsymbol{e}}(\Theta; K)/d_{\boldsymbol{e}} \tag{4.30}$$

Respectively, if we assume that the rhs of Eq.(4.22) scales exponentially with the defect weight (this is generally expected at large temperatures), we can define the area-law exponent

$$\alpha_{\boldsymbol{e}} \equiv \alpha_{\boldsymbol{e}}(\Theta^*; K^*) = -d_{\boldsymbol{e}}^{-1} \ln \left\langle \prod_b R_b^{e_b} \right\rangle_{0,\Theta^*;K^*} \tag{4.31}$$

The second GKS inequality (4.25) implies subadditivity,

$$d_{\boldsymbol{e}_1+\boldsymbol{e}_2}\alpha_{\boldsymbol{e}_1+\boldsymbol{e}_2} \leq d_{\boldsymbol{e}_1}\alpha_{\boldsymbol{e}_1} + d_{\boldsymbol{e}_2}\alpha_{\boldsymbol{e}_2} \tag{4.32}$$

The duality (4.25) also implies the relation between the defect tension and area-law exponent,

$$\tau_{\boldsymbol{e}}(\Theta; K) = \alpha_{\boldsymbol{e}}(\Theta^*; K^*) \tag{4.33}$$

Together with (4.32), we get subadditivity for defect free energy cost

$$\delta_{\boldsymbol{e}_1+\boldsymbol{e}_2} \leq \delta_{\boldsymbol{e}_1} + \delta_{\boldsymbol{e}_2} \tag{4.34}$$

4.3 Other results

Most of the results of binary QECCs can be generalized to q-ary codes straightforwardly, but some of them require special treatment. The results are followed by the proof when necessary, and the rest of the results are restated without repeating the proof. The definitions can be found in the corresponding publications.

4.3.1 Results on q-ary *CSS* codes in general

This section presents generalizations of some results from Ref.[31].

First we generalize the definition of *fixed-defect phase* and *defect-free phase*:

Definition 4.10 (Generalization of Definition 1 from Ref. [31]) *A fixed-defect phase of the Potts gauge glass model 4.13 corresponding to an infinite family of q-ary CSS codes has*

$$[Z_0(\boldsymbol{e},\beta)/Z_{tot}(\boldsymbol{s_e},\beta)] \to 1, \quad n \to \infty. \tag{4.35}$$

Definition 4.11 (Generalization of Definition 1 from Ref. [31]) *A defect-free phase of the Potts gauge glass model 4.13 corresponding to an infinite family of q-ary CSS codes has*

$$[Z_{max}(\boldsymbol{s_e},\beta)/Z_{tot}(\boldsymbol{s_e},\beta)] \to 1, \quad n \to \infty. \tag{4.36}$$

The following theorems hold,

Theorem 4.12 (Generalization of Theorem 1 from Ref. [31]) *For an infinite family of q-ary quantum stabilizer codes successful decoding with probability one implies that on the Nishimori line the corresponding Potts glass model is in the defect-free phase, i.e., in any likely configuration $\boldsymbol{e}$ of flipped bonds the largest $Z_{\boldsymbol{c}}(\boldsymbol{e};\beta_p)$ corresponds to $\boldsymbol{c}_{max}(\boldsymbol{e}) = 0$.*

Theorem 4.13 (Generalization of Theorem 2 from Ref. [31]) *For an infinite family of Potts glass models (4.13), in a fixed-defect phase the averaged over the disorder free energy increment for an additional defect corresponding to a non-trivial codeword $\boldsymbol{c} \neq 0$ diverges at large n, $[\Delta F_{\boldsymbol{c}}^{max}(\boldsymbol{s_e};\beta)] \to \infty$.*

Theorem 4.14 (Generalization of Theorem 3 from Ref. [31]) *Define the defect tension of a codeword $\boldsymbol{c}$ to be $\tau_{\boldsymbol{c}} \equiv \frac{[\Delta F_{\boldsymbol{c}}^{max}(\boldsymbol{s_e})]}{d_{\boldsymbol{c}}}$, where $\Delta F_{\boldsymbol{c}}^{max}(\boldsymbol{s_e}) \equiv \log \frac{Z_{\max}(\boldsymbol{s})}{Z_{\boldsymbol{c}_{\max}(\boldsymbol{e})+\boldsymbol{c}}(\boldsymbol{e})}$. For Potts glass models (4.13) corresponding to an infinite family of q-ary quantum codes with asymptotic rate $R = \log_q \mathcal{K}/n$, in a fixed-defect phase, the defect tension averaged over all non-trivial defect classes at large n, $\overline{\tau} \equiv (\mathcal{K}-1)^{-1} \sum_{\boldsymbol{c}\neq\boldsymbol{0}} \tau_{\boldsymbol{c}}$, satisfy the inequality $\overline{\tau} \geq \frac{R \ln q}{2}$.*

Theorem 4.15 (Generalization of Theorem 4 from Ref. [31]) *Defect-free phase cannot exist at any β for p exceeding that at the decoding transition, $p > p_c$.*

Proof. The proof goes similar to the one in the reference, except that now it is possible that the correlation functions are complex numbers, so we must prove that the averaged values are real numbers first.

Consider spin correlation functions defined as the following:

$$Q^{\boldsymbol{m}}_{\mathrm{tot}}(\boldsymbol{e},\beta) \equiv \frac{Z_{\boldsymbol{e},\boldsymbol{m}}(\tilde{G}^*,\beta)}{Z_{\boldsymbol{e},0}(\tilde{G}^*,\beta)} \tag{4.37}$$

We find that the following equality holds for any $\boldsymbol{m}$:

$$[Q^{\boldsymbol{m}}_{\mathrm{tot}}(\boldsymbol{e},\beta)] = [Q^{\boldsymbol{m}}_{\mathrm{tot}}(\boldsymbol{e},\beta)Q^{-\boldsymbol{m}}_{\mathrm{tot}}(\boldsymbol{e},\beta_p)] \tag{4.38}$$

where $[f(\boldsymbol{e})] \equiv \sum_{\boldsymbol{e}} P(\boldsymbol{e})f(\boldsymbol{e})$ is the expectation of $f(\boldsymbol{e})$ over probability distribution $P(\boldsymbol{e})$.

And the inequality

$$[Q^{\boldsymbol{m}}_{\mathrm{tot}}(\boldsymbol{e},\beta)]^2 \leq [Q^{\boldsymbol{m}}_{\mathrm{tot}}(\boldsymbol{e},\beta_p)] \tag{4.39}$$

is true for any $\boldsymbol{m}$ (proved in Appendix B.3).

Since there may be additional linear-independent rows in $\tilde{G}^*$, we can expand the partition function in terms of codewords $\boldsymbol{c}$:

$$Z_{\boldsymbol{e},\boldsymbol{m}}(\tilde{G}^*,\beta) = \sum_{\boldsymbol{c}} \omega^{\boldsymbol{c}\cdot\boldsymbol{m}} Z_{\boldsymbol{e}+\boldsymbol{c},\boldsymbol{m}}(G,\beta) \tag{4.40}$$

and so we have

$$Q^{\boldsymbol{m}}_{\mathrm{tot}}(\boldsymbol{e},\beta) = \sum_{\boldsymbol{c}} \omega^{\boldsymbol{c}\cdot\boldsymbol{m}} \frac{Z_{\boldsymbol{c}}(\boldsymbol{e},\beta)Q^{\boldsymbol{m}}_{\boldsymbol{c}}(\boldsymbol{e},\beta)}{Z_{\mathrm{tot}}(\boldsymbol{s}_{\boldsymbol{e}},\beta)} \tag{4.41}$$

Applying this to the inequality of correlation functions and summing over all the magnetic charges that equals to a dual codeword $\boldsymbol{m} = \tilde{\boldsymbol{c}}$, we find that

$$\sum_{\boldsymbol{m}=\tilde{\boldsymbol{c}}} [Q^{\boldsymbol{m}}_{\mathrm{tot}}(\boldsymbol{e},\beta)]^2 \leq \mathcal{K}\left[\frac{Z_{\boldsymbol{c}}(\boldsymbol{e},\beta_p)}{Z_{\mathrm{tot}}(\boldsymbol{s}_{\boldsymbol{e}},\beta_p)}\right] \tag{4.42}$$

This shows that the boundary of the decodable phase for q-ary code is either vertical or re-entrant as a function of temperature below the Nishimori line. ■

4.3.2 Free energy analyticity bounds of Potts models with extensive homology rank

The following results includes the generalization of the theorems in Ref [8]. The coefficient $\frac{1}{2}$ on inverse temperature K is due to the difference between the interaction energy of Ising models and Potts models, where the former is $-J$ for low energy spin alignment and J for high energy spin alignment and the latter is $-J$ for low energy alignment and 0 for high energy alignment.

Theorem 4.16 *Consider a sequence of pairs of weakly dual Potts models defined by pairs of finite q-ary matrices with mutually orthogonal rows, $G_t H_t^T = 0$,$t \in \mathbb{N}$, where row weights of each G_t do not exceed a fixed m, CSS distances d_{H_t} are increasing with t, and the sequence of CSS rates $R_t \equiv \log_q K_t/n_t$ converges, $\lim_t R_t = R$. Then, for any $K \geq 0$ such that $(m-1)\tanh\frac{K}{2} < 1$, the sequence $\Delta f_t \equiv [\Delta f_e(G_t, H_t; K)]_p$, $t \in \mathbb{N}$, converges to $R \ln q$.*

Theorem 4.17 *Let us assume that any one of the following Conditions is true:*

1. *The transition at $T_c'(G)$ is discontinuous or has a divergent specific heat;*
2. *The derivative of $\Delta f(K) = f_G(K) - f_{H^*}(K)$ is discontinuous at $K_h \equiv K_h(G,H)$, or the derivative of $\Delta f(K)$ is continuous at K_h, but its second derivative diverges at K_h;*
3. *Summation over homological defects does not increase the critical temperature, $T_c(G^*) \leq T_c(H)$.*

Then the Kramers-Wannier dual of the critical temperatures $T_c(H)$ satisfies

$$T_c^*(H) \leq T_h(G,H)$$

Theorem 4.18 *For any regular $\{f,d\}$ tiling of an infinite hyperbolic plane, $fd/(f+d) > 2$, the critical temperatures of the Potts model with free and wired boundary conditions, $T_c^f = 1/K_c^f$ and $T_c^w = 1/K_c^w$, satisfy*

$$K_c^f - K_c^w \geq 2R \ln q, \qquad R = 1 - 2/f - 2/d. \tag{4.43}$$

The subadditivity for defect free energy cost is given in Section 4.2.10.

4.3.3 Summary phase diagrams and bounds

We summarize the results on a $p - T$ diagram in Fig. 4.2, and show the plot of the corresponding bounds for Potts models with $q = 2$ and $q = 3$ on the $\{5, 5\}$ graphs in the thermodynamic limit in Fig. 4.3. The plot is obtained by setting $m = 5$, $D = 0.854$ and $R = 1/5$ in equations (4.6), (4.15) and (4.43).

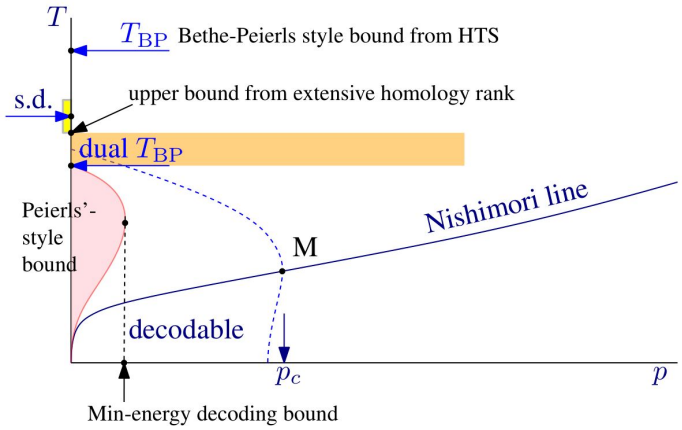

Figure 4.2: (Color online) A schematic summary phase diagram, which shows the minimum energy decoding bound (Theorem 4.7), the Peierls' style bound (Theorem 4.8) and the upper bound from extensive homology rank (Theorem 4.18).

4.4 Potts clock model formalization of multivariate probability distribution

The following formalization of multivariate probability distribution is a q-ary generalization of "multivariate Bernoulli distribution" [117].

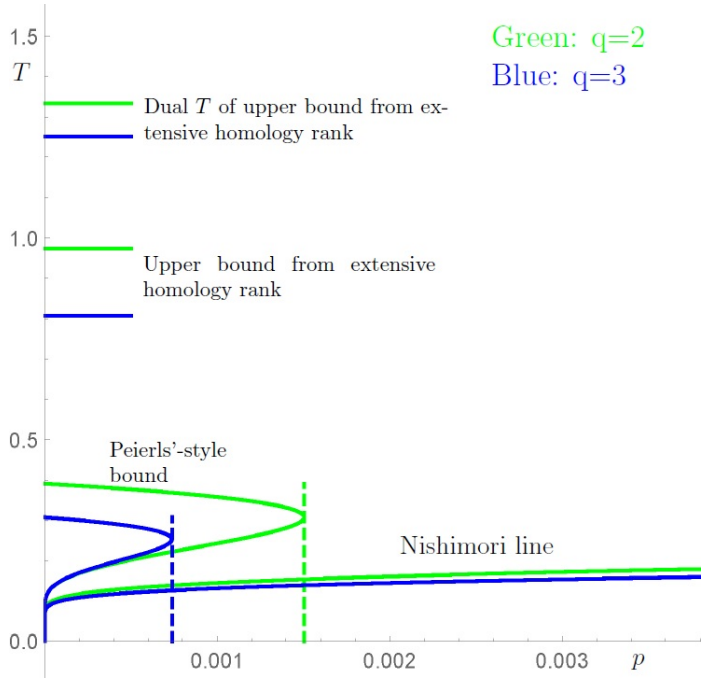

Figure 4.3: (Color online) A plot of the bounds indicated in Fig.4.2 for the Potts models with $q = 2$ (Green) and $q = 3$ (Blue) on the $\{5, 5\}$ graphs in the thermodynamic limit. The minimum energy decoding bound is given in Eq. (4.6), the Peierls' style bound in Eq. (4.15), and the extensive homology rank bound in Eq. (4.43). T_{BP} is too large to fit in, it is omitted in this plot.

4.4.1 Single variable distribution

4.4.1.1 Complex coefficients

Given any discrete probability distribution $p(x) = p_0^{\delta(x,0)} p_1^{\delta(x,1)} \dots p_{q-1}^{\delta(x,q-1)}$, we may rewrite the Kronecker delta function as the summation of powers of the root of unity $\delta(x,a) = \frac{1}{q}\sum_{j=0}^{q-1} \omega^{j(x-a)}$, where $\omega \equiv e^{i\frac{2\pi}{q}}$.

We may rewrite $p(x)$ in an exponential form:

$$p(x) = \exp\left[\frac{1}{q}(\ln(p_0)\sum_{j=0}^{q-1}\omega^{jx} + \ln(p_1)\sum_{j=0}^{q-1}\omega^{j(x-1)} + \dots + \ln(p_{q-1})\sum_{j=0}^{q-1}\omega^{j(x-(q-1))})\right]$$

Regroup the terms and it becomes:

$$p(x) = \exp[K_0 + K_1\omega^x + K_2\omega^{2x} + \dots]$$

where the constants ω^{-ja} in $\omega^{j(x-a)}$ are absorbed in the coefficients K_m.

The expression can be transformed between exponential and polynomial form:

For each term in the exponential function,

$$\begin{aligned} e^{K\omega^x} &= \sum_{m=0}^{\infty}\frac{(K\omega^x)^m}{m!} \\ &= \sum_{m=0 \bmod q}\frac{K^m}{m!} + \sum_{m=1 \bmod q}\frac{K^m}{m!}\omega^x + \dots \\ &= f_0(K) + f_1(K)\omega^x + \dots + f_{q-1}(K)\omega^{x-(q-1)} \end{aligned}$$

The exponential can then be expanded,

$$\begin{aligned} p(x) &= \exp[K_0 + K_1\omega^x + K_2\omega^{2x} + \dots] \\ &= e^{K_0}\left(f_0(K_1) + f_1(K_1)\omega^x + \dots + f_{q-1}(K_1)\omega^{(q-1)x}\right)\left(f_0(K_2) + f_1(K_2)\omega^{2x} + \dots\right. \\ &\quad \left. + f_{q-1}(K_1)\omega^{2(q-1)x)}\right)\dots\left(f_0(K_{q-1}) + f_1(K_{q-1})\omega^{(q-1)x} + \dots + f_{q-1}(K_1)\omega^{(q-1)^2x)}\right) \\ &= \tilde{K}_0 + \tilde{K}_1\omega^x + \dots + \tilde{K}_{q-1}\omega^{(q-1)x} \end{aligned}$$

and the result is in a polynomial form.

The inverse transform is given by

$$
\begin{aligned}
p(x) &= \tilde{K}_0 + \tilde{K}_1\omega^x + \cdots + \tilde{K}_{q-1}\omega^{(q-1)x} \\
&= (\tilde{K}_0 + \cdots + \tilde{K}_{q-1})^{\frac{1+\omega^x+\cdots+\omega^{(q-1)x}}{q}} (\tilde{K}_0 + \tilde{K}_1\omega + \cdots + \tilde{K}_{q-1}\omega^{q-1})^{\frac{1+\omega^{x-1}+\cdots+\omega^{(q-1)(x-1)}}{q}} \\
&\quad \ldots (\tilde{K}_0 + \tilde{K}_1\omega^{q-1} + \cdots + \tilde{K}_{q-1}\omega^{(q-1)^2})^{\frac{1+\omega^{x-(q-1)}+\cdots+\omega^{(q-1)(x-(q-1))}}{q}} \\
&= \exp\left[\frac{1}{q}\left(\ln S_0(1+\omega^x+\cdots+\omega^{(q-1)x}) + \ln S_1(1+\omega^{x-1}+\cdots+\omega^{(q-1)(x-1)}) + \ldots\right)\right] \\
&= \exp\left[K_0 + K_1\omega^x + \cdots + K_{q-1}\omega^{(q-1)x}\right]
\end{aligned}
$$

4.4.1.2 Real coefficients

Instead of complex numbers, we may only take the real part and rewrite the Kronecker delta function as a series of cosine functions, $\delta(x,a) = \frac{1}{q}\sum_{j=0}^{q-1}\cos(\frac{2\pi}{q}j(x-a))$.

$$
\begin{aligned}
p(x) &= \exp\left[\frac{1}{q}(\ln p_0(1+\cos(\frac{2\pi}{q}x) + \cos(\frac{2\pi}{q}2x) + \cdots + \cos(\frac{2\pi}{q}(q-1)x)) + \right. \\
&\qquad \left. \ln p_1(1+\cos(\frac{2\pi}{q}(x-1)) + \cos(\frac{2\pi}{q}2(x-1))) + \cdots + \cos(\frac{2\pi}{q}(q-1)(x-1)) + \ldots)\right] \\
&= \exp\left[\frac{1}{q}\left((\ln p_0 + \ln p_1 + \ldots) + \cos(\frac{2\pi}{q}x)(\ln p_0 + \cos\frac{2\pi}{q}\ln p_1 + \ldots) + \right.\right. \\
&\qquad \left.\left. \sin(\frac{2\pi}{q}x)(\sin\frac{2\pi}{q}\ln p_1 + \ldots) + \ldots\right)\right] \\
&= \exp\left(K_0 + K_1\cos(\frac{2\pi}{q}x - \alpha_1) + K_2\cos(\frac{2\pi}{q}2x - \alpha_2) + \cdots + \right. \\
&\qquad \left. K_{q-1}\cos(\frac{2\pi}{q}(q-1)x - \alpha_{q-1})\right)
\end{aligned}
$$

Here we won't be able to absorb the constants a_j into the coefficients K_j like in the case of complex numbers, so we have to include the sine functions:

$$
\begin{aligned}
p(x) = \exp\Big[&K_0 + K_1'\cos(\frac{2\pi}{q}x) + K_1''\sin(\frac{2\pi}{q}x) + K_2'\cos(\frac{2\pi}{q}2x) + K_2''\sin(\frac{2\pi}{q}2x) + \ldots \\
&+K_{q-1}'\cos(\frac{2\pi}{q}(q-1)x) + K_{q-1}''\sin(\frac{2\pi}{q}(q-1)x)\Big]
\end{aligned}
$$

To expand the exponential function, although $\cos^n(x)$ is not equivalent to $\cos(nx)$,

we can still expand it as a summation of cosine functions. Notice that

$$\cos(ax)\cos(bx) = \frac{1}{2}\left(\cos((a+b)x) + \cos((a-b)x)\right)$$

we can always expand $\cos^n(x)$ as a summation $\sum_{j=0}^{n} C_j \cos(jx)$, where C_j are constants.

As for the power of sine functions, notice that

$$\sin^2(x) = \frac{1}{2}(1 - \cos(2x))$$

$$\sin(x)\cos(ax) = \frac{1}{2}(\sin((a+1)x) - \sin((a-1)x))$$

An even power of sine functions can be expanded to a summation of cosine functions, and an odd power of sine functions becomes a summation of sine functions.

For each term of the exponential,

$$\begin{aligned} e^{K\cos(\frac{2\pi}{q}x)} &= \sum_{m=0}^{\infty} \frac{(K\cos(\frac{2\pi}{q}x))^m}{m!} \\ &= f_{c,0}(K) + f_{c,1}(K)\cos(\frac{2\pi}{q}x) + \cdots + f_{c,q-1}(K)\cos(\frac{2\pi}{q}(q-1)x) \end{aligned}$$

$$\begin{aligned} e^{K\sin(\frac{2\pi}{q}x)} &= \sum_{m=0}^{\infty} \frac{(K\sin(\frac{2\pi}{q}x))^m}{m!} \\ &= f_{s,0}(K) + f_{ss,1}(K)\sin(\frac{2\pi}{q}x) + \cdots + f_{ss,q-1}(K)\sin(\frac{2\pi}{q}(q-1)x) \\ &\quad + f_{sc,1}(K)\cos(\frac{2\pi}{q}x) + \cdots + f_{sc,q-1}(K)\cos(\frac{2\pi}{q}(q-1)x) \end{aligned}$$

After the multiplication, we can use the trigonometric identities again to convert each term into summation of sine or cosine functions. Eventually we can get

$$\begin{aligned} p(x) = \exp\Big[&K_0 + K_1'\cos(\frac{2\pi}{q}x) + K_1''\sin(\frac{2\pi}{q}x) + K_2'\cos(\frac{2\pi}{q}2x) + K_2''\sin(\frac{2\pi}{q}2x) + \dots \\ &+K_{q-1}'\cos(\frac{2\pi}{q}(q-1)x) + K_{q-1}''\sin(\frac{2\pi}{q}(q-1)x)\Big] \\ = &\tilde{K}_0 + \tilde{K}_1'\cos(\frac{2\pi}{q}x) + \tilde{K}_1''\sin(\frac{2\pi}{q}x) + \tilde{K}_2'\cos(\frac{2\pi}{q}2x) + \tilde{K}_2''\sin(\frac{2\pi}{q}2x) + \dots \\ &+ \tilde{K}_{q-1}'\cos(\frac{2\pi}{q}(q-1)x) + \tilde{K}_{q-1}''\sin(\frac{2\pi}{q}(q-1)x) \end{aligned}$$

The inverse transform is similar to the case of complex numbers. First, we let x go through $1, \ldots, q-1$ and write the polynomial as a product of constants raised to a power of delta function. Then we may expand the delta function as a series of cosine functions. Finally, convert it into exponential form, we are back to

$$\begin{aligned} p(x) &= \tilde{K}_0 + \tilde{K}'_1 \cos(\frac{2\pi}{q}x) + \tilde{K}''_1 \sin(\frac{2\pi}{q}x) + \tilde{K}'_2 \cos(\frac{2\pi}{q}2x) + \tilde{K}''_2 \sin(\frac{2\pi}{q}2x) + \ldots \\ &\quad + \tilde{K}'_{q-1} \cos(\frac{2\pi}{q}(q-1)x) + \tilde{K}''_{q-1} \sin(\frac{2\pi}{q}(q-1)x) \\ &= \exp\left(K_0 + K_1 \cos(\frac{2\pi}{q}x - \alpha_1) + K_2 \cos(\frac{2\pi}{q}2x - \alpha_2) + \ldots \right. \\ &\quad \left. + K_{q-1} \cos(\frac{2\pi}{q}(q-1)x - \alpha_{q-1}) \right) \end{aligned}$$

4.4.2 Two variables distribution

Given a two variables distribution, first rewrite the distribution as

$$p_2(\boldsymbol{x}) = p_{0,0}^{\frac{1}{q^2}[1+\cos(\frac{2\pi}{q}x_1)+\ldots][1+\cos(\frac{2\pi}{q}x_2)+\ldots]} p_{0,1}^{\frac{1}{q^2}[1+\cos(\frac{2\pi}{q}x_1)+\ldots][1+\cos(\frac{2\pi}{q}(x_2-1))+\ldots]} \ldots$$

Notice that $\cos(\frac{2\pi}{q}ax_1)\cos(\frac{2\pi}{q}bx_2) = \frac{1}{2}(\cos(\frac{2\pi}{q}ax_1 + bx_2) + \cos(\frac{2\pi}{q}ax_1 - bx_2))$, we may rewrite the distribution as

$$p_2(\boldsymbol{x}) = C \exp\left[\sum_{b=1}^{q^2-1} K_b \cos\left(\frac{2\pi}{q}[\boldsymbol{x}\Theta]_b - \alpha_b \right) \right]$$

where C is a constant and Θ is a matrix with columns consisting of all possible non-zero length 2 q-ary vectors,

$$\Theta \equiv \begin{bmatrix} 0 & \ldots & 0 & 1 & 1 & \ldots & 1 & \ldots & q-1 \\ 1 & \ldots & q-1 & 0 & 1 & \ldots & q-1 & \ldots & q-1 \end{bmatrix}$$

4.4.3 Multiple variables distribution and Potts clock model

The case of multiple variables distribution goes similarly as the 2 variables case. For an s-variables distribution,

$$p_s(\boldsymbol{x}) = \sum_{\boldsymbol{v}\in\{0,\ldots,q-1\}^s} p_{\boldsymbol{v}}^{\frac{1}{q^s}[1+\cos(\frac{2\pi}{q}(x_1-v_1))+\ldots][1+\cos(\frac{2\pi}{q}(x_2-v_2))+\ldots]\ldots[1+\cos(\frac{2\pi}{q}(x_s-v_s))+\ldots]}$$

By converting the products of cosine functions into summations, again we may rewrite the distribution as

$$p_s(\boldsymbol{x}) = C\exp\left[\sum_{b=1}^{q^s-1} K_b \cos\left(\frac{2\pi}{q}[\boldsymbol{x}\Theta]_b - \alpha_b\right)\right]$$

where C is a constant and Θ is a matrix with columns consisting of all non-zero length s q-ary vectors.

This resembles the probability distribution of Potts clock models with multi-spin interactions, where there is an interaction for any subset of the set of spins, thus for m spins there are q^s interaction terms. Each non-zero coefficient, K_b, can be viewed as a particular form of correlation; in many cases high-order correlations may be ignored, thus the number of non-zero coefficients K_b is going to be much smaller.

4.4.4 Standard Potts model

Standard Potts model considers single site and pairwise interactions, the probability distribution can be written as functions of $\delta(x_i - a, 0)$ and $\delta(x_i - x_j, 0)$, which can be expanded into cosine functions, and we may write it in exponential form with linear combinations inside cosine functions, thus converting it into the generalized Potts clock model.

4.4.5 Duality transform

Define a partition function of a Potts clock model on a hypergraph specified with a q-ary incidence matrix Θ with s spins and n interactions that has the symmetry $p(\boldsymbol{x}) = p(-\boldsymbol{x})$,

such that

$$Z(\Theta) = \sum_{\boldsymbol{x}\in\{1,\ldots,q-1\}^s} p(\boldsymbol{x},\Theta) = C\sum_{\boldsymbol{x}} \exp\left[\sum_{b=1}^{n} K_b \cos\left(\frac{2\pi}{q}[\boldsymbol{x}\Theta]_b\right)\right]$$

For each term $g(x) = e^{K\cos(\frac{2\pi}{q}x)}$, we may expand it as

$$g(x) = e^{K\cos(\frac{2\pi}{q}x)} = f_0(K) + f_1(K)\cos(\frac{2\pi}{q}x) + \cdots + f_{q-1}(K)\cos(\frac{2\pi}{q}(q-1)x)$$

The discrete Fourier transform of $g(x)$ gives

$$\begin{aligned} g^*(y) &= \frac{1}{\sqrt{q}}\left(f_0(K)\delta(y,0) + \frac{f_1(K)}{2}(\delta(y,1)+\delta(y,q-1)) + \ldots \right.\\ &\quad \left. + \frac{f_{q-1}(K)}{2}(\delta(y,q-1)+\delta(y,1))\right)\\ &= \frac{1}{\sqrt{q}}\left(f_0(K)\delta(y,0) + \frac{f_1(K)+f_{q-1}(K)}{2}\delta(y,1) + \cdots + \frac{f_{q-1}(K)+f_1(K)}{2}\delta(y,q-1)\right) \end{aligned}$$

We may expand each of the Kronecker delta as a summation of cosine functions, then use the polynomial-exponential conversion to get the exponential form. Notice that $f^*(y) = f^*(-y)$, the exponent of the resulting cosine functions must have constants all 0,

$$\begin{aligned} g^*(y) &= K_0^* + K_1^*\cos(\frac{2\pi}{q}y) + K_2^*\cos(\frac{2\pi}{q}2y) + \cdots + K_{q-1}^*\cos(\frac{2\pi}{q}(q-1)y)\\ &= \exp\left[\tilde{K}_0^* + \tilde{K}_1^*\cos(\frac{2\pi}{q}y) + \tilde{K}_2^*\cos(\frac{2\pi}{q}2y) + \cdots + \tilde{K}_{q-1}^*\cos(\frac{2\pi}{q}(q-1)y)\right] \end{aligned}$$

The inverse transform gives

$$g(x) = \frac{1}{\sqrt{q}}\sum_y \omega^{-xy}\exp\left[\tilde{K}_0^* + \tilde{K}_1^*\cos(\frac{2\pi}{q}y) + \tilde{K}_2^*\cos(\frac{2\pi}{q}2y) + \cdots + \tilde{K}_{q-1}^*\cos(\frac{2\pi}{q}(q-1)y)\right]$$

Apply the inverse transform to each term in the partition function,

$$\begin{aligned} Z(\Theta) &= \frac{C}{q^{\frac{n}{2}}}\sum_{\boldsymbol{x}\in\{1,\ldots,q-1\}^s}\prod_{b=1}^{n}\left(\sum_{y_b=1}^{q-1}\omega^{-\frac{2\pi}{q}(\boldsymbol{x}\Theta)_b y_b}e^{\tilde{K}_{b,0}^* + \tilde{K}_{b,1}^*\cos(\frac{2\pi}{q}y_b)+\cdots+\tilde{K}_{b,q-1}^*\cos(\frac{2\pi}{q}(q-1)y_b)}\right)\\ &= \frac{Ce^{\sum_{b=1}^n \tilde{K}_{b,0}^*}}{q^{\frac{n}{2}}}\sum_{\substack{\boldsymbol{x}\in\{1,\ldots,q-1\}^s\\ \boldsymbol{y}\in\{1,\ldots,q-1\}^n}}\omega^{-\frac{2\pi}{q}\boldsymbol{x}\Theta\boldsymbol{y}^T}\prod_{b=1}^{n}\left(e^{\tilde{K}_{b,1}^*\cos(\frac{2\pi}{q}y_b)+\cdots+\tilde{K}_{b,q-1}^*\cos(\frac{2\pi}{q}(q-1)y_b)}\right) \end{aligned}$$

Notice that the summation over $\boldsymbol{x}$ implies that $\Theta \boldsymbol{y}^T = 0$. Thus, the only none-zero terms have $\boldsymbol{y} = \boldsymbol{\sigma}\tilde{\Theta}$ for some arbitrary vector $\boldsymbol{\sigma}$, where $\tilde{\Theta}$ is the exact dual matrix. Let d_i^* be the non-zero invariants of the Smith normal form of $\tilde{\Theta}$, r^* be the number of d_i^*, and s^* be the number of rows in $\tilde{\Theta}$. Denote $C^* \equiv Ce^{\sum_{b=1}^{n} \tilde{K}^*_{b,0}}$,

$$\begin{aligned} Z(\Theta) &= C^* q^{s-\frac{n}{2}} \sum_{\boldsymbol{y}\in\{\boldsymbol{\sigma}\tilde{\Theta}\}} e^{\sum_{b=1}^{n}\left(\tilde{K}^*_{b,1}\cos(\frac{2\pi}{q}y_b)+\cdots+\tilde{K}^*_{b,q-1}\cos(\frac{2\pi}{q}(q-1)y_b)\right)} \\ &= \frac{C^* q^{s-\frac{n}{2}-s^*+r^*}}{\prod_{i=1}^{r^*} d_i^*} \sum_{\boldsymbol{\sigma}\in\{1,\ldots,q-1\}^{s^*}} e^{\sum_{b=1}^{n}\left(\tilde{K}^*_{b,1}\cos(\frac{2\pi}{q}(\boldsymbol{\sigma}\tilde{\Theta})_b)+\cdots+\tilde{K}^*_{b,q-1}\cos(\frac{2\pi}{q}(q-1)(\boldsymbol{\sigma}\tilde{\Theta})_b)\right)} \end{aligned}$$

To simplify the notation, let us define a new matrix $\overline{\Theta} \equiv (\tilde{\Theta}|2\tilde{\Theta}|\ldots|(q-1)\tilde{\Theta})$. Thus the summation in the exponent becomes $\sum_{b=1}^{(q-1)n} \tilde{K}^*_b \cos(\frac{2\pi}{q}(\boldsymbol{\sigma}\overline{\Theta})_b)$. The identical columns in the expanded matrix can be combined by summing up their coefficients $\tilde{K}^*_b$, so we may replace $\overline{\Theta}$ with a smaller matrix Θ^* that has the number of columns $n^* \leq (q-1)n$,

$$Z(\Theta) = \frac{C^* q^{s-\frac{n}{2}-s^*+r^*}}{\prod_{i=1}^{r^*} d_i^*} \sum_{\boldsymbol{\sigma}\in\{1,\ldots,q-1\}^{s^*}} e^{\sum_{b=1}^{n^*} \tilde{K}^*_b \cos(\frac{2\pi}{q}(\boldsymbol{\sigma}\Theta^*)_b)}$$

If for all subsets of spins there is a non-zero interaction, so that Θ consists of all q-ary vectors, then identity matrix is a submatrix of Θ, thus the invariants of Smith normal form of Θ and Θ^* must all be 1.

4.5 First order transition on non-amenable graphs

The order of phase transition of Potts model in Euclidean space depends on the parameter q and also the dimension [34]. For example, when $q \leq 4$ the 2D Potts model has a second order phase transition, while for $q > 4$ the transition is first order. The Monte Carlo simulation of the first order transition is challenging because of the free energy barrier between the two phases that it has to cross. With single-site algorithm like Metropolis or heat-bath algorithm, the relaxation time is very long on large graphs, which results in hysteresis. The cluster algorithms, e.g. Swendsen–Wang algorithm[118] and Wolff algorithm[89], are helpful in reducing the relaxation time, even though the correlation length is finite in first

order transitions so that the acceleration is not as great as in second order transitions, they can accelerate the simulation substantially comparing to single site flip algorithms like Metropolis or heat bath algorithm. The simulations can reach thermal equilibrium in practical time with the help of cluster algorithms.

On the contrary, in the case of first order transition of Potts model on hyperbolic lattices, the hysteresis remains even with cluster algorithm. One possible reason is the interface tension. In a first-order phase transition in equilibrium, the phase that has the minimum free energy density changes from one to another at the transition point. But for the transition to happen, a bubble of the stable phase must grow large enough to take over the metastable phase. During the growth of the bubble, the free energy would be decreased by an amount proportional to the volume of the bubble, but there is also an increase of interface tension by an amount proportional to the size of the interface.

Consider the free energy of a first order transition between two phases given by

$$F = f_1(\beta)V_1 + f_2(\beta)(V - V_1) + \sigma(\beta)A,$$

where f_1 and f_2 are the free energy density of the first and second phase respectively, V_1 is the volume of the first phase, σ is the interfacial tension, A is the area of the interface. In d-dimensional Euclidean space, for a bubble of radius r, its volume grows as r^d, while the size of the interface grows as r^{d-1}. So, at any temperature, eventually the free energy would be lower with a stable phase bubble if the bubble grows to a size large enough. As a result, no matter how large the system is, a large enough critical bubble would eventually form, driving the system of any size to the equilibrium phase at any $T < T_c$, no matter how close to the phase transition.

In contrast, in a hyperbolic space, the volume and the interface both grow exponentially with r, and they are proportional to each other by a constant. If the ratio between interfacial tension and free energy density difference, $\sigma/|f_1 - f_2|$, is larger than the ratio between volume and interface area, then a bubble of the "true stable" phase with smaller free energy surrounded by "metastable" phase would only increase the total free

energy regardless of how large the bubble is. Thus, there is a possibility that in hyperbolic space, in a range of the physical quantity that drives the first-order phase transition (e.g. temperature), the actual phase could be the stable or the metastable phase depending on the history, since the mechanism that drives the system from one phase to the other may no longer work, and instead of a single phase transition point, there could be two points marking the ends of the range of the physical quantity.

In application to numerical simulations on expander graphs like finite hyperbolic graphs, as the size of the system grows, in certain temperature range, the probability of switching to the phase with a lower-free energy may grow exponentially with the system size. When this is the case, it may be extremely difficult to locate the true thermodynamical phase transition temperature.

While the discussed algorithms may fail to find the transition point separating the stable phases in equilibrium, other methods may be helpful in solving the problem, such as Wang-Landau algorithm [119], which is a non-Markovian stochastic process that go through the free energy barriers and sample density of states directly. More research is needed to construct efficient simulation algorithms capable of dealing with this super-stability of overheated/overcooled phases in hyperbolic space.

Chapter 5

Conclusions And Outlook

In this dissertation, we have studied the quantum error correcting codes on closed hyperbolic surfaces and their corresponding Ising models, and we explored the generalization of binary quantum stabilizer codes to q-ary codes and their corresponding Potts models.

Chapter 3 started with the construction and the properties of hyperbolic tessellations, and also the construction of the quotient graphs. Next, we studied the quantum error correcting codes on such hyperbolic quotient graphs and their corresponding weakly-dual Ising models. The extensive homology rank of the graphs results in a non-zero homological difference of the free energy in a range of temperatures. We gave several bounds of the threshold, and we performed numerical simulations to support our results. Several open questions were listed in Section 3.2.4.2. Another possible future research direction is to find the $p - T$ phase diagram for the RBIMs on hyperbolic quotient graphs, possibly with Monte–Carlo simulation. The combinatorial method is a good option for calculating the free energy and spin correlation of RBIMs on finite subgraphs of hyperbolic graphs with open or wired boundary conditions, but it is unknown whether there is an efficient algorithm for calculating these quantities for spin models on the quotient graphs.

In Chapter 4 we discussed the construction and parameters of qudit quantum error correcting codes. We provided several examples of qudit LDPC codes and bounds on their parameters. An improvement of the upper bound of distances verification complexity index

is also given. We showed the mapping of the probability distributions to the partition functions of Potts gauge glass models, and many of the results on qubit codes were generalized to qudit codes. Further study of the generalized Potts clock model formalization of multivariate probability distribution may lead to some insight into the decoding properties of q-ary LDPC codes with correlated errors, including the correlations that necessarily occur in any circuit used for measurements. Another possible future research direction is numerical simulation of Potts models on the graphs or hypergraphs with extensive homology rank, but the first order phase transition is an obstacle, since the hysteresis makes it difficult to locate the phase transition point.

Appendix A

Appendix of Chapter 3

A.1 Proof of Theorem 3.1

Theorem 3.1 *Consider a sequence of pairs of weakly dual Ising models defined by pairs of finite binary matrices with mutually orthogonal rows, $G_t H_t^T = 0$, $t \in \mathbb{N}$, where row weights of each H_t do not exceed a fixed m. In addition, assume that the sequence of the CSS distances d_{G_t} is increasing. Then the sequence $\Delta f_t \equiv [\Delta f_{\mathbf{e}}(G_t, H_t; K)]_p$, $t \in \mathbb{N}$, converges to zero in the region*

$$(m-1)[e^{-2K}(1-p) + e^{2K}p] < 1. \tag{3.40}$$

The statement of the theorem immediately follows from the following technical Lemma, see the proof in Ref. [32]

Lemma A.1 *Consider a pair of Ising models defined in terms of weight-limited matrices G and H with orthogonal rows, such that the matrix H has a maximum row weight m. Let d_G denote the CSS distance (3.35), the minimum weight of a frustration-free homologically non-trivial defect $\mathbf{c} \in \mathcal{C}_H^{\perp} \setminus \mathcal{C}_G$. Denote $S \equiv e^{-2K}(1-p) + e^{2K}p$, and assume that $(m-1)\,S < 1$. Then, the average homological difference (3.37) satisfies*

$$[\Delta f(G, H; K)]_p \leq \frac{(m-1)^{d_G} S^{d_G+1}}{1-(m-1)\,S}. \tag{A.1}$$

A.2 Proof of inequalities in Sec. 3.2.3.1

(**i**) The proof of the monotonicity of the homological difference (in the absence of flipped bonds),

$$\frac{d}{dK}\Delta f_{\mathbf{0}}(G,H;K)\le 0, \qquad (3.39),$$

is similar to the proof[120] of the monotonicity of the tension. We combine the logarithms in Eq. (3.37), decompose $Z_{\mathbf{e}}(H^*;K)$ as a sum of $Z_{\mathbf{c}}(G;K)$ over non-equivalent codewords $\mathbf{c}$, and write

$$\frac{d}{dK}\frac{Z_{\mathbf{c}}(G;K)}{Z_{\mathbf{0}}(G;K)}=\frac{Z_{\mathbf{c}}(G;K)}{Z_{\mathbf{0}}(G;K)}\sum_{b\in\mathcal{B}}(\langle R_b\rangle_{\mathbf{c}}-\langle R_b\rangle_{\mathbf{0}})\le 0.$$

The desired inequality (3.39) follows from the monotonicity of the logarithm.

(**ii**) The first inequality in

$$|\tau_{\mathbf{c},\mathbf{e}}|\le\tau_{\mathbf{c},\mathbf{0}}\le 2K \qquad (3.42)$$

follows from the second GKS inequality[62, 63] applied in the dual system [where, according to electric-magnetic duality, the defect becomes an average of the corresponding product of spins, see Eq. (3.23)]. Depending on the sign of $\tau_{\mathbf{c},\mathbf{e}}$, duality gives $\langle R_{\mathbf{c}+\mathbf{e}}\rangle\ge\langle R_{\mathbf{e}}\rangle\langle R_{\mathbf{c}}\rangle$ or $\langle R_{\mathbf{e}}\rangle\ge\langle R_{\mathbf{c}}\rangle\langle R_{\mathbf{e}+\mathbf{c}}\rangle$, where $R_{\mathbf{e}}$ is the product of bonds corresponding to non-zero bits in the binary vector $\mathbf{e}$. The second inequality, in a more general form, $\tau_{\mathbf{e}}\equiv\tau_{\mathbf{e},\mathbf{0}}\le 2K$, follows from the Gibbs inequality

$$F_{\mathbf{e}}(G;K)-F_{\mathbf{0}}(G;K)\le 2K\sum_{b:e_b\neq 0}\langle R_b\rangle_{G;K}\le 2K\,\mathrm{wgt}(\mathbf{e}),$$

if we take a minimal-weight vector equivalent to $\mathbf{e}$, in which case $\mathrm{wgt}(\mathbf{e})=d_{\mathbf{e}}$.

(**iii**) To prove the lower bound on the average tension,

$$\zeta\bar{\tau}_p\ge R\ln 2-[\Delta f_{\mathbf{e}}]_p, \qquad (3.44)$$

we first define the constant ζ as the average minimum weight of all 2^k codewords divided by the code length n,

$$\zeta=(2^k n)^{-1}\sum_{\mathbf{c}}d_{\mathbf{c}}. \qquad (A.2)$$

An upper bound on ζ can be obtained if we take the codewords $\mathbf{c}$ as linear combinations of k inequivalent codewords $\mathbf{c}_i$, $i \in \{1, \ldots, k\}$ (it is likely that smaller-weight equivalent codewords can be found). In this case the codewords form a binary code, and the average weight is exactly a half of the length n' of the code[121], where $n' = \left|\cup_{i=1}^{k} I(\mathbf{c}_i)\right|$ is the weight of the union of the supports of the basis codewords. Clearly, $n' \leq n$, which gives $\zeta \leq 1/2$. Combining with a lower bound on the weight of non-trivial codewords, $d_{\mathbf{c}} \geq d_{\mathcal{G}}$, $\mathbf{c} \not\simeq \mathbf{0}$, we obtain

$$\frac{1-2^{-k}}{n} d_G \leq \zeta \leq \frac{1}{2}. \tag{A.3}$$

We now proceed with deriving the inequality (3.44). Start by expanding $Z_{\mathbf{e}}(H^*; K) = \sum_{\mathbf{c}} Z_{\mathbf{e}+\mathbf{c}}(G; K)$, where the summation is over all 2^k mutually inequivalent codewords $\mathbf{c}$. Each of the terms with $\mathbf{c} \not\simeq \mathbf{0}$ can be written in terms of the corresponding tension (3.41),

$$Z_{\mathbf{e}+\mathbf{c}}(G; K) = e^{-\tau_{\mathbf{c},\mathbf{e}}(G;K) d_{\mathbf{c}}} Z_{\mathbf{e}}(G; K).$$

Convexity of the exponent gives

$$\begin{aligned} \frac{Z_{\mathbf{e}}(H^*; K)}{Z_{\mathbf{e}}(G; K)} &= 1 + \sum_{\mathbf{c} \not\simeq \mathbf{0}} \exp(-\tau_{\mathbf{c},\mathbf{e}} d_c) \\ &\geq 2^k \exp\left(-2^{-k} \sum_{\mathbf{c}} \tau_{\mathbf{c},\mathbf{e}} d_{\mathbf{c}} \right), \end{aligned}$$

where for the trivial codeword $\mathbf{c} \simeq \mathbf{0}$ we set $\tau_{\mathbf{0},\mathbf{e}} d_{\mathbf{0}} = 0$. Taking the logarithm and rewriting the sum over codewords in terms of the weighted average, with the help of Eq. (A.2) we obtain

$$\Delta F_{\mathbf{e}}(G, H; K) \geq k \ln 2 - \zeta n \frac{\sum_{\mathbf{c} \not\simeq \mathbf{0}} \tau_{\mathbf{c},\mathbf{e}} d_{\mathbf{c}}}{\sum_{\mathbf{c} \not\simeq \mathbf{0}} d_{\mathbf{c}}}.$$

Eq. (3.44) trivially follows after averaging over disorder and dividing by n.

(**iv**) The inequality

$$K_h(G, H) - K_h^*(H, G) \geq R \ln 2 \tag{3.47}$$

is based on the standard inequality for the derivative of the free energy density, which is just the average energy per bond. For the case of homological difference we obtain, instead,

$$\frac{d}{dK} \Delta f(G, H; K) = \frac{1}{n} \sum_{b \in \mathcal{B}} \left(\langle R_b \rangle_{H^*;K} - \langle R_b \rangle_{G;K} \right). \tag{A.4}$$

The second term can be obtained from the first by freezing the spins corresponding to homologically non-trivial defects; with the help of GKS inequalities we obtain

$$1 \geq \langle R_b \rangle_{G;K} \geq \langle R_b \rangle_{H^*;K} \geq 0,$$

which guarantees the derivative (A.4) to be between -1 and 0. Integration gives the inequality

$$\Delta f_t(K_2) - \Delta f_t(K_1) \leq K_1 - K_2,$$

where $\Delta f_t(K) = \Delta f(G_t, H_t; K)$. We now take $K_1 = K_h(G, H)$ and $K_2 = K_h^*(H, G)$, so that in the limit of the sequence, $\lim_t \Delta f_t(K_1) = 0$ and $\lim_t \Delta f_t(K_2) = R \ln 2$. Eq. (3.47) trivially follows.

A.3 Proof of Theorem 3.2

Theorem 3.2 *Consider a sequence of pairs of weakly dual Ising models defined by pairs of finite binary matrices with mutually orthogonal rows, $G_t H_t^T = 0$, $t \in \mathbb{N}$, where row weights of each G_t do not exceed a fixed m, CSS distances d_{H_t} are increasing with t, and the sequence of CSS rates $R_t \equiv k_t/n_t$ converges, $\lim_t R_t = R$. Then, for any $K \geq 0$ such that $(m-1)\tanh K < 1$, the sequence $\Delta f_t \equiv [\Delta f_{\mathbf{e}}(G_t, H_t; K)]_p$, $t \in \mathbb{N}$, converges to $R \ln 2$.*

Proof. The proof is based on the special case of Theorem 3.1 in the absence of disorder, $p = 0$, and the duality relation (3.45), applied for each pair of matrices, G_t and H_t, with $R_t = k_t/n_t$, and K replaced with its Kramers-Wannier dual, K^*. The condition on K in Theorem 3.1 (with G_t and H_t interchanged) becomes simply $(m-1)\tanh K < 1$. Convergence of sequences $\Delta f_{\mathbf{0}}(H_t, G_t; K^*)$ to 0 and R_t to R implies that of the sequence $\Delta f_{\mathbf{0}}(G_t, H_t; K)$ to $R \ln 2$. ■

A.4 Proof of Statement 3.3

The proof is based on Theorem 9.1.7 from Ref. [69], which bounds cumulants of a random variable X,

$$\kappa_r(X) \equiv \frac{d^r}{dt^r} \ln \mathbb{E}\left(e^{tX}\right)\Big|_{t=0}, \quad r \in \{0, 1, \ldots\}, \tag{A.5}$$

where $X = \sum_{\alpha\in\mathcal{S}} Y_\alpha$ is a sum of random variables with a given *dependency graph*:

Definition A.2 *A graph $\mathcal{D}$ with vertex set $\mathcal{S}$ is called a* dependency graph *for the set of random variables $\{Y_\alpha, \alpha \in \mathcal{S}\}$ if for any two disjoint subsets $\mathcal{S}_1$ and $\mathcal{S}_2$ of $\mathcal{S}$, such that there are no edges in $\mathcal{D}$ connecting an element of $\mathcal{S}_1$ and an element of $\mathcal{S}_2$, the sets of random variables $\{Y_\alpha\}_{\alpha\in\mathcal{S}_1}$ and $\{Y_\alpha\}_{\alpha\in\mathcal{S}_2}$ are independent.*

The corresponding bound reads as follows:

Lemma A.3 (Theorem 9.1.7 from Ref. [69]) *Let $\{Y_\alpha\}_{\alpha\in\mathcal{S}}$ be a family of random variables with dependency graph $\mathcal{D}$. Denote $N = |\mathcal{S}|$ the number of vertices of $\mathcal{D}$ and Δ the maximal degree of $\mathcal{D}$. Assume that the variables Y_α are uniformly bounded by a constant A. Then, for the sum $X = \sum_{\alpha\in\mathcal{S}} Y_\alpha$, and for any $s \in \{0, 1, \ldots\}$, one has*

$$|\kappa_s(X)| \leq 2^{s-1} s^{s-2} N(\Delta + 1)^{s-1} A^s. \tag{A.6}$$

Statement 3.3 *Consider any model in the form (3.13), with an (ℓ, m)-sparse $r \times n$ coupling matrix Θ. The coefficients of the HTS expansion of the free energy density satisfy*

$$|\kappa_{\mathbf{e}}^{(s)}(\Theta; J, h')| \leq 2^{s-1} s^{s-2}\, C\, (\Delta + 1)^{s-1} A^s, \tag{3.49}$$

*where $A \equiv \max(|J|, |h'|)$ and (**a**) with J and h' both non-zero, $\Delta = \ell m$ and $C = r/n + 1$, while (**b**) with $h' = 0$, $\Delta = (\ell - 1)m$ and $C = 1$.*

Proof of Statement 3.3. The s-th coefficient of the HTS for the free energy $F(\Theta; K, h)$ is the scaled cumulant $-\kappa_s(X)/s!$, where $X = J \sum_{b\in\mathcal{B}} R_b + h' \sum_{v\in\mathcal{V}} S_v$. Define the set of random variables Y_α as the union of the set of (scaled) spins hS_v and bonds KR_b,

then $|Y_\alpha| \leq A \equiv \max(|h'|, |J|)$. The corresponding dependency graph $\mathcal{D}$ can be obtained from the bipartite graph defined by the matrix Θ by connecting any pair of nodes for bonds which share the same spin. In the original bipartite graph, each spin node has up to ℓ neighboring bond nodes, and each bond node has up to m neighboring spin nodes. In the modified graph, each bond node also connects with up to $(\ell-1)m$ bond nodes with common spins, which gives the total maximum degree of $\Delta = \ell m$. We also have $N = |\mathcal{V}|+|\mathcal{E}| = r+n$, dividing by n as appropriate for the free energy density we obtain the bound in part (a). With $h = 0$, we can drop the spin nodes from the dependency graph. In this case the maximum degree is $\Delta' = (\ell-1)m$, which gives the result in part (**b**). Notice that in this case $N = n$, and the factor $C = (r/n+1)$ is replaced with $C' = 1$. ■

A.5 Proof of Corollary 3.4.

Corollary A.4 *Any infinite sequence of (ℓ, m)-sparse Ising models, specified in terms of the matrices Θ_j, $j \in \mathbb{N}$, has an infinite subsequence $\Theta_{j(t)}$, $t \in \mathbb{N}$, where $j : \mathbb{N} \to \mathbb{N}$ is strictly increasing, such that (**a**) for each s, the sequence of the coefficients $\kappa_{\mathbf{0}}^{(s)}(\Theta_t; J, 0)$ converges with t, and (**b**) the sequence of free energy densities $f(\Theta_{j(t)}; K)$ has a limit, $\varphi_\Theta(K)$, which is an analytic function of K in the interior of the circle $|K| \leq \{2e\,[(\ell-1)m+1]\}^{-1}$. Here e is the base of natural logarithm.*

Proof. The result in Statement 3.3(b) gives a uniform in t bound on the coefficients of the HTS,

$$\begin{aligned} \frac{|\kappa_s(\Theta_j)|}{s!} &\leq \frac{2^{s-1}s^{s-2}(\Delta+1)^{s-1}J^s}{(2\pi s)^{1/2}(s/e)^s} \\ &= \frac{1}{\sqrt{8\pi}(\Delta+1)}\frac{[2eJ\,(\Delta+1)]^s}{s^{5/2}}, \end{aligned} \tag{A.7}$$

where $\Delta \equiv (\ell-1)m$ and we used the lower bound by Stirling, $r! \geq (2\pi r)^{1/2}(r/e)^r$. The bound (A.7) is uniform in the sequence index $j \in \mathbb{N}$. Thus one can select an infinite subsequence of Θ_j, $\Theta_{j'(t)}$, $t \in \mathbb{N}$, where the function $j' : \mathbb{N} \to \mathbb{N}$ is strictly increasing, so that the coefficients $\kappa_m(\Theta_{j'(t)})$ for $m = 1$ converge with t. Selecting an infinite subsequence of the

one obtained previously to ensure the convergence of the coefficients κ_m for $m = 2, 3, \ldots$, at each step we obtain an infinite subsequence such that all coefficients κ_s with $s \leq m$ converge with t. The statement in part (**a**) is obtained in the limit of $m \to \infty$. The uniform bound (A.7) also applies to the cumulants after we take the limit of the obtained subsequence, which implies absolute convergence (and thus analyticity of the limit) of the HTS for free energy density in the circle $|K| \equiv |\beta|J \leq \{2e[(\ell-1)m+1]\}^{-1}$, which is exactly the statement in part (**b**). ■

A.6 Proof of Lemma 3.5

Lemma A.5 *Consider a sequence of $r_t \times n_t$ binary matrices Θ_t, where $0 < r_t \leq n_t$, and $t \in \mathbb{N}$. For any $M > 0$, define a closed interval $I_M \equiv [0, M]$. (a) There exists a subsequence $\Theta_{t(i)}$, $i \in \mathbb{N}$, where the function $t : \mathbb{N} \to \mathbb{N}$ is strictly increasing, $t(i+1) > t(i)$ for all $i \in \mathbb{N}$, such that the sequence of Ising free energy densities converges for any $K \in I_M$, $f_i(K) \equiv f_{\mathbf{0}}(\Theta_{t(i)}; K) \to f(K)$. (b) The limit $f(K)$ is a continuous non-increasing concave function with left and right derivatives uniformly bounded,*

$$-1 \leq f'_+(K) \leq f'_-(K) \leq 0, \tag{3.50}$$

for all $K \in I_M$.

Proof. For any t, the free energy density $f_t(K) = -n_t^{-1} \ln Z_{\mathbf{0}}(G_t, K)$ is bounded from both sides,

$$-M \leq r_t \ln 2/n_t - K \leq f_t(K) \leq r_t \ln 2/n_t + K \leq \ln 2 + M.$$

Therefore, we can use a subsequence construction to ensure convergence in any point $K \in I_M$. Since the set of rational numbers $\mathbb{Q}$ is countable, we can repeat this construction sequentially on all rational points in I_M. The resulting infinite sequence $f_i(K)$ converges in any rational point $K \in I_M \cap \mathbb{Q}$. Further, the derivative of $f_i(K)$ is uniformly bounded, $-1 \leq f'_i(K) \leq 0$. Since the sequence converges on a dense subset of I_M, this guarantees

the existence and the continuity of the limit in the entire interval. Finally, each of $f_i(K)$ is concave and non-increasing; these properties survive the limit, although the resulting function may not necessarily be strictly concave. Concavity guarantees the existence of one-sided derivatives. The lower and upper bounds on these derivatives are inherited from those for $f_i'(K)$. ■

A.7 Proof of Theorem 3.6

Theorem 3.6 *Let us assume that any one of the following Conditions is true:*

1. *The transition at $T_c'(G)$ is discontinuous or has a divergent specific heat;*
2. *The derivative of $\Delta f(K) = f_G(K) - f_{H^*}(K)$ is discontinuous at $K_h \equiv K_h(G,H)$, or the derivative of $\Delta f(K)$ is continuous at K_h, but its second derivative diverges at K_h;*
3. *Summation over homological defects does not increase the critical temperature, $T_c(G^*) \leq T_c(H)$.*

Then the Kramers-Wannier dual of the critical temperatures $T_c(H)$ satisfies

$$T_c^*(H) \leq T_h(G,H). \tag{3.53}$$

Proof. There are three mutually exclusive possibilities: (a) $T_c'(G) < T_h(G,H)$, (b) $T_c'(G) > T_h(G,H)$, and (c) $T_c'(G) = T_h(G,H)$. In the case (a), $T_c^*(H) = T_c'(G)$, since the functions $f_G(K)$ and $f_{H^*}(K)$ coincide in the homological region, i.e., for $K > K_h(G,H)$; Eq. (3.53) is satisfied. In the case (b), $T_c^*(H) = T_h(G,H)$, in order to recover the non-analyticity point for the homological difference; Eq. (3.53) is saturated. The goal of the Conditions is to deal with the case (c) which implies $T_c^*(H) \geq T_h(G,H)$; a strict inequality would violate Eq. (3.53). In the following we assume (c).

Condition 1 implies that the (negative) curvature of $f_G(K)$ must diverge at $K_h = K_c'(G)$, which must be compensated by a divergent curvature of $f_{H^*}(K)$ in order to make $\Delta f(K)$ strictly convex in this point. In this case $T_c^*(H) = T_c'(G)$; Eq. (3.53) is saturated.

Condition 2 does the same, since divergent positive curvature of $\Delta f(K)$ at K_h can only come from $f_{H^*}(K)$.

Condition 3 is equivalent by duality to $T_c'(G) \geq T_c^*(H)$, which again gives Eq. (3.53) since we assumed (c). ■

A.8 Proof of the lower bound for tension

On an infinite locally planar transitive graph $\mathcal{G}$, we would like to prove the following bound for the asymptotic defect tension (3.55),

$$\frac{d\tau(K)}{dK} \geq 2[m(K)]^2, \tag{A.8}$$

the same inequality as has been previously proved on $\mathbb{Z}^D$ in Ref. [44]. This inequality is a trivial consequence of the following Lemma, which gives a version of Eq. (7) from Ref. [44] suitable to constructing a bound for the defect tension defined by Eq. (3.27).

Lemma A.6 *Let $\mathcal{G} = (\mathcal{V}, \mathcal{E})$ be a finite transitive graph, and G the corresponding vertex-edge incidence matrix with $n = |\mathcal{E}|$ columns. Take a binary vector $\mathbf{e} \in \mathbb{F}_2^n$ selecting a set of edges $\mathcal{E}_\mathbf{e} \subset \mathcal{E}$ of size $|\mathcal{E}_\mathbf{e}| = \mathrm{wgt}(\mathbf{e})$, and a set of vertices $\mathcal{A} \subset \mathcal{V}$ of twice the size, $|\mathcal{A}| = 2\,\mathrm{wgt}(\mathbf{e})$, such that the graph contains edge-disjoint paths connecting each edge to exactly two vertices in $\mathcal{A}$. Then for the Ising model defined on the same graph, at any $K, h \geq 0$, the free energy increment $\delta_\mathbf{e}(K) \equiv F_\mathbf{e}(G; K, h) - F_\mathbf{0}(G; K, h)$ associated with the defect $\mathbf{e}$ satisfies*

$$\frac{d\delta_\mathbf{e}(K)}{dK} \geq \langle S_i \rangle_\mathbf{0} \sum_{v \in \mathcal{A}} \langle S_v \rangle_\mathbf{e}, \tag{A.9}$$

where the average $\langle S_v \rangle_\mathbf{e}$ is calculated in the presence of the defect $\mathbf{e}$; by transitivity $\langle S_i \rangle_\mathbf{0}$ is independent of $i \in \mathcal{V}$.

Proof. The proof is based on two inequalities,

$$\langle S_\mathcal{A} S_\mathcal{B} \rangle_\mathbf{0} \pm \langle S_\mathcal{A} S_\mathcal{B} \rangle_\mathbf{e} \geq \left| \langle S_\mathcal{A} \rangle_\mathbf{0} \langle S_\mathcal{B} \rangle_\mathbf{e} \pm \langle S_\mathcal{A} \rangle_\mathbf{e} \langle S_\mathcal{B} \rangle_0 \right|, \tag{A.10}$$

where $\mathcal{A} \subset \mathcal{V}$ and $\mathcal{B} \subset \mathcal{V}$ are sets of vertices. The inequality with the lower (negative) signs is the Lebowitz comparison inequality[42], while the inequality with the upper signs can be proved using the same technique. In the case of an Ising model on a graph $\mathcal{G} = (\mathcal{V}, \mathcal{E})$, we have

$$\frac{d\delta_{\mathbf{e}}(K)}{dK} = \sum_{ij=b\in\mathcal{E}} \left[\langle S_i S_j\rangle_{\mathbf{0}} - (-1)^{e_b}\langle S_i S_j\rangle_{\mathbf{e}}\right].$$

Applying Eq. (A.10) for each term separately, with the help of transitivity, $\langle S_i\rangle_{\mathbf{0}} \equiv m_0 \geq 0$, $i \in \mathcal{V}$, one gets

$$\frac{d\delta_{\mathbf{e}}(K)}{dK} \geq m_0 \sum_{b=ij\in\mathcal{E}} |m'_i - (-1)^{e_b} m'_j|, \tag{A.11}$$

where $m'_i \equiv \langle S_i\rangle_{\mathbf{e}}$. The statement of the Lemma is obtained by noticing that for a path connecting 1 and f,

$$|m'_1 - m'_2| + |m'_2 - m'_3| + \ldots + |m'_{f-1} - m'_f| \geq m'_f - m'_1,$$

which allows to trade $\mathrm{wgt}(\mathbf{e})$ terms with $+$ signs in the r.h.s. of Eq. (A.11) for the sum of magnetizations m'_v on the $2\,\mathrm{wgt}(\mathbf{e})$ vertices from $\mathcal{A}$. ■

Appendix B

Appendix of Chapter 4

B.1 Proof of Theorem 4.3

Theorem 4.3 *The distance distribution of the ensemble of matrices (Definition 4.2) is given by*

$$\lim_{n\to\infty}\frac{1}{n}\ln p_{n,\theta}^{l,\alpha}=-\alpha\ln q+\max_{\eta\in[0,1-\frac{1}{q}]}\left\{\alpha H_q(\eta)\ln q+\theta l\ln\left(1-\frac{q}{q-1}\eta\right)\right\}$$

and the maximum is at the only solution for η of

$$\left(1-\frac{1}{q}-\eta\right)\left(\ln\frac{1-\eta}{\eta}+\ln(q-1)\right)=\frac{\theta l}{\alpha}$$

where $H_q(x)$ is the q-ary entropy function,

$$H_q(x)\equiv x\log_q(q-1)-x\log_q x-(1-x)\log_q(1-x).$$

Proof. For any codeword of weight w, because of symmetry we can move all the non-zero elements to the first w positions, and only consider these w columns in the matrix. We collect all the vectors that is orthogonal to it. Then we write the generating function $g(x)$ where each term represents one vector in the set. Thus $g^m(x)$ will generate all matrices of m rows that consist of those vectors. The coefficient of the term $z_1^l z_2^l\dots z_w^l$ is the number of matrices that has column weight l.

The number of vectors that is orthogonal to a given vector of full row weight w in $\mathbb{F}_q$ is listed below, the proof is given in Appendix B.5:

weight 1: 0

weight 2: $(q-1)$

weight 3: $(q-1)^2-(q-1)$

...

weight u: $((q-1)^{u-1}+(-1)^u)(1-\frac{1}{q})$

The generating function is given by

$$\begin{aligned} g(x) &= \sum_{\{\boldsymbol{z_u}\}} \left((q-1)^{u-1}+(-1)^u\right)\left(1-\frac{1}{q}\right)(z_{i_1}z_{i_2}\dots z_{i_u}) \\ &= \sum_{\{\boldsymbol{z_u}\}} \frac{1}{q}(q-1)^u(z_{i_1}z_{i_2}\dots z_{i_u}) + \sum_{\{\boldsymbol{z_u}\}} \frac{q-1}{q}(-1)^u(z_{i_1}z_{i_2}\dots z_{i_u}) \\ &= \frac{1}{q}\prod(1+(q-1)z_i) + \frac{q-1}{q}\prod(1+(-1)z_i) \end{aligned}$$

Raise $g(x)$ to mth power,

$$\begin{aligned} g^m(x) &= \frac{1}{q^m}\sum_{j=0}^{m}\binom{m}{j}\left(\prod_i(1+(q-1)z_i)\right)^{m-j}\left((q-1)\prod_i(1-z_i)\right)^j \\ &= \frac{1}{q^m}\sum_{j=0}^{m}\binom{m}{j}(q-1)^j\prod_i(1+(q-1)z_i)^{m-j}(1-z_i)^j \\ &= \frac{1}{q^m}\sum_{j=0}^{m}\binom{m}{j}(q-1)^j\prod_i\left(\sum_{l=0}^{m}K_l^m(j)z_i^l\right) \end{aligned}$$

where $K_l^m(x)=\sum_{i=0}^{l}(-1)^i(q-1)^{l-i}\binom{x}{i}\binom{m-x}{l-i}$ is the q-ary Kravchuk polynomial.

The coefficient of $z_1^l z_2^l\dots z_w^l$ is

$$\frac{1}{q^m}\sum_{j=0}^{m}\binom{m}{j}(q-1)^j(K_l^m(j))^w$$

The total number of matrices orthogonal to the codeword is

$$|\Delta_{n,\theta}^{l,\alpha}| = \frac{1}{q^m}\left(\sum_{j=0}^{m}\binom{m}{j}(q-1)^j(K_l^m(j))^w\right)\left(\binom{m}{l}(q-1)^l\right)^{n-w}$$

while the total number of matrices is

$$|\Delta_n^{l,\alpha}| = \left(\binom{m}{l}(q-1)^l\right)^n$$

Next, we need to estimate $p_{n,\theta}^{l,\alpha}$ as $n \to \infty$

$$\begin{aligned} p_{n,\theta}^{l,\alpha} &= \frac{|\Delta_{n,\theta}^{l,\alpha}|}{|\Delta_n^{l,\alpha}|} \\ &= \frac{\frac{1}{q^m}\left(\sum_{j=0}^{m}\binom{m}{j}(q-1)^j(K_l^m(j))^w\right)}{\left((q-1)^l\binom{m}{l}\right)^w} \\ &= \frac{1}{q^m}\sum_{j=0}^{m}\binom{m}{j}(q-1)^j\left(\frac{K_l^m(j)}{(q-1)^l\binom{m}{l}}\right)^w \end{aligned}$$

Asymptotic form of $K_l^m(x)$ is given by

$$\begin{aligned} K_l^m(x) &= \sum_{i=0}^{l}(-1)^i(q-1)^{l-i}\binom{x}{i}\binom{m-x}{l-i} \\ &\approx (q-1)^l\sum_{i=0}^{l}(-1)^i(q-1)^{-i}\frac{x^i}{i!}\frac{(m-x)^{l-i}}{(l-i)!} \\ &= (q-1)^l\frac{1}{l!}\sum_{i=0}^{l}(-1)^i(q-1)^{-i}\binom{l}{i}x^i(m-x)^{l-i} \\ &= (q-1)^l\frac{1}{l!}(m-x-\frac{1}{q-1}x)^l \\ &= \frac{1}{l!}((q-1)m-qx)^l \end{aligned}$$

Substitute that in $p_{n,\theta}^{l,\alpha}$,

$$\begin{aligned} p_{n,\theta}^{l,\alpha} &\approx \frac{1}{q^m}\sum_{j=0}^{m}\binom{m}{j}(q-1)^j\left(\frac{\frac{1}{l!}((q-1)m-qj)^l}{(q-1)^l\binom{m}{l}}\right)^w \\ &\approx \frac{1}{q^m}\sum_{j=0}^{m}\binom{m}{j}(q-1)^j\left(1-\frac{q}{q-1}\frac{j}{m}\right)^{lw} \\ &\approx \frac{1}{q^m}\max_{\eta}\left\{q^{mH_q(\eta)}\left(1-\frac{q}{q-1}\eta\right)^{lw}\right\} \end{aligned}$$

Substitute with $m = \alpha n$, $w = \theta n$, we find that

$$\lim_{n\to\infty}\frac{1}{n}\ln p_{n,\theta}^{l,\alpha} = -\alpha\ln q + \max_{\eta\in\left[0,1-\frac{1}{q}\right]}\left\{\alpha H_q(\eta)\ln q + \theta l\ln\left(1-\frac{q}{q-1}\eta\right)\right\}$$

and the maximum is at the only solution for η of

$$(1-\frac{1}{q}-\eta)\left(\ln\frac{1-\eta}{\eta}+\ln(q-1)\right)=\frac{\theta l}{\alpha}$$

■

B.2 Duality of Partition Function (4.18)

Define q-ary discrete Fourier transform (DFT) of f_α, a function of a q-ary variable α, to be $f^*_\beta \equiv \sum_{\alpha=0}^{q-1}\frac{\omega^{\alpha\beta}\cdot f_\alpha}{\sqrt{q}}$, where $\omega \equiv e^{\frac{2\pi i}{q}}$. The reverse transform is given by $\sum_\beta \frac{f^*_\beta \omega^{-\alpha\beta}}{\sqrt{q}} = \frac{1}{q}\sum_\beta \omega^{-\alpha\beta}(\sum_j \omega^{j\beta}f_j) = \frac{1}{q}\sum_j\sum_\beta \omega^{(-\alpha+j)\beta}f_j = \frac{1}{q}\sum_j q\delta(j,\alpha)f_j = f_\alpha$.

For the simplicity of notation, we introduce a reduced partition function Z_r, which is the partition function (4.17) without the constant in the front:

$$Z = \frac{1}{q^{N_s-r}\prod_{i=1}^r d_i}\left(\frac{1}{e^K+q-1}\right)^{N_b} Z_r,$$
$$Z_r \equiv \sum_{\{s_i\}}\prod_b \omega^{\sum_i s_i\Theta_{ib}m_b}e^{K\delta(\sum_i s_i\Theta_{ib}-e_b,0)}$$

Take $\alpha_b \equiv \sum_i s_i\Theta_{ib}-e_b$ as a variable, and apply the reverse Fourier transform to the function $f_{\alpha_b}=e^{K\delta(\alpha_b,0)}$:

$$\begin{aligned}
Z_r &= \sum_{\{s_i\}}\prod_b \omega^{\sum_i s_i\Theta_{ib}m_b}\sum_{\beta_b}\frac{f^*_\beta\omega^{-(\sum_i s_i\Theta_{ib}-e_b)\beta_b}}{\sqrt{q}}\\
&= q^{-N_b/2}\sum_{\{s_i\}}\prod_b\sum_{\beta_b} f^*_{\beta_b}\omega^{(\sum_i s_i\Theta_{ib}(m_b-\beta_b))+e_b\beta_b}\\
&= q^{-N_b/2}\sum_{\{s_i\}}\sum_{\{\beta_b\}}\prod_b f^*_{\beta_b}\omega^{(\sum_i s_i\Theta_{ib}(m_b-\beta_b))+e_b\beta_b}\\
&= q^{-N_b/2}\sum_{\{s_i\}}\sum_{\{\beta_b\}}(\prod_b f^*_{\beta_b})\omega^{\sum_b(\sum_i s_i\Theta_{ib}(m_b-\beta_b))+e_b\beta_b}\\
&= q^{-N_b/2}\sum_{\{\beta_b\}}(\prod_b f^*_{\beta_b})\sum_{\{s_i\}}\omega^{\sum_b(\sum_i s_i\Theta_{ib}(m_b-\beta_b))+e_b\beta_b}\\
&= q^{-N_b/2}\sum_{\{\beta_b\}}(\prod_b f^*_{\beta_b})\omega^{\sum_b e_b\beta_b}\sum_{\{s_i\}}\prod_i\omega^{s_i\sum_b(\Theta_{ib}(m_b-\beta_b))}\\
&= q^{-N_b/2}\sum_{\{\beta_b\}}(\prod_b f^*_{\beta_b})\omega^{\sum_b e_b\beta_b}\prod_i\sum_{s_i}\omega^{s_i\sum_b(\Theta_{ib}(m_b-\beta_b))}
\end{aligned}$$

All the terms that have $\sum_b \Theta_{ib}(m_b - \beta_b) \neq 0$ will be zero, so all the non zero terms must satisfy $\sum_b \Theta_{ib}(m_b - \beta_b) = 0$. We can rewrite $\beta_b = m_b - \sum_i \sigma_i \Theta^*_{ib}$, where Θ^*_{ib} is the exact dual matrix of Θ_{ib}, which can be found through Smith normal form. So we have

$$\begin{aligned} Z_r &= q^{-N_b/2} \sum_{\{\beta_b = m_b - \sigma_i \Theta^*_{ib}\}} (\prod_b f^*_{\beta_b}) q^{N_s} \omega^{\sum_b e_b \beta_b} \\ &= q^{N_s - N_b/2} \sum_{\{\beta_b = m_b - \sigma_i \Theta^*_{ib}\}} (\prod_b f^*_{\beta_b}) \omega^{\sum_b e_b \beta_b} \end{aligned}$$

For any vector $\boldsymbol{\sigma}$, if $\boldsymbol{v}\Theta^* = 0$, $\boldsymbol{\sigma}\Theta^* = (\boldsymbol{\sigma} + \boldsymbol{v})\Theta^*$. The total number of vectors $\boldsymbol{v}$ such that $\boldsymbol{v}\Theta^* = 0$ is $q^{N^*_s - r^*} \prod_{i=1}^{r^*} d^*_i$, where d^*_i are the non-zero invariants of the Smith normal form of Θ^* and r^* is the number of them.

$$\begin{aligned} Z_r &= \left(q^{N_s - \frac{N_b}{2} - N^*_s + r^*} \frac{1}{\prod_{i=1}^{r^*} d^*_i} \right) \sum_{\{\sigma_i\}} \prod_b f^*_{m_b - \sigma_i \Theta^*_{ib}} \omega^{e_b (m_b - \sum_i \sigma_i \Theta^*_{ib})} \\ &= \left(q^{N_s - \frac{N_b}{2} - N^*_s + r^*} \frac{1}{\prod_{i=1}^{r^*} d^*_i} \right) \omega^{\sum_b e_b m_b} \sum_{\{\sigma_i\}} \prod_b f^*_{m_b - \sigma_i \Theta^*_{ib}} \omega^{-\sum_i \sigma_i \Theta^*_{ib} e_b} \end{aligned}$$

Next we evaluate f^*_β explicitly. Given that $f_\alpha = e^{K\delta(\alpha,0)} = (e^K - 1)\delta(\alpha, 0) + 1$,

$$\begin{aligned} f^*_\beta &= \sum_{\alpha=0}^{q-1} \frac{\omega^{\alpha\beta} e^{K\delta(\alpha,0)}}{\sqrt{q}} \\ &= \begin{cases} \frac{q-1+e^K}{\sqrt{q}}, & \text{when } \beta = 0 \\ \frac{e^K - 1}{\sqrt{q}}, & \text{when } \beta \neq 0 \end{cases} \\ &= \left(\frac{e^K - 1}{\sqrt{q}} \right) \left[\frac{q}{e^K - 1} \delta(\beta, 0) + 1 \right] \\ &= \left(\frac{e^K - 1}{\sqrt{q}} \right) \left[(e^{K^*} - 1)\delta(\beta, 0) + 1 \right] \end{aligned}$$

In the last equality we define K^*, the dual of K, by the equation $e^{K^*} - 1 = \frac{q}{e^K - 1}$. So the self-dual temperature is at $K_{sd} = \ln(1 + \sqrt{q})$.

Apply the duality transform to the full partition function,

$$
\begin{aligned}
Z =& \frac{1}{q^{N_s-r}\prod_{i=1}^{r} d_i}\left(\frac{1}{e^K+q-1}\right)^{N_b} Z_r \\
=& \frac{1}{q^{N_s-r}\prod_{i=1}^{r} d_i}\left(\frac{1}{e^K+q-1}\right)^{N_b} \\
& \left(q^{N_s-\frac{N_b}{2}-N_s^*+r^*}\frac{1}{\prod_{i=1}^{r^*} d_i^*}\right)\left(\frac{e^K-1}{\sqrt{q}}\right)^{N_b}\omega^{\sum_b e_b m_b}\sum_{\{\sigma_i\}}\prod_b \omega^{-\sum_i \sigma_i \Theta_{ib}^* e_b} e^{K^*\delta(m_b-\sigma_i\Theta_{ib}^*,0)} \\
=& \frac{q^{N_s^*-r^*}\prod_{i=1}^{r^*} d_i^*}{q^{N_s-r}\prod_{i=1}^{r} d_i}\left(\frac{e^{K^*}+q-1}{e^K+q-1}\right)^{N_b}\left(q^{N_s-\frac{N_b}{2}-N_s^*+r^*}\frac{1}{\prod_{i=1}^{r^*} d_i^*}\right)\left(\frac{e^K-1}{\sqrt{q}}\right)^{N_b}\omega^{\sum_b e_b m_b} Z^* \\
=& \frac{q^r}{\prod_{i=1}^{r} d_i} q^{-\frac{N_b}{2}}\left(\frac{e^{K^*}+q-1}{e^K+q-1}\right)^{N_b}\left(\frac{e^K-1}{\sqrt{q}}\right)^{N_b}\omega^{\sum_b e_b m_b} Z^*
\end{aligned}
$$

where Z^* is the partition function of the dual model, defined as

$$
Z^* \equiv \frac{1}{q^{N_s^*-r^*}(\prod_{i=1}^{r^*} d_i^*)(e^{K^*}+q-1)^{N_b}}\sum_{s_i}\prod_b \omega^{\sum_i s_i\Theta_{ib}^* m_b^*} e^{K^*\delta(\sum_i s_i\Theta_{ib}^*-e_b^*,0)}
$$

Apply the following identities:

$$
\begin{aligned}
e^{K^*}+q-1 &= \frac{q}{e^K-1}+q = \frac{qe^K}{e^K-1} \\
e^K+q-1 &= \frac{qe^{K^*}}{e^{K^*}-1} \\
\sqrt{q} &= \sqrt{(e^K-1)(e^{K^*}-1)} \\
q^{N_b} &= \frac{q^r}{\prod_{i=1}^{r} d_i}\frac{q^{r^*}}{\prod_{i=1}^{r^*} d_i^*}
\end{aligned}
$$

One can see that

$$
Z = (\frac{q^r}{\prod_{i=1}^{r} d_i})^{\frac{1}{2}}(\frac{q^{r^*}}{\prod_{i=1}^{r^*} d_i^*})^{-\frac{1}{2}}(\frac{e^K}{\sqrt{e^K-1}})^{N_b}(\frac{\sqrt{e^{K^*}-1}}{e^{K^*}})^{N_b}\omega^{\sum_b e_b m_b} Z^*,
$$

so the duality reads

$$
(\frac{\prod_{i=1}^{r} d_i}{q^r})^{\frac{1}{2}}(\frac{\sqrt{e^K-1}}{e^K})^{N_b} Z_{\boldsymbol{e},\boldsymbol{m}}(\Theta,K) = (\frac{\prod_{i=1}^{r^*} d_i^*}{q^{r^*}})^{\frac{1}{2}}(\frac{\sqrt{e^{K^*}-1}}{e^{K^*}})^{N_b}\omega^{\boldsymbol{e}\cdot\boldsymbol{m}} Z_{\boldsymbol{e^*},\boldsymbol{m^*}}(\Theta^*,K^*) \tag{B.1}
$$

where $\boldsymbol{m^*} \equiv \boldsymbol{e}$, $\boldsymbol{e^*} \equiv -\boldsymbol{m}$, $K^* \equiv \ln(1+\frac{q}{e^K-1})$, and Θ^* is the exact dual of Θ.

B.3 Proof of Correlation Function Equality (4.38) and Inequality (4.39)

The correlation function is defined as

$$[Q^{\boldsymbol{m}}_{tot}(\boldsymbol{e},\beta)] \equiv \left[\frac{Z_{\boldsymbol{e},\boldsymbol{m}}(\tilde{G}^*,\beta)}{Z_{\boldsymbol{e},0}(\tilde{G}^*,\beta)}\right] = \sum_{\boldsymbol{e}} \left(P(\boldsymbol{e}) \frac{Z_{\boldsymbol{e},\boldsymbol{m}}(\tilde{G}^*,\beta)}{Z_{\boldsymbol{e},0}(\tilde{G}^*,\beta)} \right)$$

where

$$P(\boldsymbol{e}) = \prod_{i=1}^{N_b} (\frac{p}{q-1})^{\delta(e_i,0)} (1-p)^{1-\delta(e_i,0)} = \prod_b \frac{e^{\beta_p J \delta(e_b,0)}}{e^{\beta_p J}+q-1}$$

$$Z_{\boldsymbol{e},\boldsymbol{m}}(\Theta,\beta) = \frac{1}{q^{N_s-r}\prod_{i=1}^r d_i} \sum_{\boldsymbol{\sigma}} \prod_b \omega^{\sum_s \sigma_s \Theta_{sb} m_b} \frac{e^{\beta J \delta(\sum_s \sigma_s \Theta_{sb} - e_b, 0)}}{e^{\beta J}+q-1}$$

Define the gauge transformation (G.T.) of a partition function on a graph with an incidence matrix Θ to be:

$$Z_{\boldsymbol{e}}(\Theta) = \sum_{\boldsymbol{\sigma}} f(\boldsymbol{\sigma}\Theta, \boldsymbol{e}) \overset{G.T.}{\rightarrow} \frac{1}{q^{N_s}} \sum_{\boldsymbol{\alpha}} \sum_{\boldsymbol{\sigma}} f((\boldsymbol{\sigma}+\boldsymbol{\alpha})\Theta, \boldsymbol{e}+\boldsymbol{\alpha}\Theta) = \frac{1}{q^{N_s}} \sum_{\boldsymbol{\alpha}} Z_{\boldsymbol{e}+\boldsymbol{\alpha}\Theta}(\Theta) \quad \text{(B.2)}$$

Here we introduced an extra set of spins $\boldsymbol{\alpha}$ that runs through all possible combinations of length N_s q-ary vectors, just like $\boldsymbol{\sigma}$. For each term inside the summation, the transformation goes as $\sigma_s \rightarrow \sigma_s + \alpha_s$ and $\boldsymbol{e} \rightarrow \boldsymbol{e} + \boldsymbol{\alpha}\Theta$. Notice the identity $\sum_{\boldsymbol{\sigma}} f((\boldsymbol{\sigma}+\boldsymbol{\alpha})\Theta, \boldsymbol{e}+\boldsymbol{\alpha}\Theta) = \sum_{\boldsymbol{\sigma}} f(\boldsymbol{\sigma}\Theta, \boldsymbol{e}+\boldsymbol{\alpha}\Theta)$, since for any $\boldsymbol{\alpha}$, $\boldsymbol{\sigma}+\boldsymbol{\alpha}$ runs through all vectors just like $\boldsymbol{\sigma}$ alone, thus we have the equality after the gauge transformation.

For a function of a summation of partition functions over $\boldsymbol{e}$, the gauge transformation is

$$\sum_{\boldsymbol{e}} F(Z_{\boldsymbol{e}}(\Theta)) \overset{G.T.}{=} \frac{1}{q^{N_s}} \sum_{\boldsymbol{e}} \sum_{\boldsymbol{\alpha}} F(Z_{\boldsymbol{e}+\boldsymbol{\alpha}\Theta}(\Theta)) = \frac{1}{q^{N_s}} \sum_{\boldsymbol{e}} \sum_{\boldsymbol{\alpha}} F(f((\boldsymbol{\sigma}+\boldsymbol{\alpha})\Theta, \boldsymbol{e}+\boldsymbol{\alpha}\Theta)) \quad \text{(B.3)}$$

Notice that for any $\boldsymbol{\alpha}$, as $\boldsymbol{e}$ runs through all possible vectors, $\boldsymbol{e}+\boldsymbol{\alpha}\Theta$ runs through all possible vectors as well, and the summation of $\boldsymbol{\alpha}$ gives a factor of q^{N_s}, and the equality follows.

Proof of Eq. (4.38). Apply the gauge transformation to the correlation functions:

$$\begin{aligned}
[Q^{\boldsymbol{m}}_{tot}(\boldsymbol{e},\beta)] &\overset{G.T.}{=} \frac{1}{q^{N_s^*}}\sum_{\boldsymbol{e}}\left(\sum_{\boldsymbol{\alpha}} P(\boldsymbol{e}+\boldsymbol{\alpha}\tilde{G}^*)\omega^{\sum_s\sum_b \alpha_s \tilde{G}^*_{sb}m_b}\frac{Z_{\boldsymbol{e},\boldsymbol{m}}(\tilde{G}^*,\beta)}{Z_{\boldsymbol{e},0}(\tilde{G}^*,\beta)}\right)\\
&= \frac{1}{q^{N_s^*}}\sum_{\boldsymbol{e}}\left(q^{N_s^*-r^*}\prod_{i=1}^{r} d_i^* Z_{-\boldsymbol{e},\boldsymbol{m}}(\tilde{G}^*,\beta_p)\frac{Z_{\boldsymbol{e},\boldsymbol{m}}(\tilde{G}^*,\beta)}{Z_{\boldsymbol{e},0}(\tilde{G}^*,\beta)}\right)\\
&= \frac{\prod_{i=1}^{r} d_i^*}{q^{r^*}}\sum_{\boldsymbol{e}}\left(\frac{Z_{\boldsymbol{e},\boldsymbol{m}}(\tilde{G}^*,\beta)Z_{-\boldsymbol{e},\boldsymbol{m}}(\tilde{G}^*,\beta_p)}{Z_{\boldsymbol{e},0}(\tilde{G}^*,\beta)}\right)
\end{aligned}$$

$$\begin{aligned}
[Q^{\boldsymbol{m}}_{tot}(\boldsymbol{e},\beta)Q^{-\boldsymbol{m}}_{tot}(\boldsymbol{e},\beta_p)] &= \left[\frac{Z_{\boldsymbol{e},\boldsymbol{m}}(\tilde{G}^*,\beta)}{Z_{\boldsymbol{e},0}(\tilde{G}^*,\beta)}\frac{Z_{\boldsymbol{e},-\boldsymbol{m}}(\tilde{G}^*,\beta_p)}{Z_{\boldsymbol{e},0}(\tilde{G}^*,\beta_p)}\right]\\
&= \sum_{\boldsymbol{e}}\left(P(\boldsymbol{e})\frac{Z_{\boldsymbol{e},\boldsymbol{m}}(\tilde{G}^*,\beta)}{Z_{\boldsymbol{e},0}(\tilde{G}^*,\beta)}\frac{Z_{\boldsymbol{e},-\boldsymbol{m}}(\tilde{G}^*,\beta_p)}{Z_{\boldsymbol{e},0}(\tilde{G}^*,\beta_p)}\right)\\
&\overset{G.T.}{=} \frac{1}{q^{N_s^*}}\sum_{\boldsymbol{e}}\left(\sum_{\boldsymbol{\alpha}} P(\boldsymbol{e}+\boldsymbol{\alpha}\tilde{G}^*)\frac{Z_{\boldsymbol{e},-\boldsymbol{m}}(\tilde{G}^*,\beta)}{Z_{\boldsymbol{e},0}(\tilde{G}^*,\beta)}\frac{Z_{\boldsymbol{e},\boldsymbol{m}}(\tilde{G}^*,\beta_p)}{Z_{\boldsymbol{e},0}(\tilde{G}^*,\beta_p)}\right)\\
&= \frac{1}{q^{N_s^*}}\sum_{\boldsymbol{e}}\left(q^{N_s^*-r^*}\prod_{i=1}^{r} d_i^* Z_{-\boldsymbol{e},0}(\tilde{G}^*,\beta_p)\frac{Z_{\boldsymbol{e},\boldsymbol{m}}(\tilde{G}^*,\beta)}{Z_{\boldsymbol{e},0}(\tilde{G}^*,\beta)}\frac{Z_{\boldsymbol{e},-\boldsymbol{m}}(\tilde{G}^*,\beta_p)}{Z_{\boldsymbol{e},0}(\tilde{G}^*,\beta_p)}\right)\\
&= \frac{\prod_{i=1}^{r} d_i^*}{q^{r^*}}\sum_{\boldsymbol{e}}\left(\frac{Z_{-\boldsymbol{e},0}(\tilde{G}^*,\beta_p)}{Z_{\boldsymbol{e},0}(\tilde{G}^*,\beta_p)}\frac{Z_{\boldsymbol{e},\boldsymbol{m}}(\tilde{G}^*,\beta)Z_{\boldsymbol{e},-\boldsymbol{m}}(\tilde{G}^*,\beta_p)}{Z_{\boldsymbol{e},0}(\tilde{G}^*,\beta)}\right)
\end{aligned}$$

We can see that $Z_{\boldsymbol{e},\boldsymbol{m}}(\tilde{G}^*,\beta)$ is unchanged under $\boldsymbol{\sigma}\to-\boldsymbol{\sigma},\boldsymbol{e}\to-\boldsymbol{e},\boldsymbol{m}\to-\boldsymbol{m}$, so we have $Z_{\boldsymbol{e},\boldsymbol{m}}(\tilde{G}^*,\beta)=Z_{-\boldsymbol{e},-\boldsymbol{m}}(\tilde{G}^*,\beta)$. The equality $[Q^{\boldsymbol{m}}_{tot}(\boldsymbol{e},\beta)]=[Q^{\boldsymbol{m}}_{tot}(\boldsymbol{e},\beta)Q^{-\boldsymbol{m}}_{tot}(\boldsymbol{e},\beta_p)]$ follows. ■

Proof of Eq. (4.39). Another identity $[f(\boldsymbol{e})]=\sum_{\boldsymbol{e}}(P(\boldsymbol{e})f(\boldsymbol{e}))=\sum_{\boldsymbol{e}}(P(-\boldsymbol{e})f(-\boldsymbol{e}))=\sum_{\boldsymbol{e}}(P(\boldsymbol{e})f(-\boldsymbol{e}))=[f(-\boldsymbol{e})]$ shows that $[Q^{\boldsymbol{m}}_{tot}(\boldsymbol{e},\beta)]=[Q^{-\boldsymbol{m}}_{tot}(-\boldsymbol{e},\beta)]=[Q^{-\boldsymbol{m}}_{tot}(\boldsymbol{e},\beta)]$. And we also have $Z_{\boldsymbol{e},-\boldsymbol{m}}(\Theta,\beta)=\overline{Z}_{\boldsymbol{e},\boldsymbol{m}}(\Theta,\beta)$, where $\overline{f}$ is the complex conjugate of f. Now we define $A=Q^{\boldsymbol{m}}_{tot}(\boldsymbol{e},\beta)$, $B=Q^{\boldsymbol{m}}_{tot}(\boldsymbol{e},\beta_p)$, we see that $[A]=[\overline{A}]=[A\overline{B}]=[\overline{A}B]$, $[B]=[\overline{B}]=[B\overline{B}]$, so they must be real.

For any real number t, the following inequality holds:

$$[(A+tB)(\overline{A}+t\overline{B})]\geq 0$$

so that

$$[A\overline{A}]+[A\overline{B}]t+[\overline{A}B]t+[B\overline{B}]t^2\geq 0$$

$$[A\overline{A}] + 2[A\overline{B}]t + [B\overline{B}]t^2 \geq 0$$

which implies

$$4[A\overline{B}]^2 - 4[A\overline{A}][B\overline{B}] \leq 0$$

$$[A\overline{B}]^2 \leq [A\overline{A}][B\overline{B}]$$

thus

$$[A]^2 = [A\overline{B}]^2 \leq [A\overline{A}][B\overline{B}] \leq [B\overline{B}] = [B]$$

And the inequality $[Q^{\boldsymbol{m}}_{\text{tot}}(\boldsymbol{e}, \beta)]^2 \leq [Q^{\boldsymbol{m}}_{\text{tot}}(\boldsymbol{e}, \beta_p)]$ follows. ■

B.4 Proof of Theorem 4.7

Theorem 4.7 *Any sequence of q-ary CSS codes whose distances scale with n at least logarithmically ($d \geq D \ln n$, $D > 0$) with generator weights not exceeding m_X, m_Z can be decoded with vanishing error probabilities if channel probabilities (p_X, p_Z) for independent X/Z errors satisfy*

$$\begin{aligned} (m_X - 1)\Upsilon_{CSS}(p_Z) &\leq e^{-1/D} \\ (m_Z - 1)\Upsilon_{CSS}(p_X) &\leq e^{-1/D} \end{aligned} \tag{4.6}$$

where $\Upsilon_{CSS}(p) \equiv \left(\sqrt{1-p} + \sqrt{p(q-1)}\right)^2 - 1$.

Proof. This is a generalization of Theorem 2 in [98] for q-ary code.

For any random qudit error $\boldsymbol{e}$ and a codeword $\boldsymbol{c}$, the probability distribution of an element in the error is:

$$\begin{cases} P_{\boldsymbol{c}}(e_i = 0) = 1 - p \\ P_{\boldsymbol{c}}(e_i = c_i) = \frac{p}{q-1} \\ P_{\boldsymbol{c}}(e_i \neq 0, e_i \neq c_i) = \frac{q-2}{q-1}p \end{cases}$$

for any $1 \leq i \leq n$.

Denote the weight of the codeword to be ω. For any error $\boldsymbol{e}$, denote the number of error positions corresponding to the second and third cases above to be a and b, respectively.

To successfully decode by minimum energy decoding, it is required that $P_{\boldsymbol{c}}(\boldsymbol{e}) < P_{\boldsymbol{c}}(\boldsymbol{e}+\boldsymbol{c})$ for any $\boldsymbol{c}$, where $P_{\boldsymbol{c}}(\boldsymbol{e})$ and $P_{\boldsymbol{c}}(\boldsymbol{e}+\boldsymbol{c})$ are given by

$$P_{\boldsymbol{c}}(\boldsymbol{e}) = (1-p)^{w-a-b}(\frac{p}{q-1})^{a}\left(\frac{q-2}{q-1}p\right)^{b}$$

and

$$P_{\boldsymbol{c}}(\boldsymbol{e}+\boldsymbol{c}) = (\frac{p}{q-1})^{w-a-b}(1-p)^{a}\left(\frac{q-2}{q-1}p\right)^{b}$$

respectively. The ratio

$$\frac{P_{\boldsymbol{c}}(\boldsymbol{e})}{P_{\boldsymbol{c}}(\boldsymbol{e}+\boldsymbol{c})} = \left(\frac{p}{(q-1)(1-p)}\right)^{2a+b-w}$$

must be less than 1 for successful decoding.

Consider $p < 1-\frac{1}{q}$, the decoding will fail whenever $a+\frac{b}{2} > \frac{w}{2}$. Summing the probability over all errors that would result in decoding failure for any codeword:

$$
\begin{aligned}
P_{\boldsymbol{c},\text{fail}} &= \sum_{\{\boldsymbol{e}|a+\frac{b}{2}>\frac{w}{2}\}} P_{\boldsymbol{c}}(\boldsymbol{e}) \\
&\leq \sum_{\{\boldsymbol{e}|\text{any } a,b\}} P_{\boldsymbol{c}}(\boldsymbol{e}) \sqrt{\frac{P_{\boldsymbol{c}}(\boldsymbol{e}+\boldsymbol{c})}{P_{\boldsymbol{c}}(\boldsymbol{e})}} \\
&= \sum_{\{\boldsymbol{e}|\text{any } a,b\}} (\sqrt{1-p})^{w-b} \left(\sqrt{\frac{p}{q-1}}\right)^{w-b} \left(\frac{q-2}{q-1}p\right)^{b} \\
&= \sum_{0\leq a,b\leq w} \binom{w}{b}\binom{w-b}{a} \left(\sqrt{\frac{p(1-p)}{q}}\right)^{w-b} \left(\frac{q-2}{q-1}p\right)^{b} \\
&= \sum_{b=0}^{w} \left(\sum_{a=0}^{w-b} \binom{w-b}{a}\right) \binom{w}{b} \left(\sqrt{\frac{p(1-p)}{q}}\right)^{w-b} \left(\frac{q-2}{q-1}p\right)^{b} \\
&= \sum_{b=0}^{w} 2^{w-b} \binom{w}{b} \left(\sqrt{\frac{p(1-p)}{q}}\right)^{w-b} \left(\frac{q-2}{q-1}p\right)^{b} \\
&= \sum_{b=0}^{w} \binom{w}{b} \left(2\sqrt{\frac{p(1-p)}{q}}\right)^{w-b} \left(\frac{q-2}{q-1}p\right)^{b} \\
&= \left(\frac{q-2}{q-1}p + 2\sqrt{(1-p)\frac{p}{q-1}}\right)^{w} \\
&= \left(1-\left(\sqrt{1-p}-\sqrt{\frac{p}{q-1}}\right)^{2}\right)^{w}
\end{aligned}
$$

Thus the probability of decoding failure is upper bounded:

$$P_{\text{fail}} \leq \sum_{\boldsymbol{c}} P_{\boldsymbol{c},\text{fail}} = \sum_{w=d}^{\infty} N_w P_{\boldsymbol{c},\text{fail}}$$

where N_w is the number of irreducible codewords with weight w. We only need to consider irreducible codewords because for a reducible codeword $c' = c_1 + c_2$ where c_1 and c_2 have non-overlapping supports, any error that would result in decoding failure for c' will also result in failure for c_1 or c_2, so we can exclude reducible codewords in the summation so that we don't count the same errors multiple times.

Next, we bound the number of irreducible codewords with weight w for a LDPC code of row weight m: $N_w(m) \leq (q-1)n((q-1)(m-1))^{w-1}$. The logic goes as the following:

Suppose we want to construct an irreducible codeword. Starting from a zero vector, first we assign a non-zero value to any position, there are $(q-1)n$ choices. Then, some rows in the generator matrix are not satisfied. The finished codeword must be orthogonal to all the rows in the generator, so it must have at least one other non-zero element in the support of any of the unsatisfied rows. We need to assign another non-zero value to a position in the support of an unsatisfied row. There are $m-1$ positions to choose from. The weight of the codeword is w, so there are at most $(q-1)n((q-1)(m-1))^{w-1}$ choices.

Thus the upper bound of the failure probability is:

$$\begin{aligned} P_{\text{fail}} &\leq \sum_{w=d}^{\infty} \frac{n}{m-1} \left((q-1)(m-1) \left(1 - \left(\sqrt{1-p} - \sqrt{\frac{p}{q-1}} \right)^2 \right) \right)^w \\ &= \frac{n}{m-1} \frac{\left((m-1) \left(\left(\sqrt{1-p} + \sqrt{p(q-1)} \right)^2 - 1 \right) \right)^d}{1 - (m-1) \left(\left(\sqrt{1-p} + \sqrt{p(q-1)} \right)^2 - 1 \right)} \end{aligned}$$

For a code of which distance increases as $\lim_{n\to\infty} \frac{d}{\ln(n)} = D$, the probability of decoding failure converges to 0 if

$$(m-1) \left(\left(\sqrt{1-p} + \sqrt{p(q-1)} \right)^2 - 1 \right) < e^{-1/D} \tag{B.4}$$

In the case where $\lim_{n\to\infty} \frac{d}{\ln(n)} = \infty$ as in toric code or hypergraph-product code, the condition is simply

$$(m-1) \left(\left(\sqrt{1-p} + \sqrt{p(q-1)} \right)^2 - 1 \right) < 1$$

■

B.5 Proof of Theorem 4.6

Theorem 4.6 *A codeword of weight δn in any q-ary (l,m)-limited quantum or classical LDPC code can be found with complexity 2^{Fn}, where*

$$F = \delta \log_2(\gamma_m(m-1)),$$

$\gamma_m \in (1, \gamma_\infty)$ *grows monotonically with* m *and is upper bounded as the following:*

If all entries of the parity check matrix are coprime with q, γ_m *is upper bounded by*

$$\gamma_m \leq \min\left[\frac{q-2}{(m-1)((q-1)^{\frac{1}{m-1}}-1)}, \frac{1}{q^{\frac{1}{q-1}}-1}\right] \tag{4.5}$$

More generally, with some entries in the parity check matrix that are not coprime with q, γ_m *is upper bounded by*

$$\gamma_m \leq \frac{q-2}{(m-1)((3-\frac{4}{q})^{\frac{1}{m-1}}-1)}.$$

Here we improve the upper bound on the complexity coefficient γ_m of distance verification algorithm in the coprime case (explained below) by finding a better estimation on $N_v(q, b)$, defined in Section V of [93]. A different upper bound was found for codes in general case.

B.5.1 Coprime case

Consider a vector $\boldsymbol{b}$ of which all elements are coprime with q. Let $N_v(q)$ denote the number of q-ary vectors $\boldsymbol{c}$ of length v that satisfy the restrictions

$$\boldsymbol{c} \cdot \boldsymbol{b} = a$$

$$\forall I \subsetneq \{1, 2, \ldots, v\}, \sum_{i \in I} c_i b_i \neq 0$$

where a is an arbitrary number in $\mathbb{Z}_q$. The second inequality is the irreducible property, which can only be satisfied for $v \leq q-1$.

We prove the following upper bound

$$N_v(q) \leq (q-2)(q-3)\ldots(q-v) = \frac{(q-2)!}{(q-v-1)!} \tag{B.5}$$

Proof. If $v = 1$, $N_v(q)$ is just 1. For any other v, the first element has $q-2$ choices, not 0 or a. And every time another element is selected, it will remove at least one possible value from which the next element can be chosen.

Consider this sequence of summations: $c_1b_1, c_1b_1+c_2b_2, c_1b_1+c_2b_2+c_3b_3, \ldots, c_1b_1+\cdots+c_vb_v$. If any two of them are equal, the vector is reducible. So every time a new element

is added, the list of summation of all combinations of subsets of the elements will increase by at least one, which means the choices for the value of the next element will decrease by at least one. And after the first $v-1$ elements are determined, the last element doesn't have a choice, so the product has $v-1$ terms. This gives the upper bound of $N_v(q)$ above. ■

Next, we follow the proof in [93] except that we replace the upper bound on $N_v(q)$ with the one given above. We look for the root of the polynomial of variable z,

$$\sum_{v=1}^{m-1} z^v N_v(q) \binom{m-1}{v} = 1$$

and find better upper bounds on $\gamma_m \equiv 1/((m-1)z)$.

Proof of the inequality $\gamma_m \leq \frac{1}{q^{\frac{1}{q-1}}-1}$.

$N_v(q) = 0$ for $v \geq q-1$. As $m \to \infty$ the equation becomes

$$\sum_{v=1}^{q-1} \frac{(m-1)^v}{v!} N_v(q) z^v \geq 1$$

replace $(m-1)z$ with $\frac{1}{\gamma_\infty}$,

$$\sum_{v=1}^{q-1} \frac{N_v(q)}{v!} (\frac{1}{\gamma_\infty})^v \geq 1$$

$$\sum_{v=1}^{q-1} \frac{(q-2)!}{(q-v-1)!v!} (\frac{1}{\gamma_\infty})^v \geq 1$$

$$\frac{1}{q-1} \sum_{v=1}^{q-1} \binom{q-1}{v} (\frac{1}{\gamma_\infty})^v \geq 1$$

$$(1+\frac{1}{\gamma_\infty})^{q-1} - 1 \geq q-1$$

$$\gamma_\infty \geq \frac{1}{q^{\frac{1}{q-1}}-1}$$

And since $\gamma_m \leq \gamma_\infty$, this also upper bounds γ_m. ■

Proof of the inequality $\gamma_m \leq \frac{q-2}{(m-1)((q-1)^{\frac{1}{m-1}}-1)}$.

The bound (B.5) can only be applied on γ_∞, and for γ_m there is no simple expression for the solution. So instead we may use a different bound for $N_v(q)$, since from (B.5) we can easily see that $N_v(q) \leq (q-2)^{v-1}$.

Then we can upper bound γ_m as the following:

$$\sum_{v=1}^{m-1} z^v N_v(q) \binom{m-1}{v} = 1$$

$$\sum_{v=1}^{m-1} z^v (q-2)^{v-1} \binom{m-1}{v} \geq 1$$

$$\frac{1}{q-2}((1+(q-2)z)^{m-1} - 1) \geq 1$$

$$z \geq \frac{(q-1)^{\frac{1}{m-1}} - 1}{q-2}$$

Replacing with $z = \frac{1}{\gamma_m(m-1)}$ gives

$$\gamma_m \leq \frac{q-2}{(m-1)((q-1)^{\frac{1}{m-1}} - 1)}$$

■

By combining the two upper bounds above, we proved that

$$\gamma_m \leq \min\left[\frac{q-2}{(m-1)((q-1)^{\frac{1}{m-1}} - 1)}, \frac{1}{q^{\frac{1}{q-1}} - 1}\right]$$

for $q \geq 3$. (In the case $q = 2$, $\gamma_m = 1$.)

B.5.2 General case

If the non-zero elements of the rows of the stabilizer generator matrix are not necessarily coprime with q, the bound (B.5) is no longer valid.

Counterexample: Consider the trivial upper bound $N_v(q) \leq (q-1)^{v-1}$. Assume $q = 6$, $v = 2$, the check is $(3, 2)$, so we look for irreducible solutions of $3x_1 + 2x_2 = 1$, where $3x_1 \neq 0$ and $2x_2 \neq 0$. Solutions are $\{(x_1, x_2) | x_1 \in \{1, 3, 5\} \text{ and } x_2 \in \{2, 5\}\}$. The number of solutions $N = 6 > 5$.

On the other hand, there is no solution for $3x_1 + 2x_2 = a$, with $a \in \{2, 3, 4\}$. On average, the number of solutions is $12/5$, so there might be a way to use such a bound. Unfortunately, so far we are not aware of the corresponding argument.

That being said, a larger upper bound can still be found:

$$\gamma_m \leq \frac{q-2}{(m-1)((3-\frac{4}{q})^{\frac{1}{m-1}}-1)}$$

Proof. First we find an upper bound on $N_v(q)$ to be $\frac{q}{2}(q-2)^{v-1}$. For any x_i that is not coprime with q, the number of solutions of $c_i x_i = 0 \pmod q$ for c_i equals $\gcd(x_i, q)$, which is at least two since x_i and q are not coprime. Thus, the requirement $c_i x_i \neq 0 \pmod q$ upper-bounds the number of choices for c_i by $q - \gcd(x_i, q) \leq q-2$. And the solution for the last number is at most $\frac{q}{2}$, which is the largest possible value of $\gcd(x_v, q)$ for any $2 \leq x_v \leq q-1$.

Applying this upper bound on z:

$$\sum_{v=1}^{m-1} z^v (q-2)^{v-1} \frac{q}{2} \binom{m-1}{v} \geq 1$$

$$z \geq \frac{(3-\frac{4}{q})^{\frac{1}{m-1}}-1}{q-2}$$

Replacing with $z = \frac{1}{\gamma_m(m-1)}$ gives the upper bound on γ_m. ■

B.6 Proof of Theorem 4.8 and Theorem 4.9

Theorem 4.8 *Consider a sequence of quantum CSS codes $Q(G_t, H_t)$, $t \in \mathbb{N}$, of increasing lengths n_t, where row weights of each G_t and H_t do not exceed a fixed m, and the code distances $d_t \geq D \ln n_t$, with some $D > 0$. Then the sequence $\Delta F_t \equiv [\Delta F_{\boldsymbol{e}}(G_t, H_t; K)]_p$, $t \in \mathbb{N}$, converges to zero in the region*

$$(m-1)\left((1-p)(q-1)e^{-K} + pe^{K} + (q-2)p\right) < e^{-1/D} \tag{4.15}$$

Theorem 4.9 *Consider a sequence of pairs of weakly dual Potts models defined by pairs of finite q-ary matrices with mutually orthogonal rows, $G_t H_t^T = 0$, $t \in \mathbb{N}$, where row weights of each H_t do not exceed a fixed m. In addition, assume that the sequence of the CSS distances*

d_{G_t} is increasing. Then the sequence $\Delta f_t \equiv [\Delta f_{\mathbf{e}}(G_t, H_t; K)]_p$, $t \in \mathbb{N}$, converges to zero in the region

$$(m-1)\left((1-p)(q-1)e^{-K} + pe^{K} + (q-2)p\right) < 1. \tag{4.16}$$

The proofs are similar, and follow the line of argument in the proof of Theorem 3.1.

Proof. Consider a q-ary quantum CSS LDPC code with generator matrix G for X or Z errors. The following upper bound on the ratio $r(K, \boldsymbol{e}) \equiv \frac{Z_{tot}(\boldsymbol{e})}{Z_0(\boldsymbol{e})} - 1 = \sum_{\boldsymbol{c}\neq 0} \frac{Z_{\boldsymbol{c}}(\boldsymbol{e})}{Z_0(\boldsymbol{e})}$ are proved for any fixed error $\boldsymbol{e}$.

For any $\boldsymbol{\varepsilon} \equiv \boldsymbol{c} + \boldsymbol{\alpha} P$, consider an irreducible vector decomposition: $\boldsymbol{\varepsilon} = \boldsymbol{\varepsilon}_1 + \boldsymbol{\varepsilon}_2 + ...$, where the support of $\boldsymbol{\varepsilon}_i$ don't overlap, and they each satisfies the parity check $G\boldsymbol{\varepsilon}_i^T = 0$. Take the sum of non-trivial codewords to be $\boldsymbol{\varepsilon}' \not\simeq 0$ and the sum of trivial ones to be $\boldsymbol{\varepsilon}'' \simeq 0$, we write $\boldsymbol{\varepsilon} = \boldsymbol{\varepsilon}' + \boldsymbol{\varepsilon}''$ where the support of $\boldsymbol{\varepsilon}'$ and $\boldsymbol{\varepsilon}''$ don't overlap. So the ratio $r(K, \boldsymbol{e})$ can be written as

$$\begin{aligned} r(K, \boldsymbol{e}) &\equiv \frac{Z_{\text{tot}}(\boldsymbol{e})}{Z_0(\boldsymbol{e})} - 1 \\ &= \sum_{\boldsymbol{\varepsilon}'} \frac{\sum_{\boldsymbol{\varepsilon}''\simeq 0 : \boldsymbol{\varepsilon}'\cap\boldsymbol{\varepsilon}''=\emptyset} e^{-K\text{wgt}(\boldsymbol{e}+\boldsymbol{\varepsilon}'+\boldsymbol{\varepsilon}'')}}{\sum_{\boldsymbol{\varepsilon}''\simeq 0} e^{-K\text{wgt}(\boldsymbol{e}+\boldsymbol{\varepsilon}'')}} \\ &\leq \sum_{\boldsymbol{\varepsilon}'} \frac{\sum_{\boldsymbol{\varepsilon}''\simeq 0 : \boldsymbol{\varepsilon}'\cap\boldsymbol{\varepsilon}''=\emptyset} e^{-K\text{wgt}(\boldsymbol{e}+\boldsymbol{\varepsilon}'+\boldsymbol{\varepsilon}'')}}{\sum_{\boldsymbol{\varepsilon}''\simeq 0 : \boldsymbol{\varepsilon}'\cap\boldsymbol{\varepsilon}''=\emptyset} e^{-K\text{wgt}(\boldsymbol{e}+\boldsymbol{\varepsilon}'')}} \end{aligned}$$

where in the last equation, the summation in the denominator is restricted to vectors $\boldsymbol{\varepsilon}'' \simeq 0$ that don't overlap with $\boldsymbol{\varepsilon}'$.

For each $\boldsymbol{\varepsilon}'$, we can also decompose $\boldsymbol{e} = \boldsymbol{e}'(\boldsymbol{\varepsilon}') + \boldsymbol{e}''(\boldsymbol{\varepsilon}') + \boldsymbol{e}'''(\boldsymbol{\varepsilon}')$. Here the support of $\boldsymbol{e}'$ is in the support of $\boldsymbol{\varepsilon}'$ and their corresponding elements add up to 0 (mod q), the support of $\boldsymbol{e}'''$ is also in the support of $\boldsymbol{\varepsilon}'$ but their corresponding elements add up to some non-zero value, which doesn't change the weight. The support of $\boldsymbol{e}''$ is the part of the support of $\boldsymbol{e}'$ that doesn't overlap with $\boldsymbol{\varepsilon}'$. So the weight can be decomposed as: $\text{wgt}(\boldsymbol{e}' + \boldsymbol{e}'' + \boldsymbol{e}''' + \boldsymbol{\varepsilon}' + \boldsymbol{\varepsilon}'') = \text{wgt}(\boldsymbol{e}' + \boldsymbol{\varepsilon}') + \text{wgt}(\boldsymbol{e}'' + \boldsymbol{\varepsilon}'')$, and $\text{wgt}(\boldsymbol{e}' + \boldsymbol{e}'' + \boldsymbol{e}''' + \boldsymbol{\varepsilon}'') = \text{wgt}(\boldsymbol{e}' + \boldsymbol{e}''') + \text{wgt}(\boldsymbol{e}'' + \boldsymbol{\varepsilon}'')$. Thus the inequality becomes

$$
\begin{aligned}
r(K,e) &\le \sum_{\boldsymbol{\varepsilon}'} \frac{\sum_{\boldsymbol{\varepsilon}''\simeq 0:\boldsymbol{\varepsilon}'\cap\boldsymbol{\varepsilon}''=\emptyset} e^{-K\mathrm{wgt}(\boldsymbol{e}'+\boldsymbol{e}''+\boldsymbol{e}'''+\boldsymbol{\varepsilon}'+\boldsymbol{\varepsilon}'')}}{\sum_{\boldsymbol{\varepsilon}''\simeq 0:\boldsymbol{\varepsilon}'\cap\boldsymbol{\varepsilon}''=\emptyset} e^{-K\mathrm{wgt}(\boldsymbol{e}'+\boldsymbol{e}''+\boldsymbol{e}'''+\boldsymbol{\varepsilon}'')}} \\
&= \sum_{\boldsymbol{\varepsilon}'} \frac{e^{-K\mathrm{wgt}(\boldsymbol{e}'+\boldsymbol{\varepsilon}')} \sum_{\boldsymbol{\varepsilon}''\simeq 0:\boldsymbol{\varepsilon}'\cap\boldsymbol{\varepsilon}''=\emptyset} e^{-K\mathrm{wgt}(\boldsymbol{e}''+\boldsymbol{\varepsilon}'')}}{e^{-K\mathrm{wgt}(\boldsymbol{e}'+\boldsymbol{e}''')} \sum_{\boldsymbol{\varepsilon}''\simeq 0:\boldsymbol{\varepsilon}'\cap\boldsymbol{\varepsilon}''=\emptyset} e^{-K\mathrm{wgt}(\boldsymbol{e}''+\boldsymbol{\varepsilon}'')}} \\
&= \sum_{\boldsymbol{\varepsilon}'} \frac{e^{-K\mathrm{wgt}(\boldsymbol{e}'+\boldsymbol{\varepsilon}')}}{e^{-K\mathrm{wgt}(\boldsymbol{e}'+\boldsymbol{e}''')}} \\
&= \sum_{\boldsymbol{\varepsilon}'} e^{-K\mathrm{wgt}(\boldsymbol{\varepsilon}')+2K\mathrm{wgt}(\boldsymbol{e}')+K\mathrm{wgt}(\boldsymbol{e}''')} \\
&= \sum_{l\ge 1} \sum_{1\le j_1<j_2<\ldots j_l\le t} e^{\sum_{i=1}^{l}(-K\mathrm{wgt}(\boldsymbol{c}_{j_i})+2K\mathrm{wgt}(\boldsymbol{e}'_{j_i})+K\mathrm{wgt}(\boldsymbol{e}'''_{j_i}))} \\
&= -1+\prod_{j=1}^{t}\left(1+e^{-K\mathrm{wgt}(\boldsymbol{c}_j)+2K\mathrm{wgt}(\boldsymbol{e}'_j)+K\mathrm{wgt}(\boldsymbol{e}'''_j)}\right) \\
&= -1+\exp\left(\sum_{j=1}^{t}\ln\left(1+e^{-K\mathrm{wgt}(\boldsymbol{c}_j)+2K\mathrm{wgt}(\boldsymbol{e}'_j)+K\mathrm{wgt}(\boldsymbol{e}'''_j)}\right)\right) \\
&\le -1+\exp\left(\sum_{j=1}^{t} e^{-K\mathrm{wgt}(\boldsymbol{c}_j)+2K\mathrm{wgt}(\boldsymbol{e}'_j)+K\mathrm{wgt}(\boldsymbol{e}'''_j)}\right)
\end{aligned}
$$

where we have decomposed every $\boldsymbol{\varepsilon}'$ into t irreducible codewords $\boldsymbol{c}_1, \boldsymbol{c}_2, \ldots, \boldsymbol{c}_t$, j_i are the indices in the list of irreducible codewords, and $\boldsymbol{e}_j$ are the restriction of $\boldsymbol{e}$ to the support of $\boldsymbol{c}_j$. The last inequality used the trivial inequality $\ln(1+x) \le x$ for any $x > -1$.

Denote error averaging with square brackets $[f(e)] \equiv \sum_e P(e) f(e)$, the successful decoding probability

$$
\begin{aligned}
\mathbb{P}_{\mathrm{succ}} \equiv \left[\frac{Z_0(\boldsymbol{e})}{Z_{\mathrm{tot}(\boldsymbol{e})}}\right] &= \left[\frac{1}{1+r(K,\boldsymbol{e})}\right] \ge \left[\exp\left(-\sum_{j=1}^{t} e^{-K\mathrm{wgt}(\boldsymbol{c}_j)+2K\mathrm{wgt}(\boldsymbol{e}'_j)+K\mathrm{wgt}(\boldsymbol{e}'''_j)}\right)\right] \\
&\ge \exp\left(-\sum_{j=1}^{t}\left[e^{-K\mathrm{wgt}(\boldsymbol{c}_j)+2K\mathrm{wgt}(\boldsymbol{e}'_j)+K\mathrm{wgt}(\boldsymbol{e}'''_j)}\right]\right) \\
&= \exp\left(-\sum_{j=1}^{t}\left((1-p)e^{-K}+\frac{p}{q-1}e^{K}+\frac{q-2}{q-1}p\right)^{\mathrm{wgt}(\boldsymbol{c}_j)}\right)
\end{aligned}
$$

where we have used the convexity of the exponential function in the last inequality.

Applying the upper bound on the number of irreducible codewords from Appendix B.4, we find

$$\begin{aligned}\mathbb{P}_{\text{succ}} &\geq \exp\left(-n(q-1)\sum_{w=d}^{\infty}\left((m-1)\left((1-p)(q-1)e^{-K}+pe^{K}+(q-2)p\right)\right)^{w}\right)\\ &= \exp\left(-n(q-1)\frac{\left((m-1)\left((1-p)(q-1)e^{-K}+pe^{K}+(q-2)p\right)\right)^{d}}{1-(m-1)\left((1-p)(q-1)e^{-K}+pe^{K}+(q-2)p\right)}\right)\end{aligned}$$

For a code of which distance increases as $\lim_{n\to\infty}\frac{d}{\ln(n)} = D$, the probability of decoding failure converges to 0 if

$$(m-1)\left((1-p)(q-1)e^{-K}+pe^{K}+(q-2)p\right) < e^{-1/D}$$

In the case where $\lim_{n\to\infty}\frac{d}{\ln(n)} = \infty$ which is true in toric code or hypergraph-product code, the condition is simply

$$(m-1)\left((1-p)(q-1)e^{-K}+pe^{K}+(q-2)p\right) < 1$$

The inverse temperature that maximizes $\mathbb{P}_{\text{succ}}$ is when

$$e^{K} = \sqrt{\frac{(1-p)(q-1)}{p}}$$

which is half of the inverse Nishimori temperature $K_p = \ln\left(\frac{(1-p)(q-1)}{p}\right)$. And the lower bound on the error rate threshold at this temperature becomes

$$(m-1)\left(\left(\sqrt{1-p}+\sqrt{p(q-1)}\right)^{2}-1\right) < e^{-1/D}$$

The free energy density homological difference, $\Delta f \equiv \frac{1}{n}(\ln Z_{\text{tot}}(\boldsymbol{e}) - \ln Z_0(\boldsymbol{e}))$, is given by

$$\Delta f = \frac{1}{n}\ln(\frac{Z_{\text{tot}}(\boldsymbol{e})}{Z_0(\boldsymbol{e})}) = (q-1)\frac{\left((m-1)\left((1-p)(q-1)e^{-K}+pe^{K}+(q-2)p\right)\right)^{d}}{1-(m-1)\left((1-p)(q-1)e^{-K}+pe^{K}+(q-2)p\right)}$$

which converges to 0 if

$$(m-1)\left((1-p)(q-1)e^{-K}+pe^{K}+(q-2)p\right) < 1.$$

■

B.7 Proof of Theorem 4.4 and discussion on the upper bounds for code distance

Theorem 4.4 *Given that the distances of the codes $C_{H_1}^{\perp}$ and $C_{H_2}^{\perp}$ are d_1 and d_2 respectively and the corresponding codes with transposed matrices are $\tilde{d}_1$ and $\tilde{d}_2$ respectively, the lower bound of the distance d of the code $\mathcal{C}$ is $d \geq \min(d_1, d_2)$ and $d \geq \min(\tilde{d}_1, \tilde{d}_2)$.*

B.7.1 Code dimension

Given the generator matrices $G_x = (I \otimes H_2, H_1 \otimes I)$ and $G_z = (H_1^T \otimes I, -I \otimes H_2^T)$ of a CSS code $\mathcal{C}$, write H_1 and H_2 in Smith normal form: $H_1 = V_1 P_1 U_1$, $H_2 = V_2 P_2 U_2$, where V_i and U_i are reversible matrices with determinant ± 1 and P_1 and P_2 are diagonal matrices with diagonal elements $\{a_i\}$ and $\{b_j\}$.

Let N_x be the number of different vectors $\boldsymbol{v} = \boldsymbol{\alpha} G_x$ and N_z be that of $\boldsymbol{\alpha} G_z$, where $\boldsymbol{\alpha}$ is an arbitrary vector in $\mathbb{Z}_q$. First we find out N_x

$$N_x = \frac{q^{r_1 r_2}}{|\{\boldsymbol{\sigma} : \boldsymbol{\sigma} G_x = 0\}|}$$

where $r1$, $r2$ are the ranks of H_1 and H_2, respectively. To calculate the number of solutions, we can expand the product

$$\begin{aligned} 0 &= \boldsymbol{\sigma} G_x \\ &= \boldsymbol{\sigma}(I_1 \otimes V_2 P_2 U_2, V_1 P_1 U_1 \otimes I_2) \\ &= \boldsymbol{\sigma}(V_1 \otimes V_2)[(I_1 \otimes P_2)(V_1^{-1} \otimes U_2), (P_1 \otimes I_2)(U_1 \otimes V_2^{-1})] \end{aligned}$$

To simplify the symbols, let $\tilde{\boldsymbol{\sigma}} \equiv \boldsymbol{\sigma}(V_1 \otimes V_2)$. Then we may write

$$\begin{cases} \tilde{\boldsymbol{\sigma}}(I_1 \otimes P_2) = 0 \\ \tilde{\boldsymbol{\sigma}}(P_1 \otimes I_2) = 0 \end{cases}$$

so that

$$\begin{aligned} |\{\tilde{\boldsymbol{\sigma}}\}| =& (|\{\tilde{\sigma}_1 : \tilde{\sigma}_1 b_1 = 0 \text{ and } \tilde{\sigma}_1 a_1 = 0\}|)(|\{\tilde{\sigma}_2 : \tilde{\sigma}_2 b_2 = 0 \text{ and } \tilde{\sigma}_2 a_1 = 0\}|) \\ & (|\{\tilde{\sigma}_3 : \tilde{\sigma}_3 b_3 = 0 \text{ and } \tilde{\sigma}_3 a_1 = 0\}|) \ldots \end{aligned}$$

Since ($\tilde{\sigma}_1 b_1 = 0$ and $\tilde{\sigma}_1 a_1 = 0$) is equivalent to $\tilde{\sigma}_1 \gcd(a_1, b_1) = 0$, we may rewrite the number of solutions as:

$$|\{\tilde{\boldsymbol{\sigma}}\}| = \prod_{\substack{1\le i\le t_1\\ 1\le j\le t_2}} \gcd(a_i, b_j) \cdot \prod_{1\le i\le t_1} a_i^{r_2-t_2} \cdot \prod_{1\le j\le t_2} b_j^{r_1-t_1} \cdot q^{(r_1-t_1)(r_2-t_2)}$$

And we find the number

$$N_x = \frac{q^{t_1 r_2 + t_2 r_1 - t_1 t_2}}{D_{12} D_1^{r_2-t_2} D_2^{r_1-t_1}}$$

where t_1 and t_2 are the ranks of P_1 and P_2 respectively, $D_1 \equiv \prod_i a_i$, $D_2 \equiv \prod_j b_j$ and $D_{12} \equiv \prod_{i,j} \gcd(a_i, b_j)$.

Similarly,

$$N_z = \frac{q^{t_1 n_2 + t_2 n_1 - t_1 t_2}}{D_{12} D_1^{n_2-t_2} D_2^{n_1-t_1}}$$

Thus the total number of codewords is

$$\mathcal{K} = \frac{q^n}{N_x N_z} = q^{n+2t_1t_2-t_1(r_2+n_2)-t_2(r_1+n_1)} D_{12}^2 D_1^{r_2+n_2-2t_2} D_2^{r_1+n_1-2t_1}$$

where $n \equiv n_1 r_2 + n_2 r_1$.

Let the number of solutions for $H_1 \boldsymbol{c} = 0$ be $\mathcal{K}_1 \equiv q^{n_1-t_1} D_1$ and the number of solutions for $H_2 \boldsymbol{c} = 0$ be $\mathcal{K}_2 \equiv q^{n_2-t_2} D_2$, and those for H_1^T and H_2^T be $\tilde{\mathcal{K}}_1$ and $\tilde{\mathcal{K}}_2$ respectively.

To simplify the notations, let us define

$$\begin{aligned}
k &\equiv \log_q \mathcal{K} \\
k_1 &\equiv \log_q \mathcal{K}_1 = n_1 - t_1 + \log_q D_1 \\
k_2 &\equiv \log_q \mathcal{K}_2 = n_2 - t_2 + \log_q D_2 \\
\tilde{k}_1 &\equiv \log_q \tilde{\mathcal{K}}_1 = r_1 - t_1 + \log_q D_1 \\
\tilde{k}_2 &\equiv \log_q \tilde{\mathcal{K}}_2 = r_2 - t_2 + \log_q D_2
\end{aligned}$$

where we simply define k to be the logarithm of the number of codewords in base q, which is not necessarily an integer. It is easy to see that

$$k = k_1 \tilde{k}_2 + k_2 \tilde{k}_1 - 2 \log_q D_1 \log_q D_2 + 2 \log_q D_{12}$$

B.7.2 Bounds on code distance

We find the lower bound of the distance as in the following statement:

Theorem B.1 *Given that the distance of H_1 and H_2 is d_1 and d_2 respectively and the distance of H_1^T and H_2^T is $\tilde{d}_1$ and $\tilde{d}_2$ respectively, the lower bound of the distance d of the code $\mathcal{C}$ is $d \geq \min(d_1, d_2)$ and $d \geq \min(\tilde{d}_1, \tilde{d}_2)$.*

Lemma B.2 *If $\mathcal{K}_1 = \mathcal{K}_2 = 1$, then $\mathcal{K} = 1$.*

Proof of Lemma: Denote the invariants of the Smith normal form of H_1 and H_2 by $\{a_i\}$ and $\{b_j\}$ respectively, $D_1 \equiv \prod_i a_i$, $D_2 \equiv \prod_j b_j$ and $D_{12} \equiv \prod_{i,j} \gcd(a_i, b_j)$. If $\mathcal{K}_1 = \mathcal{K}_2 = 1$, D_1 and D_2 must be 1, so that $a_i = 1$ and $b_j = 1$ are true for all i, j, so $D_{12} = 1$, which implies $\mathcal{K} = 1$.

Proof. To prove the lower bound, suppose there is a vector $\boldsymbol{v}$ that satisfies $G_x \boldsymbol{v}^T = 0$ and $\mathrm{wt}(\boldsymbol{v}) < \min(d_1, d_2)$ and we prove that it can be written as a linear combination of rows of G_z: $\boldsymbol{v} = \boldsymbol{\alpha} G_z$.

In vector $\boldsymbol{v}$, the non-zero elements multiply certain columns in G_x, and these columns correspond to certain columns in H_1 and H_2. Now drop those columns in H_1 and H_2 that don't correspond to any non-zero element of $\boldsymbol{v}$, and define the resulting matrices to be H_1' and H_2', and the number of columns to be n_1' and n_2'. And also drop the elements of $\boldsymbol{v}$ that correspond to the dropped columns in $G_x' = (I \otimes H_2', H_1' \otimes I)$, which results in a shorter vector $\boldsymbol{v}'$.

The number of columns of H_1' is $n_1' < d_1$, which is the distance of H_1, so it must be a full rank matrix with all diagonal elements to be 1 in Smith normal form, otherwise we can find a vector $\boldsymbol{c}_1'$ with $\mathrm{wt}(\boldsymbol{c}_1') \leq n_1'$ that satisfies $H_1' {\boldsymbol{c}_1'}^T = 0$, and by putting zeros in $\boldsymbol{c}_1'$ we find an codeword of H_1 with weight less than d_1, resulting in a contradiction. Similarly, H_2' must also be a full rank matrix with all diagonal elements to be 1.

From the lemma above, we can see that the QHP code based on matrices G_x', G_z' contains only the trivial vector 0, so $\mathcal{K}' = 1$. Thus, the matrix $G_z' = ({H_1'}^T \otimes I, -I \otimes {H_2'}^T)$

also has dimension 1, which means that $\boldsymbol{v}'$ can be written as linear combinations of rows of G'_z since $G'_x \boldsymbol{v}'^T = 0$ and $G'_x G'^T_z = 0$. By expanding $\boldsymbol{v}'$ back to length n, where we fill the columns that was dropped when we created $\boldsymbol{v}'$ from $\boldsymbol{v}$ with zeros, we recover $\boldsymbol{v}$ and show that it can be written as linear combinations of rows of G_z, which completes the proof.

In the above we proved $d \geq \min(d_1, d_2)$. The second inequality, $d \geq \min(\tilde{d}_1, \tilde{d}_2)$, is proved in a similar way. ■

Let us now discuss the upper bounds on the distance. In the binary case, the upper bound reads $d \leq \min(d_1, d_2)$ if we set the distance of an empty code equal infinity. However, the method to prove the upper bound of the distance of the code in the binary case: "$d \leq d_1$ when $k_2 \neq 0$, and $d \leq d_2$ when $k_1 \neq 0$; similarly $d \leq \tilde{d}_1$ when $\tilde{k}_2 \neq 0$, and $d \leq \tilde{d}_2$ when $\tilde{k}_1 \neq 0$", is no longer valid in $\mathbb{Z}_q$ when q is composite, as shown in the following argument:

In the case $k_1 \neq 0$, to prove $d \leq d_2$, we need to find an error $\boldsymbol{e}$ with $wt(\boldsymbol{e}) = d_2$, where $G_x \boldsymbol{e}^T = 0$ and $\boldsymbol{e}$ can't be written as any linear combination of rows of G_z.

Take all the vectors $\{\boldsymbol{e}\}$ that can be written as $\boldsymbol{e} = (\boldsymbol{\beta} \otimes \boldsymbol{c}_2^T, 0)$ where $\boldsymbol{\beta}$ goes through all the vectors that has an element 1 and other elements 0, $\boldsymbol{c}_2$ goes through all the vectors that satisfies $H_2 \boldsymbol{c}_2 = 0$ and $wt(\boldsymbol{c}_2) = d_2$. Suppose any $\boldsymbol{e}$ can be written as $\boldsymbol{\alpha} G_z$. Expand $\boldsymbol{\alpha}$ in the basis $\boldsymbol{\alpha}_1 \otimes \boldsymbol{\alpha}_2$:

$$\begin{cases} \boldsymbol{\beta} \otimes \boldsymbol{c}_2^T = \sum_{i,j} \alpha_{ij} (\boldsymbol{\alpha}_{1i} \otimes \boldsymbol{\alpha}_{2j})(H_1^T \otimes I) \\ 0 = \sum_{i,j} \alpha_{ij} (\boldsymbol{\alpha}_{1i} \otimes \boldsymbol{\alpha}_{2j})(I \otimes H_2^T) \end{cases}$$

which leads to

$$\begin{cases} \boldsymbol{\beta} \otimes \boldsymbol{c}_2^T = \sum_{i,j} \alpha_{ij} \boldsymbol{\alpha}_{1i} H_1^T \otimes \boldsymbol{\alpha}_{2j} \\ 0 = \sum_{i,j} \alpha_{ij} \boldsymbol{\alpha}_{2j} H_2^T \end{cases}$$

In the case q is prime, all α_{ij} can be taken as 1, and as $\boldsymbol{\beta}$ goes through all the vectors that has one position to be 1 and all the rest 0, we see that any vector that can be written as linear combinations of rows of H_1^T and H_1^T must be full rank, which implies that k_1 must be 0. However in $\mathbb{Z}_q$, it is possible that the elements of $\boldsymbol{c}_2^T$ have a common factor which may also appear in α_{ij} or H_1^T, which causes this method to be inapplicable.

Although the bounds on the code parameters defined on $\mathbb{Z}_q$ are much more complicated for general q, numeric evidence shows that a large random sparse matrix most likely has its Smith normal form invariants all being 1, which simplifies the situation so that it is similar to the algebra defined on fields, and the bounds are valid again.

Bibliography

[1] Richard P. Feynman. Simulating Physics with Computers. *International Journal of Theoretical Physics*, 21(6-7):467–488, June 1982.

[2] John Preskill. Quantum computing and the entanglement frontier. *arXiv preprint arXiv:1203.5813*, 2012.

[3] M. A. Nielsen and I. L. Chuang. *Quantum Computation and Quantum Infomation.* Cambridge Unive. Press, Cambridge, MA, 2000.

[4] A. R. Calderbank and P. W. Shor. Good quantum error-correcting codes exist. *Phys. Rev. A*, 54(2):1098–1105, Aug 1996.

[5] Andrew M Steane. Error correcting codes in quantum theory. *Physical Review Letters*, 77(5):793, 1996.

[6] E. Dennis, A. Kitaev, A. Landahl, and J. Preskill. Topological quantum memory. *J. Math. Phys.*, 43:4452, 2002.

[7] A. Yu. Kitaev. Quantum computations: algorithms and error correction. *Uspekhi Mat. Nauk*, 52:53–112, 1997. [Russian Math. Surveys, 52:6 (1997), 1191-1249].

[8] Yi Jiang, Ilya Dumer, Alexey A Kovalev, and Leonid P Pryadko. Duality and free energy analyticity bounds for few-body ising models with extensive homology rank. *Journal of Mathematical Physics*, 60(8):083302, 2019.

[9] N. B. Birrel and P. C. W. Davies. *Quantum fields in curved space.* Cambridge University Press, Cambridge, UK, 1982.

[10] Guido Cognola, Klaus Kirsten, and Sergio Zerbini. One-loop effective potential on hyperbolic manifolds. *Phys. Rev. D*, 48:790–799, Jul 1993.

[11] Roberto Camporesi. ζ-function regularization of one-loop effective potentials in anti-de Sitter spacetime. *Phys. Rev. D*, 43:3958–3965, Jun 1991.

[12] Gennaro Miele and Patrizia Vitale. Three-dimensional Gross-Neveu model on curved spaces. *Nuclear Physics B*, 494(1):365 – 387, 1997.

[13] Benjamin Doyon. Two-point correlation functions of scaling fields in the Dirac theory on the Poincaré disk. *Nuclear Physics B*, 675(3):607 – 630, 2003.

[14] G. Evenbly and G. Vidal. Tensor network states and geometry. *Journal of Statistical Physics*, 145(4):891–918, Nov 2011.

[15] Hiroaki Matsueda, Masafumi Ishihara, and Yoichiro Hashizume. Tensor network and a black hole. *Phys. Rev. D*, 87:066002, Mar 2013.

[16] David R. Nelson. Order, frustration, and defects in liquids and glasses. *Phys. Rev. B*, 28:5515–5535, Nov 1983.

[17] G. Tarjus, S. A. Kivelson, Z. Nussinov, and P. Viot. The frustration-based approach of supercooled liquids and the glass transition: a review and critical assessment. *Journal of Physics: Condensed Matter*, 17(50):R1143, 2005.

[18] Vincenzo Vitelli, J. B. Lucks, and D. R. Nelson. Crystallography on curved surfaces. *Proceedings of the National Academy of Sciences*, 103(33):12323–12328, 2006.

[19] F. Sausset and G. Tarjus. Periodic boundary conditions on the pseudosphere. *Journal of Physics A: Mathematical and Theoretical*, 40(43):12873, 2007.

[20] Luca Giomi and Mark Bowick. Crystalline order on Riemannian manifolds with variable Gaussian curvature and boundary. *Phys. Rev. B*, 76:054106, Aug 2007.

[21] Ari M. Turner, Vincenzo Vitelli, and David R. Nelson. Vortices on curved surfaces. *Rev. Mod. Phys.*, 82:1301–1348, Apr 2010.

[22] Nicolas A. Garcia, Aldo D. Pezzutti, Richard A. Register, Daniel A. Vega, and Leopoldo R. Gomez. Defect formation and coarsening in hexagonal 2D curved crystals. *Soft Matter*, 11:898–907, 2015.

[23] Dario Benedetti. Critical behavior in spherical and hyperbolic spaces. *Journal of Statistical Mechanics: Theory and Experiment*, 2015(1):P01002, 2015.

[24] Reuven Cohen, Keren Erez, Daniel ben-Avraham, and Shlomo Havlin. Resilience of the internet to random breakdowns. *Phys. Rev. Lett.*, 85:4626–4628, Nov 2000.

[25] R. Albert and A.-L. Barabási. Statistical mechanics of complex networks. *Rev. Mod. Phys.*, 74:47–97, Jan 2002.

[26] Prasanna Gai and Sujit Kapadia. Contagion in financial networks. *Proc. Royal Soc. A: Math., Phys. and Eng. Sci.*, 466(2120):2401–2423, 2010.

[27] K. Börner, S. Sanyal, and A. Vespignani. Network science. *Annual Review of Information Science and Technology*, 41(1):537–607, 2007.

[28] L. M. Sander, C. P. Warren, I. M. Sokolov, C. Simon, and J. Koopman. Percolation on heterogeneous networks as a model for epidemics. *Mathematical Biosciences*, 180(1-2):293 – 305, 2002.

[29] L. da Fontoura Costa, O. N. Oliveira, G. Travieso, F. A. Rodrigues, P. R. Villas Boas, L. Antiqueira, M. P. Viana, and L. E. Correa Rocha. Analyzing and modeling real-world phenomena with complex networks: a survey of applications. *Advances in Physics*, 60(3):329–412, 2011.

[30] L. Danon, A. P. Ford, T. House, C. P. Jewell, M. J. Keeling, G. O. Roberts, J. V. Ross, and M. C. Vernon. Networks and the epidemiology of infectious disease. *Interdisciplinary Perspectives on Infectious Diseases*, 2011:284909, 2011.

[31] A. A. Kovalev and L. P. Pryadko. Spin glass reflection of the decoding transition for quantum error-correcting codes. *Quantum Inf. & Comp.*, 15:0825, 2015.

[32] A. A. Kovalev, S. Prabhakar, I. Dumer, and L. P. Pryadko. Numerical and analytical bounds on threshold error rates for hypergraph-product codes. *Phys. Rev. A*, 97:062320, Jun 2018.

[33] A. R. Calderbank, E. M. Rains, P. W. Shor, and N. J. A. Sloane. Quantum error correction and orthogonal geometry. *Phys. Rev. Lett.*, 78:405–408, 1997.

[34] Fa-Yueh Wu. The potts model. *Reviews of modern physics*, 54(1):235, 1982.

[35] W. K. Wootters and W. H. Zurek. A single quantum cannot be cloned. *Nature*, 299(5886):802–803, October 1982.

[36] Hidetoshi Nishimori. *Statistical Physics of Spin Glasses and Information Processing: An Introduction*. Clarendon Press, Oxford, 2001.

[37] Nicolas Sourlas. Spin-glass models as error-correcting codes. *Nature*, 339(6227):693–695, 1989.

[38] Harold Scott Macdonald Coxeter. *Non-euclidean geometry*. Cambridge University Press, 1998.

[39] Nikolas P. Breuckmann. *Homological Quantum Codes Beyond the Toric Code*. PhD thesis, RWTH Aachen University, 2017.

[40] Matthias Keller, Daniel Lenz, and Simone Warzel. An invitation to trees of finite cone type: random and deterministic operators. *arXiv preprint arXiv:1403.4426*, 2014.

[41] R. Griffiths. Rigorous results and theorems. In C. Domb and M. S. Green, editors, *Phase Transitions and Critical Phenomena*, volume 1. Exact results, chapter 2, pages 7–109. Acad. Press, London, 1972.

[42] Joel L. Lebowitz. Coexistence of phases in Ising ferromagnets. *Journal of Statistical Physics*, 16(6):463–476, 1977.

[43] C. Gruber and J. L. Lebowitz. On the equivalence of different order parameters and coexistence of phases for Ising ferromagnet. II. *Communications in Mathematical Physics*, 59(2):97–108, 1978.

[44] J. L. Lebowitz and C. E. Pfister. Surface tension and phase coexistence. *Phys. Rev. Lett.*, 46:1031–1033, Apr 1981.

[45] Russell Lyons. The Ising model and percolation on trees and tree-like graphs. *Communications in Mathematical Physics*, 125(2):337–353, 1989.

[46] Russell Lyons. Phase transitions on nonamenable graphs. *Journal of Mathematical Physics*, 41(3):1099–1126, 2000.

[47] P. Gerl. Random walks on graphs with a strong isoperimetric property. *J. Theor. Probab.*, 1:171–187, 1988.

[48] R. M. Burton and M. Keane. Density and uniqueness in percolation. *Comm. Math. Phys.*, 121(3):501–505, 1989.

[49] Itai Benjamini and Oded Schramm. Percolation beyond Z^d, many questions and a few answers. *Electronic Communications in Probability*, 1:71–82, 1996.

[50] Olle Häggström and Johan Jonasson. Uniqueness and non-uniqueness in percolation theory. *Probability Surveys*, 3:289–344, 2006.

[51] Itai Benjamini and Oded Schramm. Percolation in the hyperbolic plane. *Journal of the American Mathematical Society*, 14(2):487–507, 2001.

[52] Johan Jonasson and Jeffrey E. Steif. Amenability and phase transition in the Ising model. *Journal of Theoretical Probability*, 12(2):549–559, 1999.

[53] C. M. Fortuin and P. W. Kasteleyn. On the random-cluster model: I. introduction and relation to other models. *Physica*, 57(4):536 – 564, 1972.

[54] C. M. Fortuin. On the random-cluster model: II. The percolation model. *Physica*, 58(4):393 – 418, 1972.

[55] H. Roberto Schonmann. Multiplicity of phase transitions and mean-field criticality on highly non-amenable graphs. *Communications in Mathematical Physics*, 219(2):271–322, 2001.

[56] Olle Häggström, Johan Jonasson, and Russell Lyons. Explicit isoperimetric constants and phase transitions in the random-cluster model. *Ann. Probab.*, 30(1):443–473, 01 2002.

[57] C. Chris Wu. Ising models on hyperbolic graphs II. *Journal of Statistical Physics*, 100(5):893–904, Sep 2000.

[58] F. Wegner. Duality in generalized Ising models and phase transitions without local order parameters. *J. Math. Phys.*, 2259:12, 1971.

[59] R. Tanner. A recursive approach to low complexity codes. *IEEE Trans. Info. Th.*, 27:533–547, 1981.

[60] J. K. Percus. Correlation inequalities for Ising spin lattices. *Communications in Mathematical Physics*, 40(3):283–308, 1975.

[61] S. B. Shlosman. Correlation inequalities and their applications. *Journal of Soviet Mathematics*, 15(2):79–101, 1981.

[62] Robert B. Griffiths. Correlations in Ising ferromagnets. I. *J. Math. Phys.*, 8:478, 1967.

[63] D. G. Kelly and S. Sherman. General Griffiths' inequalities on correlations in Ising ferromagnets. *Journal of Mathematical Physics*, 9(3):466–484, 1968.

[64] H. A. Kramers and G. H. Wannier. Statistics of two-dimensional ferromagnet. Part I. *Phys. Rev.*, 60:252–262, Aug. 1941.

[65] Daniel Gottesman. *Stabilizer Codes and Quantum Error Correction*. PhD thesis, Caltech, 1997.

[66] A. R. Calderbank, E. M. Rains, P. M. Shor, and N. J. A. Sloane. Quantum error correction via codes over GF(4). *IEEE Trans. Info. Theory*, 44:1369–1387, 1998.

[67] John Preskill. *Course Information for Physics 219/Computer Science 219 Quantum Computation*. Caltech, 2000.

[68] A. M. Steane. Simple quantum error-correcting codes. *Phys. Rev. A*, 54:4741–4751, 1996.

[69] Valentin Féray, Pierre-Loïc Méliot, and Ashkan Nikeghbali. *Mod-ϕ convergence I: Normality zones and precise deviations*. Springer International Publishing, Cham, 2016.

[70] I. Benjamini and O. Schramm. Recurrence of distributional limits of finite planar graphs. *Electron. J. Probab.*, 6:23/1–13, 2001.

[71] Christian Borgs, Jennifer Chayes, Jeff Kahn, and László Lovász. Left and right convergence of graphs with bounded degree. *Random Structures & Algorithms*, 42(1):1–28, 2013.

[72] L. M. Lovász. A short proof of the equivalence of left and right convergence for sparse graphs. *Eur. J. Comb.*, 53(C):1–7, April 2016.

[73] C. Domb and M. S. Green, editors. *Phase transitions and critical phenomena*, volume 3. Academic, London, 1974.

[74] S. Bravyi and B. Terhal. A no-go theorem for a two-dimensional self-correcting quantum memory based on stabilizer codes. *New Journal of Physics*, 11(4):043029, 2009.

[75] S. Bravyi, D. Poulin, and B. Terhal. Tradeoffs for reliable quantum information storage in 2D systems. *Phys. Rev. Lett.*, 104:050503, Feb 2010.

[76] J.-P. Tillich and G. Zemor. Quantum LDPC codes with positive rate and minimum distance proportional to $\sqrt{n}$. In *Proc. IEEE Int. Symp. Inf. Theory (ISIT)*, pages 799–803, June 2009.

[77] A. A. Kovalev and L. P. Pryadko. Quantum Kronecker sum-product low-density parity-check codes with finite rate. *Phys. Rev. A*, 88:012311, July 2013.

[78] L. Guth and A. Lubotzky. Quantum error correcting codes and 4-dimensional arithmetic hyperbolic manifolds. *Journal of Mathematical Physics*, 55(8):082202, 2014.

[79] Andrea Montanari, Elchanan Mossel, and Allan Sly. The weak limit of Ising models on locally tree-like graphs. *Probability Theory and Related Fields*, 152(1):31–51, 2012.

[80] Jozef Širáň. Triangle group representations and constructions of regular maps. *Proceedings of the London Mathematical Society*, 82(3):513–532, 2001.

[81] N. Delfosse and G. Zémor. Quantum erasure-correcting codes and percolation on regular tilings of the hyperbolic plane. In *Information Theory Workshop (ITW), 2010 IEEE*, pages 1–5, Aug 2010.

[82] N. Delfosse and G. Zémor. Upper bounds on the rate of low density stabilizer codes for the quantum erasure channel. *Quantum Info. Comput.*, 13(9-10):793–826, September 2013.

[83] N. Delfosse. Tradeoffs for reliable quantum information storage in surface codes and color codes. In *Information Theory Proceedings (ISIT), 2013 IEEE International Symposium on*, pages 917–921. IEEE, 2013.

[84] N. Delfosse and G. Zémor. A homological upper bound on critical probabilities for hyperbolic percolation. *Ann. Inst. Henri Poincaré Comb. Phys. Interact.*, 3:139–161, 2016.

[85] N. P. Breuckmann and B. M. Terhal. Constructions and noise threshold of hyperbolic surface codes. *IEEE Trans. on Inf. Th.*, 62(6):3731–3744, June 2016.

[86] N. P. Breuckmann, C. Vuillot, E. Campbell, A. Krishna, and B. M. Terhal. Hyperbolic and semi-hyperbolic surface codes for quantum storage. *Quantum Science and Technology*, 2(3):035007, 2017.

[87] A. Yu. Kitaev. Fault-tolerant quantum computation by anyons. *Ann. Phys.*, 303:2, 2003.

[88] Nicholas Metropolis, Arianna W. Rosenbluth, Marshall N. Rosenbluth, Augusta H. Teller, and Edward Teller. Equation of state calculations by fast computing machines. *The Journal of Chemical Physics*, 21(6):1087–1092, 1953.

[89] Ulli Wolff. Collective Monte Carlo updating for spin systems. *Phys. Rev. Lett.*, 62:361–364, Jan 1989.

[90] K. Binder. Finite size scaling analysis of Ising model block distribution functions. *Zeitschrift für Physik B Condensed Matter*, 43(2):119–140, 1981.

[91] The GAP Group. *GAP – Groups, Algorithms, and Programming, Version 4.8.10*, 2018.

[92] I. Dumer, A. A. Kovalev, and L. P. Pryadko. Numerical techniques for finding the distances of quantum codes. In *Information Theory Proceedings (ISIT), 2014 IEEE International Symposium on*, pages 1086–1090, Honolulu, HI, June 2014. IEEE.

[93] I. Dumer, A. A. Kovalev, and L. P. Pryadko. Distance verification for classical and quantum LDPC codes. *IEEE Trans. Inf. Th.*, 63(7):4675–4686, July 2017.

[94] Christian Borgs, Jennifer T Chayes, Remco Van Der Hofstad, Gordon Slade, Joel Spencer, et al. Random subgraphs of finite graphs. ii. the lace expansion and the triangle condition. *The Annals of Probability*, 33(5):1886–1944, 2005.

[95] Gady Kozma and Asaf Nachmias. A note about critical percolation on finite graphs. unpublished.

[96] Markus Heydenreich and Remco van der Hofstad. *Progress in High- Dimensional Percolation and Random Graphs*. CRM Short Courses. Springer International Publishing, Switzerland, 2017.

[97] Michael Woolls and Leonid Pryadko. Homology-changing percolation transitions on finite graphs. *arXiv preprint arXiv:2011.02603*, 2020.

[98] I. Dumer, A. A. Kovalev, and L. P. Pryadko. Thresholds for correcting errors, erasures, and faulty syndrome measurements in degenerate quantum codes. *Phys. Rev. Lett.*, 115:050502, Jul 2015.

[99] Michael E. Fisher. Critical temperatures of anisotropic Ising lattices. II. General upper bounds. *Phys. Rev.*, 162:480–485, Oct 1967.

[100] Joel L. Lebowitz. Bounds on the correlations and analyticity properties of ferromagnetic Ising spin systems. *Communications in Mathematical Physics*, 28(4):313–321, 1972.

[101] Mark Kac and John C Ward. A combinatorial solution of the two-dimensional ising model. *Physical Review*, 88(6):1332, 1952.

[102] Dmitry Chelkak, David Cimasoni, and Adrien Kassel. Revisiting the combinatorics of the 2d ising model. *AIHPD*, 4(3):309–385, 2017.

[103] Michael Wimmer. Algorithm 923: Efficient numerical computation of the pfaffian for dense and banded skew-symmetric matrices. *ACM Transactions on Mathematical Software (TOMS)*, 38(4):1–17, 2012.

[104] Henry J Stephen Smith. On systems of linear indeterminate equations and congruences. *Philosophical Transactions of the Royal Society of London*, pages 293–326, 1861.

[105] William C Brown. *Matrices over commutative rings*. Marcel Dekker, Inc., 1993.

[106] R. G. Gallager. *Low-Density Parity-Check Codes*. M.I.T. Press, Cambridge, Mass., 1963.

[107] S. Litsyn and V. Shevelev. On ensembles of low-density parity-check codes: asymptotic distance distributions. *IEEE Trans. Inf. Theory*, 48(4):887–908, Apr 2002.

[108] Vlad Gheorghiu. Standard form of qudit stabilizer groups. *Physics Letters A*, 378(5-6):505–509, 2014.

[109] A. A. Kovalev and L. P. Pryadko. Fault tolerance of quantum low-density parity check codes with sublinear distance scaling. *Phys. Rev. A*, 87:020304(R), Feb 2013.

[110] Weilei Zeng and Leonid P. Pryadko. Higher-dimensional quantum hypergraph-product codes with finite rates. *Phys. Rev. Lett.*, 122:230501, Jun 2019.

[111] H. Bombin and M. A. Martin-Delgado. Homological error correction: Classical and quantum codes. *Journal of Mathematical Physics*, 48(5):052105, 2007.

[112] Weilei Zeng and Leonid P. Pryadko. Iterative decoding of row-reduced quantum LDPC codes. unpublished, 2020.

[113] Jesper Lykke Jacobsen and Marco Picco. Phase diagram and critical exponents of a potts gauge glass. *Physical Review E*, 65(2):026113, 2002.

[114] Chiaki Yamaguchi. The derivation of the exact internal energies for spin glass models by applying the gauge theory to the fortuin-kasteleyn representation. *Progress of theoretical physics*, 127(2):199–208, 2012.

[115] Jo Ginibre. General formulation of griffiths' inequalities. *Communications in mathematical physics*, 16(4):310–328, 1970.

[116] Geoffrey Grimmett. Correlation inequalities for the potts model. *Mathematics and Mechanics of Complex Systems*, 4(3):327–334, 2016.

[117] Bin Dai, Shilin Ding, and Grace Wahba. Multivariate Bernoulli distribution. *Bernoulli*, 19:1465–1483, 2013.

[118] Robert H Swendsen and Jian-Sheng Wang. Nonuniversal critical dynamics in monte carlo simulations. *Physical review letters*, 58(2):86, 1987.

[119] Fugao Wang and David P Landau. Efficient, multiple-range random walk algorithm to calculate the density of states. *Physical review letters*, 86(10):2050, 2001.

[120] Jean Bricmont, Joel L. Lebowitz, and Charles E. Pfister. On the surface tension of lattice systems. *Annals of the New York Academy of Sciences*, 337(1):214–223, 1980.

[121] F. J. MacWilliams and N. J. A. Sloane. *The Theory of Error-Correcting Codes*. North-Holland, Amsterdam, 1981.